

Origami-Inspired Muscle Augmentation

An exploration of inflatable structured sheets to support the muscle function in individuals with muscle impairments



J.P.G. van de Kamp

 **TU Delft**

Origami-Inspired Muscle Augmentation

An exploration of inflatable structured sheets to support the muscle function in individuals with muscle impairments

Origami-Inspired Muscle Augmentation

An exploration of inflatable structured sheets to support the muscle function in individuals with muscle impairments

M.Sc. Thesis

In partial fulfilment of the requirements for the degree of
Master of Science in BioMedical Engineering.
Department of Biomechanical Engineering,
Delft University of Technology, Delft, The Netherlands
to be defended on Thursday, July 11th, 2024 at 13:30

By

Johannes Petrus Gerardus van de Kamp

Supervisor: Dr. ir. A.H.A. Stienen
Specialization: Neuromusculoskeletal Biomechanics
Type of report: M.Sc. Thesis
Date: July 11, 2024

This thesis was approved by the thesis committee:

Dr. ir. A.H.A. Stienen	Chairman
	BME, ME TU Delft
Dr ir. G. Smit	BME, ME TU Delft
Ir. P.H. de Jong	BME, ME TU Delft



Keywords: Inflatable structured sheets, muscle augmentation, Origami-inspired patterns, Biceps brachii.

Preface

Ever since I was young, I've been fascinated by the human body. The idea that every organ, tissue, and cell works together in harmony to sustain life has always captivated me. My passion for sports has given me a deep appreciation for the movements and interactions of muscles. Whether I am running, playing tennis, or dancing, I am constantly amazed by how our muscles work together to perform even the simplest actions.

As I pursued my bachelor's degree in mechatronics, I discovered profound parallels between the complexities of engineering and the intricate mechanisms of the human body. The fascination with the intersection of technology and healthcare propelled me towards continuing my studies in biomedical engineering, with a focus on neuromuscular biomechanics. During this masters, I studied the physical and biological principles that govern muscle function and control, deepening my admiration for the intricacies of the human body.

Despite its remarkable capabilities, the human body is not without its imperfections. Neuromuscular disorders, affecting over 14 million people worldwide. These disorders highlight the fragility and complexity of our biological systems and can significantly impact a person's quality of life, making it difficult to perform even basic tasks.

Fortunately, just as technological designs can be refined and improved, advancements in medical research and treatments offer hope for those affected by neuromuscular disorders. Through innovative solutions, many individuals can regain mobility and enhance their quality of life. This thesis contributes to ongoing research in biomedical engineering by designing origami-inspired inflatable structured sheets to support muscle function in individuals with muscle impairments.

By embracing advancements in neuromuscular biomechanics, I envision a future where neuromuscular conditions no longer impede the lives of those affected.

*Jeroen van de Kamp
Delft, July 2024*

Abstract

This thesis explores the application of origami-inspired inflatable structured sheets to enhance muscle function for individuals with muscle impairments, specifically focusing on the biceps brachii muscle. These sheets induce muscle contraction through pneumatic pressure, aimed at facilitating forearm flexion by strategically incorporating patterns that create air pockets.

These sheets hold significant potential for assisting individuals with conditions such as muscular dystrophy, cerebral palsy, or spinal cord injuries. Compared to traditional solutions, they offer less bulkiness and greater adaptability, promoting natural movement and improving limb mobility. Furthermore, these sheets can be customized to fit various muscle contours and integrated with mechatronics for real-time adjustments, enhancing stability and resilience in muscle support applications.

The study begins with the development of a comprehensive test setup that simulates muscle extension and flexion, integrating mechanical and electrical components. This setup includes a silicone muscle model of the biceps brachii muscle, essential for evaluating sheet performance.

Subsequent chapters delve into the evaluation of materials and patterns for the sheets. Materials such as PVC-film, TPU-film, PET-film, and Nylon are assessed for biocompatibility, flexibility, temperature sensitivity, and adhesion characteristics. Here, TPU-film emerges as the most promising material due to its durability and adhesive properties under pressure.

For the evaluation of the patterns, a preliminary study is conducted to determine optimal patterns that effectively respond to pneumatic pressure for inducing muscle contraction. This study reveals that combinations of parallel lines and zigzag structures show the most promising results among the tested patterns.

Building on these findings, various structured sheets are tested around the muscle model to assess their ability to activate and contract muscles. An optimal structure is selected that conforms closely to the contours of the muscle model, ensuring optimal airflow and maximizing the potential for effective muscle contraction. However, challenges such as leakage affecting pressure retention and muscle activation are identified, underscoring the need for further optimization to achieve practical muscle activation and flexion.

In conclusion, while this research provides valuable insights into the feasibility of origami-inspired structured sheets for muscle augmentation, ongoing refinement is crucial to address practical challenges and optimize performance.

Contents

Preface	v
Abstract	vi
Chapter 1	1
1.1 <i>Introduction to origami-inspired muscle augmentation</i>	2
1.1.1 Muscle augmentation	2
1.1.2 Origami-inspired inflatable structured sheets	3
1.2 <i>Background</i>	4
1.3 <i>Objectives</i>	6
1.4 <i>Thesis outline</i>	7
Chapter 2	8
2.1 <i>Introduction</i>	9
2.2 <i>Bicep brachii muscle model</i>	10
2.2.1 Analysis of the bicep brachii muscle	10
2.2.2 Requirements	12
2.2.3 Method	12
2.2.4 Results	13
2.2.5 Discussion	15
2.3 <i>Mechanical design</i>	16
2.3.1 Requirements	16
2.3.2 Method	17
2.3.3 Results	20
2.3.4 Discussion	21
2.4 <i>Electrical design</i>	22
2.4.1 Requirements	22
2.4.2 Method	23
2.4.3 Results	24
2.4.4 Discussion	27
2.5 <i>Conclusion</i>	28
Chapter 3	29
3.1 <i>Introduction</i>	30
3.2 <i>Materials</i>	30
3.2.1 Requirements	31
3.2.2 Method	31
3.2.3 Results	33
3.2.4 Conclusion	37
3.2.5 Discussion	37

Chapter 4	38
4.1 <i>Introduction</i>	39
4.2 <i>Preliminary study</i>	39
4.2.1 <i>Conclusion</i>	48
4.3 <i>Implementation around the muscle model</i>	49
4.3.1 <i>Requirements</i>	49
4.3.2 <i>Method</i>	49
4.3.3 <i>Results</i>	55
4.3.4 <i>Conclusion</i>	56
4.3.5 <i>Discussion</i>	57
Chapter 5	58
5.1 <i>Conclusion</i>	59
5.2 <i>Recommendations and Future Work</i>	60
Acknowledgements	65
References.....	66
Appendices	69
<i>Appendix A</i>	70
<i>Appendix B</i>	74
<i>Appendix C</i>	75
<i>Appendix D</i>	81

Chapter 1

Introduction: Origami-Inspired muscle augmentation

Jeroen van de Kamp

In this chapter, the concept of muscle augmentation is first introduced. Then, the main focus of this thesis is presented, emphasizing sheets designed to deform under pneumatic pressure through embedded structures inspired by origami, including their applications and relevance. Following this, the background is discussed, exploring artificial muscles and origami-inspired designs within this field. Lastly, the research objectives and thesis outline are presented.

1.1 Introduction to origami-inspired muscle augmentation

Throughout human history, there has been a profound interest in the workings of our muscles, the mechanisms driving our movements and powering our actions. However, when these muscles weaken or fail due to injury, disease or age, restoring mobility can become quite challenging. Conventional approaches typically focus on rehabilitation or support. But imagine if we could directly augment existing muscles to restore or enhance their function. This approach would promote greater flexibility, natural movement, and personalized support, tailored to fit various muscle groups and conditions. Therefore, the focus of this thesis is on exploring a way to directly augment muscle function.

1.1.1 Muscle augmentation

Muscle augmentation is an innovative advancement in medical technology that improves the power and functionality of human muscles. This approach holds promise across various applications, such as restoring mobility in individuals affected by paralysis or muscular dystrophy. A well-known example of muscle augmentation technology are robotic exoskeletons [1][2]. These exoskeletons integrate mechanical structures, sensors, and motors to support and enhance movement, enabling people with spinal cord injuries to walk again [3] (Fig. 1a). Another notable technology for muscle augmentation includes myoelectric prosthetic limbs [4] (Fig. 1b). Myoelectric prosthetic limbs use sensors to detect electrical signals from residual muscles in the user's limb, translating these signals into movements that replicate natural muscle function. This advancement provides amputees with increased strength and mobility, enabling them to perform a wide range of tasks effectively. Similarly, powered orthoses are a form of muscle augmentation that assists individuals with weakened muscles. For example, powered ankle-foot orthoses (Fig. 1c) can help improve gait and stability by providing additional support and movement control to the foot and ankle [5].



Figure 1: Muscle augmentation technologies: (a) robotic exoskeleton, (b) myoelectric prosthetic arm, (c) powered ankle-foot orthosis.

While many of these technologies offer significant benefits, they also present several drawbacks. These devices are often expensive, making them inaccessible to a wide range of users. Their bulky design can restrict natural movement and cause discomfort over prolonged use. Also their rigid design may also lack flexibility, potentially further impacting user comfort and compliance. In addition, users often require extensive training or rehabilitation to adapt to these technologies. In contrast, the field of soft robotics represents a promising alternative within the field of muscle augmentation [6].

1.1.2 Origami-inspired inflatable structured sheets

In this thesis, the focus lies within the field of soft robotics exploring the suitability of origami-inspired inflatable structured sheets designed to enhance muscle function in individuals with muscle impairments. These sheets are designed to wrap around muscles, specifically targeting the contraction of the biceps brachii in order to enable the flexion of the forearm. Inspired by origami principles, the design incorporates folding patterns that allow the sheets to dynamically deform and contract when subjected to pneumatic pressure. Ultimately, the aim is to place these sheets invasively in order to provide direct support (Fig. 2). When these sheets are placed around the muscle and activated, the contraction of the sheet induces the muscle to contract as well, thereby flexing the forearm and enhance the muscle function.

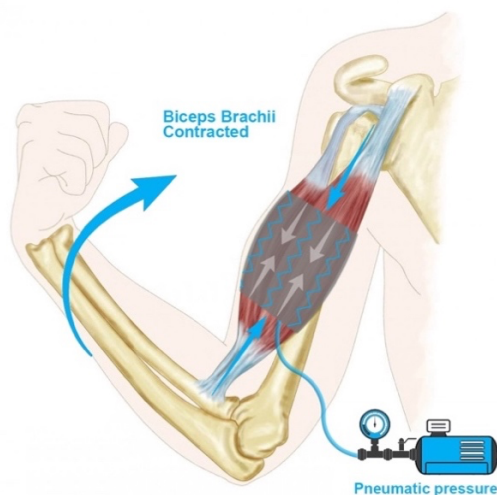


Figure 2: Concept drawing: Origami-inspired structured sheet wrapped around the biceps brachii muscle, inducing contraction and flexion of the forearm through pneumatic pressure.

Application and relevance

When the origami-inspired structured sheets are placed around muscles, they can induce contraction and extension to influence movement, making them useful for conditions like muscular dystrophy, cerebral palsy, or spinal cord injuries, where muscle function is limited.

These sheets offer several advantages when incorporated into muscle augmentation strategies. They are less bulky than traditional methods, promoting more natural movement and greater limb mobility. Their flexibility frees users from the constraints of rigid orthoses or exoskeletons, offering targeted and efficient support to enhance muscle strength and function. The adaptability of these sheets allows for personalized support, fitting various muscle groups and conditions, with customization to meet the specific contours and needs of different muscles.

Additionally, these sheets have the possibility to be integrated with mechatronics (a combination of mechanical, electrical, and computer engineering disciplines) such as sensors, springs, and dampers, enabling real-time adjustments for optimal muscle support and making them resilient and stable. For instance, they could potentially stabilize tremors in individuals with Parkinson's disease, offering greater control over movements.

1.2 Background

In order to delve into the design of these sheets, the thesis leverages expertise from artificial muscles, with a particular focus on origami-inspired designs. Traditional artificial muscles provide valuable insights into creating and controlling flexible, responsive materials that can mimic natural muscle behaviour. This capability is crucial for designing sheets that can dynamically adapt to muscle movements. Origami-inspired designs, in conjunction with artificial muscles, offer innovative solutions for creating structures that can efficiently fold and unfold. This capability enables the sheets to deform and contract as needed to enhance muscle function and support.

Artificial muscles

Artificial muscles are materials or devices engineered to mimic or support the function of biological muscles. Through the application of various stimuli such as tension, electric current, pressure, or temperature, these muscles can perform actions such as expansion, contraction, and rotation, enabling this technology to replicate the movements of real muscles [7].

In recent years, extensive research has focused on various forms of artificial muscles and ways to control them. For example, improvements have resulted in the development of artificial muscles that can be controlled pneumatically [8] or hydraulically [9]. A prominent example of such technology is the McKibben Muscle [8] (Fig. 3a), which utilizes compressed air or gas to induce contractions. Furthermore, there are materials such as Shape Memory Alloys [10] (Fig. 3b) that have the extraordinary capacity to return to their previous state in response to temperature, whereas Electroactive Polymers [11] (Fig. 3c) deform in reaction to electric current.

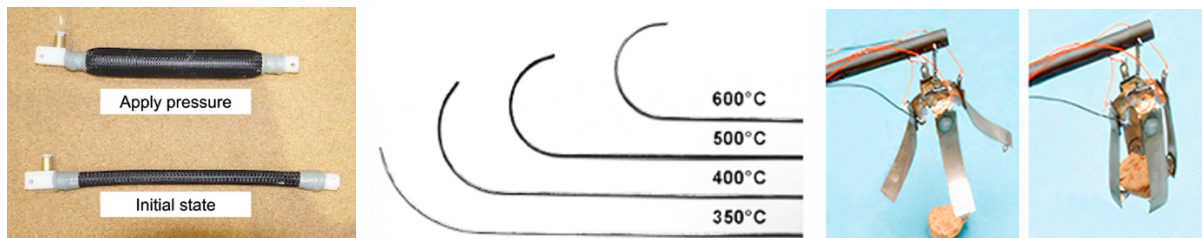


Figure 3: Forms of artificial muscles: (a) McKibben muscle, (b) Shape memory alloys (nitinol), (c) electroactive polymers applied as a gripper

In conclusion, artificial muscles provide innovative solutions for enhancing muscle function by replicating biological movements. Understanding how artificial muscles achieve motion that mimics biological muscles is valuable for designing structured sheets that are pneumatically controlled to enhance natural muscle movements.

Given the ultimate aim of invasively placing these sheets, the literature review on mechatronics suitable for implantation to facilitate skeletal movement also provides valuable insights (Appendix D). Among the conventional artificial muscle types evaluated, the McKibben muscle stands out as particularly suitable due to its biocompatibility, weight, flexibility, force output, and durability. With its pneumatic control mechanisms and applicability for invasive placement, this muscle type offers valuable information for designing inflatable structures to enhance muscle function.

Origami-inspired artificial muscles

Origami-inspired artificial muscles hold great potential for advancing the development of artificial muscles, offering new possibilities for research in this field. These muscles rely on geometric folding patterns to achieve motion and deformation, mimicking the flexibility and adaptability of natural muscles. These artificial muscles often incorporate well-known origami patterns, such as the Yoshimura, Miura-ori, Waterbomb, Kresling, and Resch patterns to achieve specific motion characteristics [12] (Fig. 4).



Figure 4: Examples of origami patterns. (a) Yoshimura pattern, (b) Miura-ori pattern, (c) waterbomb pattern, (d) Kresling pattern, (e) Resch Pattern

The operation of these muscles typically involves pneumatic or hydraulic mechanisms, leveraging flexible skins, usually in the form plastic sheets of various types that deform under the influence of pressure differentials. These sheets feature crease patterns, much like origami, strategically designed to create air pockets that influence the shape of the artificial muscle, enabling dynamic deformation and motion when subjected to pneumatic or hydraulic forces [13] (Fig. 5a). Additionally, within these sheets, a skeletal structure can be embedded, acting as a framework to guide the muscle's deformation [14] (Fig. 5b). As a result, the muscle can adapt to various shapes and execute tasks such as gripping, lifting or rotating [15] (Fig. 5c).



Figure 5: (a) Crease patterns creating air pockets, (b) skeletal structure inside plastic sheet (c) origami gripper

In conclusion, origami-inspired artificial muscles offer fascinating possibilities for advancing artificial muscle technology. These muscles exhibit remarkable biocompatibility, adaptability in size and shape and a wide range of motion capabilities. The intricate folding patterns contribute significantly to understanding patterned configurations and deformation under pneumatic pressure. Additionally, they provide insights into various materials and additional possibilities and applications

Similarly to the McKibben muscle, the literature review on mechatronics suitable for implantation highlights the invasive suitability of origami-inspired artificial muscles (Appendix D). Given the ultimate aim of invasively placing these sheets, the insights from these muscles are valuable for designing structured sheets.

1.3 Objectives

During this thesis, the focus will be on developing origami-inspired structured sheets, designed to wrap around muscles, specifically targeting the flexion of the biceps brachii. When this muscle is extended, as in when the arm is stretched, it lengthens. whereas during flexion, it shortens (Fig. 6). Therefore, the sheet must induce activation that contracts the muscle. This activation process combines origami folding principles and pneumatic manipulation techniques on the sheet.

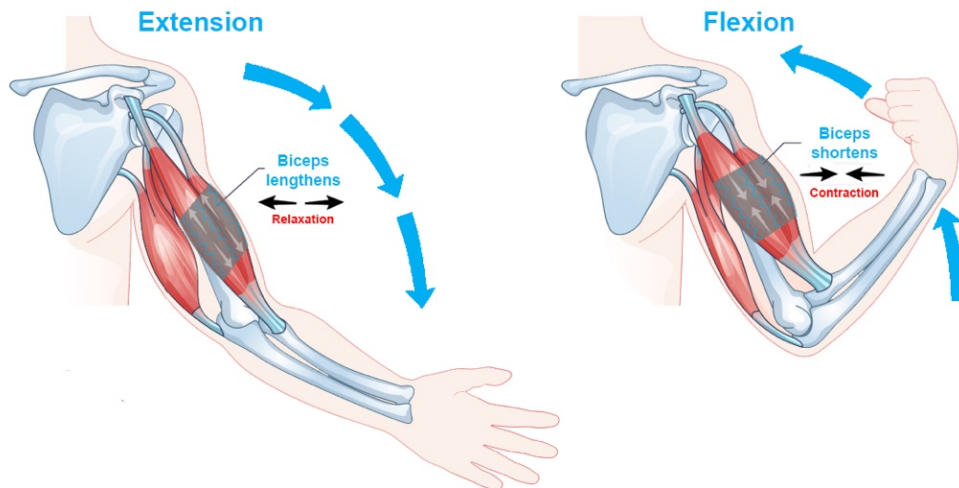


Figure 6: Deformation of the biceps brachii, illustrated with the structured sheet wrapped around the muscle.

This research focuses on identifying suitable patterns and materials for these sheets. Prioritizing factors such as compatibility and durability will ensure the sheet's viability for potential medical applications. To evaluate the efficacy of these origami sheets, a comprehensive test setup must be developed. This setup should simulate both the extension and flexion of the biceps brachii muscle, allowing for a thorough examination of the sheet's performance in activating muscle movement.

This thesis is guided by the following sub-questions:

1. *How can a test setup be developed to evaluate the performance of the sheet in simulating the extension and flexion of the biceps brachii muscle?*
2. *Which materials are most suitable for wrapping around a muscle and incorporating structures to undergo deformations?*
3. *What specific structural designs can be developed to effectively induce contraction, similar to the biceps brachii muscle during flexion?*
4. *How effective are the chosen structural designs in replicating the contraction and functionality of the biceps brachii muscle within the test setup?*

Leading to the main question:

Are inflatable structures suitable to support the functionality of biological muscles in individuals with muscle impairments?

1.4 Thesis outline

In this thesis the main line of research is designing an origami-inspired sheet for muscle contraction in order to induce flexion of the forearm. The following subtopics are included: designing a test setup, testing different materials, and experimenting with various patterns.

The second chapter of this thesis focuses on the design of a test setup essential for evaluating the efficacy of origami-inspired sheets in simulating muscle extension and flexion. This chapter covers both the mechanical and electrical aspects of the test setup, including the replication of the biceps brachii muscle and the integration of mechanical and electrical components to facilitate precise measurements and analysis.

The third chapter explores different materials to identify the most suitable material for wrapping around the muscle and incorporating structures into it.

The fourth chapter is dedicated to incorporating patterns into the sheet. In this chapter, various structures are evaluated to identify the optimal pattern that creates air pockets and contracts the sheet, aiming to induce contraction of the biceps brachii muscle.

The fifth and final chapter encapsulates the culmination of the thesis journey, offering a comprehensive overview of the key findings, conclusions, and recommendations derived from the research. Furthermore, this chapter provides insights into future directions and potential avenues for further exploration, paving the way for continued advancements in the field of origami-inspired muscle assistance technology.

To preserve a clear focus on the work that did not directly add value to the main conclusion was not included in the thesis. Instead the following appendices were added; [Appendix A](#) includes detailed technical drawings. [Appendix B](#) shows the MATLAB program that was used during testing. In [Appendix C](#), the electrical diagram used for the test setup is presented [Appendix D](#) contains the literature review on the classification and review of mechatronics that are suitable for implantation to facilitate skeletal movement.

Chapter 2

Mechanical and electrical design of a test setup to simulate the extension and flexion of the biceps brachii muscle

Jeroen van de Kamp

This chapter focuses on the test setup for measuring the efficacy of origami sheets in simulating extension and flexion of the biceps brachii muscle. It includes an analysis and description of the replication of the biceps brachii muscle, as well as the integration of both the mechanical and electrical aspects of the test setup.

2.1 Introduction

A test setup has been developed to evaluate the effectiveness of an origami-inspired sheet in enclosing the biceps brachii muscle and precisely targeting its flexion to induce movement. The test setup aims to replicate the bending motion of the forearm by incorporating an antagonistic system, mimicking the stretching and contracting of the triceps and biceps brachii muscles, which facilitates the rotation of the arm. To further (Fig. 7) test whether the origami-inspired sheet can be applied to the biceps brachii muscle to induce arm flexion, it is essential to accurately analyse the dynamics, shape, and dimensions of this muscle. In order to test and gather data from the origami-inspired sheets, electronics are also included.

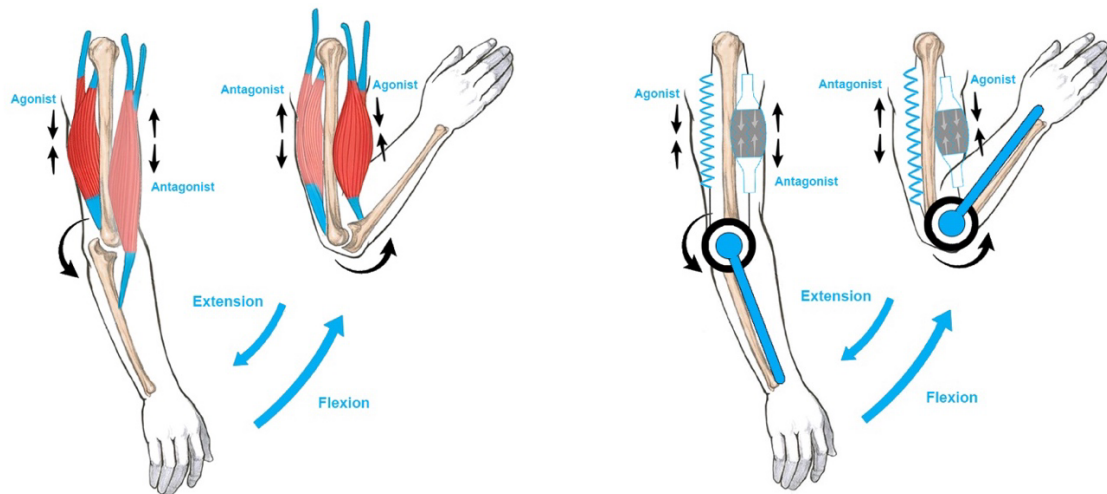


Figure 7: Antagonistic system: (a) biceps and triceps brachii, (b) concept drawing: depicting the biceps brachii muscle with a structured sheet inducing flexion and a spring representing the triceps brachii inducing extension.

In this chapter, first the biceps brachii muscle is described in order to mimic the muscle accurately for testing purposes. This includes discussing the muscle's dimensions, deformation characteristics, and behaviour during contraction and extension. Then the requirements for replicating the muscle are outlined, along with the methods used to create a silicone muscle model, including material selection, design considerations, and fabrication techniques are described.

Next, the chapter delves into the mechanical design, detailing a system capable of accurately replicating the extension and contraction of the muscles while simultaneously simulating arm movement. This chapter covers the design requirements, methodology, and results of integrating the silicone muscle with mechanical components.

Subsequently, electrical design necessary to assess the performance of the origami-inspired sheets is addressed, including requirements, methodology, results, and discussion. This involves the integration of electrical components, measurements, and the overall setup used to evaluate the effectiveness of the sheets in replicating muscle behaviour.

Finally, the conclusion is presented, describing a comprehensive test setup that is produced by integrating all of these components into a framework.

2.2 Bicep brachii muscle model

To effectively evaluate structured sheets that can be wrapped around the biceps brachii muscle, a muscle model must be developed that closely replicates its anatomical and physiological characteristics. This model forms the foundation for testing the sheets' effect on the muscle's deformation.

2.2.1 Analysis of the bicep brachii muscle

Anatomy

The biceps brachii muscle, a prominent muscle in the upper arm, is composed of two distinct heads: the short head and the long head (Fig. 8). These two heads originate from different points on the scapula bone. Both the short and long heads of the biceps brachii muscle merge together as they descend towards the arm, forming a single muscle belly. This belly gives rise to the biceps tendon, a strong and fibrous structure that attaches the muscle to the radius bone in the forearm [16][17].

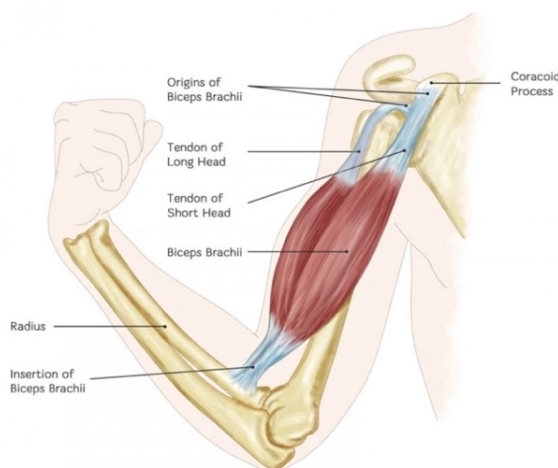


Figure 8: Anatomy of the bicep brachii muscle

Dimensions

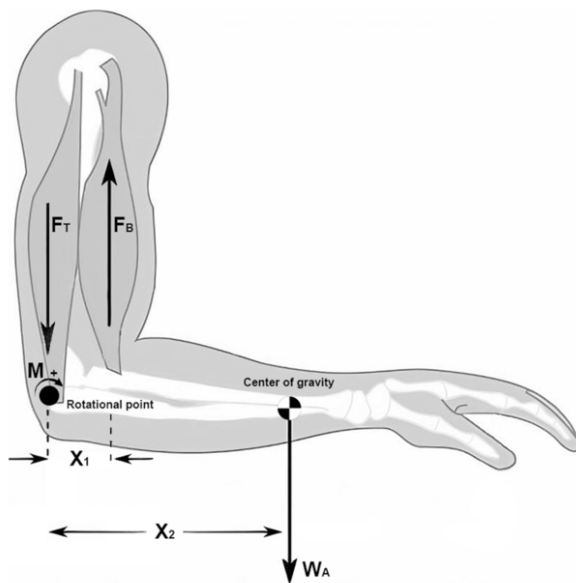
The total length of a muscle comprises the length of the fascicles and the tendons combined. Variations in the length and width of the biceps brachii muscle have been documented in the literature. For example, Nelson et al. [18] observed systematic and significant differences in measured fascicle lengths between elbow positions for the biceps, with in vivo measurements revealing a range of 82.6 mm to 155.1 mm for the muscle length. Additionally, in the study; A Proposal for a New Classification of the Supernumerary Heads of the Biceps Brachii Muscle [19], the distal tendon was measured at 63 mm in length, while the proximal tendons were found to be approximately 80.91 [20] and 80.95 mm [19] for the long head and short head, respectively. Similarly, the width of a muscle exhibits significant variation among individuals and populations as well, ranging from 22.9 mm to 40 mm [21][22][23].

Physiology

This muscle plays a crucial role in various upper limb movements, including elbow flexion and forearm supination. When the muscle contracts, it pulls on the biceps tendon, causing the forearm to move towards the upper arm and enabling actions such as lifting and bending the elbow [16].

The biceps brachii, undergoes notable changes in shape and length during arm movements. During extension of the arm, the biceps brachii elongates, stretching along with the movement to maintain tension and provide support as the forearm is lowered. This elongation causes the muscle to appear lengthened. In contrast, when the arm flexes, the biceps brachii contracts concentrically, resulting in a shortening of its fibers. This contraction causes the muscle to bulge and appear more pronounced as it exerts force to pull the forearm upward towards the shoulder [24].

A simplified analysis of the upper- and forearm suggests that the biceps needs to generate approximately 153.8N to flex the forearm (Fig. 9). The relationship between the distal tendon and the pivot point, was obtained from an article by Athwal et al. [25] and the forearm dimensions were obtained from a cadaver study [26].



$$M = W_a \cdot x_2 - F_B \cdot x_1 = 0$$

$$F_B = \frac{W_a \cdot x_2}{x_1}$$

$$x_1 = 0.023 \text{ m}$$

$$x_2 = 0.25 \text{ m}$$

$$W_a = 1.44 \text{ kg}$$

$$F_B = \frac{1.44 \cdot 9.81 \cdot 0.25}{0.023}$$

$$F_B \approx 153.55 \text{ N}$$

Figure 9: Free body diagram, upper- and forearm

Mechanical properties

The mechanical properties of the biceps brachii muscle encompass its dynamic behaviour and response to external forces. Research by Zhang et al. [27] revealed that the Young's modulus of the biceps brachii muscle exhibits non-linear behaviour during elbow extension, indicating that the muscle becomes stiffer as the elbow extends. According to the provided research, the Young's modulus of the healthy volunteer group varied depending on the elbow position. at 90°, the Young's modulus was 8.100 kPa, while at 180°, it increased to 19.700 kPa. Additionally, Nelson et al. [18] concluded that biceps fascicles increased by an average of 25 mm as the elbow was extended.

2.2.2 Requirements

To effectively develop a muscle model that accurately mimics the biceps brachii muscle and allows for the placement of origami-inspired sheets around it to test their effects, several key requirements must be addressed:

- Identifying a suitable material is critical to accurately simulate both extension and contraction of the biceps brachii. Criteria such as elasticity, durability, and ease of moulding were considered during this evaluation.
- To accurately mimic and test how the origami-inspired sheet would behave on a real biceps brachii muscle, it is essential that the muscle closely resembles the actual muscle in terms of shape and dimensions.
- Another considerations in designing the test setup is the ability to properly evaluate the origami-inspired sheets while maintaining a practical approach. Hence, it is crucial to ensure that the biceps brachii muscle is sufficiently large enough to facilitate the testing of these sheets.
- Finally, the biceps brachii muscle must be deformable to simulate both its extension and contraction accurately. This deformation capability is essential for validating and testing whether the origami-inspired sheets placed on the muscle have an effect on its extension and contraction.

Therefore, it is imperative to conduct a thorough assessment of the muscle's deformation characteristics. This ensures accurate validation and testing of the effects of the sheets.

2.2.3 Method

Materials

Several material options were evaluated for their potential to mimic the deformation characteristics of the biceps brachii muscle. Rubber was considered for its good elasticity and durability [28], but was ultimately deemed unsuitable due to its moderate ease of moulding, making it less flexible for precise shapes. Polyurethane, known for its durability and high elasticity [29], was also considered. However, its moderate ease of moulding, complex curing process, potential for inconsistent results, and higher cost led to its exclusion.

Silicone with a shore hardness of A25 [30] was chosen as the preferred material. Silicone is a synthetic polymer with excellent elasticity and durability, allowing the muscle to stretch during extension and return to its original shape during contraction. It can be easily poured into a mould, offering great shaping flexibility. The pouring method involves mixing liquid silicone with a curing agent before pouring it into a mould cavity, where it hardens and adopts the mould's shape. Once cured, silicone retains its flexibility, allowing it to be stretched and bent without losing structural integrity.

Shape and dimensions

Before casting the silicone, a mould was made in order to shape the muscle (Appx. A, fig. 74). Utilizing 3D printing technology, the mould was constructed with two outer shells made out of PLA material that interlocked with each other, enclosing an inner TPU component for casting the silicone. TPU was chosen for its ability to dissolve in water post-casting, leaving the muscle hollow. To ensure the stability of the inner component, specific shapes were incorporated on both sides of the mould. It was crucial to prevent the entrapment of air during the silicone casting process, hence strategically positioned holes were incorporated into one side of the mould to facilitate air escape and ensure smooth flow of the silicone mixture into the mould cavity.

In the process of design simplification, the short head and long head of the biceps were combined to define the muscle's shape. The chosen design typically exhibits an elongated structure with a rounded apex and a tapered base, resembling the natural anatomy of the biceps brachii muscle. As the design evolved, it became apparent that a thickness ranging from 22.9 to 40 mm would be too small and therefore insufficient for rigorous testing purposes. Consequently, a magnification factor of around 2 times the original size was implemented to ensure adequate dimensions for testing accuracy. Subsequently, the length of the muscle was also augmented to maintain proportional fidelity to the original muscle anatomy. Additionally, the incorporation of a hollow interior in the muscle model was deemed essential to maximize its stretchable properties, allowing for more authentic replication of muscle behaviour.

Assessing the deformability

To evaluate the silicone muscle's stretchability and deformation, a stiffness test was conducted. The silicone muscle was suspended vertically, and a 5 kg load was applied to simulate muscle movement forces. Measurements of the silicone muscle's displacement under load provided insights into its elasticity and deformation characteristics.

2.2.4 Results

The silicone muscle model, designed to mimic the behaviour of the biceps brachii muscle, measured 188 mm in length and 67 mm in width (Fig. 10):



Figure 10: Bicep brachii muscle model out of silicone

The stiffness value obtained provides insights into the mechanical properties of the silicone muscle model, demonstrating its resistance to deformation under the applied load and its ability to emulate the behaviour of the biceps brachii muscle. During the stiffness evaluation, the silicone muscle model exhibited linear displacement. To measure the stiffness of the silicone muscle model the muscle model was subjected to a single load of 5 kg, simulating the forces experienced by the biceps brachii during extension. The observed displacement of the muscle under this load was recorded at 5.75 cm.

To quantify the stiffness of the silicone muscle model, Hooke's Law was applied:

$$k = \frac{F}{\Delta L} = \frac{5 \cdot 9.81}{0.0575} \approx 853.04 \text{ N/m}$$

where:

- k is the stiffness in Newtons per meter (N/m)
- F is the force in Newtons (N), calculated as mass (kg) times gravity (9.81 m/s²)
- ΔL is the displacement in meters (m)

Additionally, the Young's modulus of the silicone muscle model was calculated. Utilizing the provided dimensions and experimental data, including the muscle length of 18.8 cm, an average cross-sectional area of approximately 402.14 mm², a displacement of 5.75 cm, and an applied force of approximately 49.05 N.

$$E = \frac{F \cdot L}{A_{gem} \cdot \Delta L} \approx \frac{49.05 \cdot 0.188}{402.14 \cdot 10^{-6} \cdot 0.0575} \approx 398.97 \text{ N/m}^2 \approx 0.4 \text{ kPa}$$

where:

- E is the Young's modulus in kilopascals (kPa),
- F is the force applied in Newtons (N),
- L is the original length of the muscle in meters (m),
- A is the cross-sectional area in square meters (m²),
- ΔL is the displacement in meters (m).

It can be inferred that the silicone muscle model exhibits a significant capacity to resist deformation when subjected to a 5 kg applied load, and upon removal of the weight, the muscle returns to its original state, indicating its ability to recover from external forces. Moreover, the Young's modulus, provides further insights into its mechanical behaviour.

2.2.5 Discussion

The results of this study demonstrate that the silicone muscle model effectively replicates certain mechanical properties of the biceps brachii muscle, suggesting its suitability for testing purposes. However, several important points should be considered in interpreting these findings.

One notable difference between the silicone muscle model and the actual biceps brachii muscle is their size. While the silicone model accurately mimics the general shape of the muscle, its dimensions are larger compared to the real muscle. This size disparity may affect how accurately the model replicates the behaviour of the biceps brachii under various loads.

Another aspect to consider is the difference in stiffness between the silicone muscle model and biological muscle. The stiffness value obtained for the silicone model in this study, approximately 853.04 N/m, indicates its significant resistance to deformation under an applied load of 5 kg. However, when comparing the Young's modulus of the silicone muscle model to values reported in literature for biological muscle stiffness (ranging from 8.1 to 19.7 kPa for different elbow positions), the measured stiffness of approximately 0.4 kPa falls outside this range, indicating that the silicone muscle model does not precisely mimic the stiffness properties of the biological biceps brachii muscle.

Furthermore, it's essential to acknowledge the limitations of the silicone muscle model in fully capturing the complex mechanical behaviour of biological muscles. Factors such as viscoelasticity, non-linear stress-strain relationships, and muscle fibre recruitment patterns contribute to the dynamic nature of muscle mechanics, which may not be entirely replicated by the silicone model. Additionally, variations in muscle architecture and composition further complicate direct comparisons between the model and the actual muscle.

Despite these discrepancies, the silicone muscle model holds value for testing purposes. Its ability to withstand external forces and return to its original state make it a useful tool for biomechanical studies and testing applications related to muscle behaviour and performance. By providing a simplified yet representative model of muscle mechanics, the silicone muscle model enables researchers to conduct experiments and investigations that would otherwise be challenging or impractical to perform on biological specimens.

In conclusion, the silicone muscle model exhibits significant stiffness characteristics and proves to be a valuable testing tool in biomechanical investigations. However, its results should be interpreted cautiously, considering its limitations in fully replicating the mechanical complexity of biological muscles. While the model demonstrates notable resistance to deformation and mimics certain aspects of muscle behaviour, such as returning to its original state after loading, it may not precisely replicate the stiffness profile and dynamic behaviour of actual muscles due to factors like viscoelasticity and non-linear stress-strain relationships.

2.3 Mechanical design

In order to manipulate the silicone muscle model for extension and contraction and to test the origami inspired sheets that are wrapped around the muscle, a mechanical design is essential.

The objective of this design is to create a system capable of accurately replicating the extension and contraction of the muscles, while simultaneously simulating arm movement for a comprehensive visual representation. In order to achieve this an antagonistic setup is made by emulating the dynamics of the triceps- and biceps brachii. Through this integration, the mechanical design enables the stretching of the muscle model and allows the sheets to induce the muscle model to contract. This enables comprehensive testing of the sheets' efficacy in deforming the muscle, providing valuable insights into their ability to induce muscle contraction.

2.3.1 Requirements

- The key requirements is that the design must incorporate an antagonistic system to effectively simulate the actions of both the biceps and triceps muscles, allowing for extension and contraction while emulating the natural movement of the arm. This involves a visual representation by creating an arm structure capable of angular displacement to replicate the motion observed during muscle contraction and extension.
- Additionally, the system must provide adequate support for the silicone biceps brachii muscle while allowing for controlled manipulation to induce extension and contraction. This requires designing frames or structures capable of securely holding the muscle and applying the necessary forces for movement.
- All components of the mechanical system should be durable and reliable to withstand repeated use over the course of experimentation, selecting materials and structures that can endure the forces applied during muscle manipulation without experiencing degradation or failure.
- Furthermore, the mechanical design should be compatible with the overall testing setup and experimental requirements, considering factors such as space constraints, integration with other, mechanical and electrical components, and ease of setup and operation.
- Overall, the mechanical design must have a balance between structural integrity and flexibility to ensure accurate simulation of muscle movement and to effectively support experimental objectives, contributing significantly to accurately test the origami inspired sheets.

2.3.2 Method

Support of the muscle model

To maintain the integrity of the silicone muscle model throughout the experimental process, careful measures were taken to provide adequate support while allowing for axial deformation. Ensuring a stable yet flexible setup was imperative to prevent unwanted distortion of the muscle and to facilitate accurate measurements.

The muscle needed to be securely held in place to prevent displacement during manipulation. Traditional fixation methods, such as screws or wires, were unsuitable for securing the muscle, as they risked damaging the silicone. Instead, custom 3D-printed caps were used, fitting the ends of the muscle (*Appx. A, fig. 70*). These caps were tightened with hose clamps, providing a secure grip without compromising the integrity of the silicone. To prevent the clamps from cutting the silicone, rubber pieces were placed beneath them.

The caps feature top-mounted holes designed for connecting them to the arm mechanism using Dyneema® wire. The choice of Dyneema® wire over conventional options like steel cable or nylon was based on its advantageous properties [31]. Dyneema® wire exhibits minimal elongation under load, ensuring it maintains its length and shape without significant stretching. This characteristic is crucial for precise muscle manipulation, preventing undesired slack or deformation in the wire and enabling accurate movements. Additionally, Dyneema® wire's flexibility allows it to conform to the contours of system components, enhancing adaptability within the mechanical setup. Its compatibility with adhesive bonding streamlines integration, enabling secure attachment without the need for additional fixtures or fasteners.

The wire was affixed to the arm mechanism via a pulley for smooth transitions between muscle contraction and extension (*Fig. 11*).

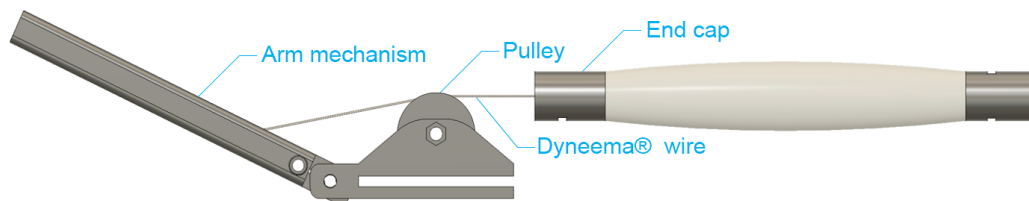


Figure 11: Biceps brachii muscle model with end cap, Dyneema® wire, pulley and arm mechanism

All components, including the caps and arm mechanism, were 3D-printed from PLA material, allowing for custom designs with precise dimensions.

Additionally, a pulley system was employed to relocate force displacement from beneath the muscle, providing space for the arm mechanism. These pulleys, connected by Dyneema® wire, ensure efficient force transmission and minimize frictional losses. The first pulley, integrated into the arm, rotates synchronously with it. The second pulley, positioned below, ensures force displacement operates in the opposite direction of the biceps brachii muscle, leveraging the tension of the spring below (*Fig. 12*) (*Appx. A, fig. 73*).

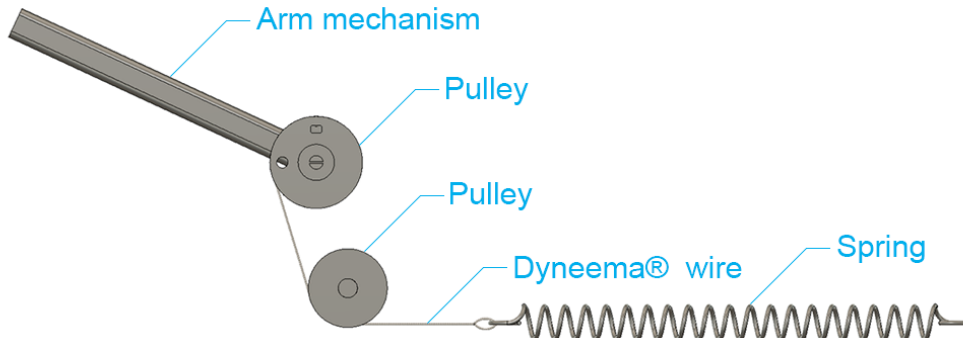
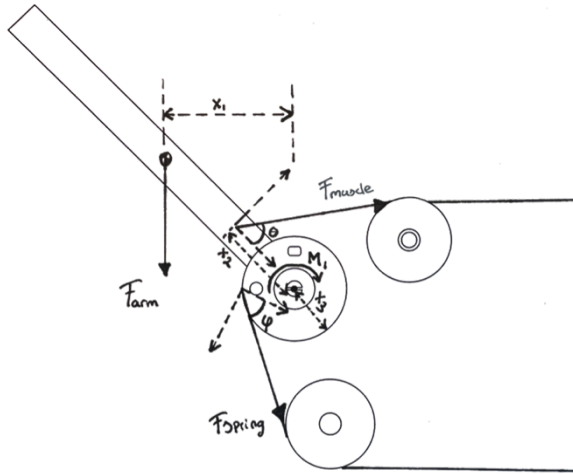


Figure 12: Arm mechanism with the pulley system, Dyneema cable® and spring

Antagonistic system

In order to create an antagonistic system mimicking the actions of the biceps and triceps muscles, careful consideration was given to muscle stretching and compression. A spring mechanism was selected for this purpose due to its ability to stretch and return to its original state, analogous to the function of the biceps muscle. The stiffness of the biceps brachii, measured at 853.04 N/m, informed the choice of a spring with a minimum stiffness to ensure effective muscle stretching.

To identify a spring with adequate capacity to stretch the muscle, it is imperative to analyse the forces applied to the test setup (Fig. 13).



$$M = F_{muscle} \cdot \sin(\theta) \cdot x_2 - F_{spring} \cdot \sin(\varphi) \cdot x_3 - F_{arm} \cdot x_1 = 0$$

$$F_{spring} = \frac{F_{muscle} \cdot \sin(\theta) \cdot x_2 - F_{arm} \cdot x_1}{\sin(\varphi) \cdot x_3}$$

$$\begin{aligned} x_1 &= 0.076 \text{ m} \\ x_2 &= 0.038 \text{ m} \\ x_3 &= 0.018 \text{ m} \\ \theta &= 21.8^\circ \\ \varphi &= 72.1^\circ \\ F_{muscle} &= 38.4 \text{ N} \\ F_{arm} &= 0.3 \text{ N} \end{aligned}$$

$$F_{spring} = \frac{38.4 \cdot \sin(21.8^\circ) \cdot 0.038 - 0.3 \cdot 0.076}{\sin(72.1^\circ) \cdot 0.018}$$

$$F_{spring} \approx 30.36 \text{ N}$$

Figure 13: Free body diagram, test setup

These calculations reveal that the spring must deliver a minimum force of 30.36 N.

Considering the selection criteria for the spring, which permits a maximum length of 230 mm, a spring initially measured at a length of 65 mm must meet a specific spring constant (i.e. its stiffness).

To quantify the stiffness of the spring, Hooke's Law was applied:

$$k = \frac{F}{\Delta L} = \frac{30.36}{0.230 - 0.065} \approx 184 \text{ N/m}$$

where:

- k is the stiffness in Newtons per meter (N/m)
- F is the force in Newtons (N), calculated as mass (kg) times gravity (9.81 m/s^2)
- ΔL is the displacement in meters (m)

Considering the selection criteria, the spring must have a minimum spring constant of 184 N/m.

Subsequently, testing of the spring confirms a spring constant of 384.11 N/m and an extension of 0.113 meters, resulting in a force of 43.4 N.

This force significantly exceeds the required 30.36 N necessary to stretch the muscle. Therefore, it has been demonstrated to be sufficient for muscle stretching, confirming that it meets the requirements for the muscle model.

Frame

To support all of these components, a frame made out of PETG (Polyethylene Terephthalate Glycol) was implemented. PETG, selected for its flexibility and adaptability, has desired features like as easy deformability and precise moulding capabilities.

During fabrication, the PETG material is shaped using a heat wire technique for precise moulding. The heat wire, typically heated to a specific temperature, is used to soften the PETG material at precise points or along specific lines. This controlled heating process enables the material to become pliable without compromising its structural integrity.

Once heated, the softened PETG can be manipulated into exact shapes and forms required for the frame construction. This method ensures that complex geometries and intricate details can be achieved with accuracy.

Additionally, a CNC milling machine is employed to integrate precise holes and shapes into the PETG frame. This technology guarantees the exact positioning and alignment of components within the frame structure (*Appx. A, fig. 69*).

2.3.3 Results

The culmination of the design resulted in a mechanical system that effectively emulates the antagonistic system of the biceps and triceps brachii while simulating natural arm movement.

The integration of the silicone muscle model with custom-designed caps and hose clamps ensured secure fixation and controlled manipulation without compromising the integrity of the silicone material. The implementation of rubber pieces beneath the hose clamps significantly improved the integrity of the silicone muscle model. Initial tests with pipe clamps resulted in unintended incisions, compromising both the model and the accuracy of the experiment.

The utilization of Dyneema® wire, with its minimal elongation and flexibility, enabled smooth transitions between muscle contraction and extension, enhancing the accuracy of movements. The incorporation of a spring mechanism, tailored to match the stiffness of the biceps brachii, provided effective stretching and compression, closely mimicking muscle behaviour.

The pulley system efficiently transmitted forces, ensuring synchronized movement of the arm mechanism while minimizing frictional losses. Integration of potentiometers enabled real-time monitoring of movement, contributing to precise control and data collection.

The implementation of three separate PETG frames, in contrast to the initial PETG single-piece frame, yielded significant improvements in the stability and adjustability of the experimental setup. Through the implementation of these separate frames, the system's ability to withstand forces generated during operation was significantly improved, ensuring reliable functionality and reinforcing the adaptability of the mechanical design. Furthermore, the use of a CNC milling machine ensured precise positioning and alignment of other components within each frame, contributing to improved functionality and performance.

In summary, the results demonstrate the successful implementation of a comprehensive mechanical system capable of accurately replicating muscle actions and arm movement, laying a solid foundation for biomechanical studies and testing applications in muscle behaviour and performance evaluation.

2.3.4 Discussion

The development and implementation of the mechanical system showed positive results. The silicone muscle model, arm mechanism, caps, Dyneema® wire and spring can be successfully integrated, making an antagonistic setup mimicking the contraction and elongation of the triceps- and biceps brachii.

The integration of the silicone muscle model with custom caps and hose clamps prevents potential damage to the silicone material while ensuring attachment, this approach bolsters the system's reliability and longevity. However, exploring alternative fixation methods could enhance the emulation of tendon connections observed in biological systems, thus improving the realism of muscle behaviour replication.

The spring mechanism chosen for muscle stretching, with a stiffness of 384.11 N/m and an extension force of 43.4 N, meets the minimum force requirement of 30.36 N for effective muscle stretching. This approach ensures the system's capability to simulate muscle elongation accurately, yet it may not fully capture the dynamic complexities observed in living muscles. Future iterations could explore advanced actuation methods or materials with superior biomechanical properties to enhance fidelity to biological muscle behaviour.

The selection of PETG material for the frame signifies a meticulous balance between structural integrity and adaptability, addressing the requisite durability while accommodating customization and precise moulding. This holistic design approach factors in both mechanical requisites and practical considerations such as fabrication ease and seamless integration with other components. However, considering alternative materials with improved biomechanical properties could enhance the system's performance and longevity.

Certain aspects emerge that do not entirely mirror the intricacies of real-world musculoskeletal structures and dynamics. Specifically, the endpoints (caps) of the muscle and the connection to the arm mechanism via Dyneema® wire do not emulate a true tendon connection as observed in biological systems. In reality, tendons play a crucial role in transmitting forces from muscles to bones, providing stability, and enabling precise control of movement. The current design does not address these aspects nor provide data on how closely it mimics tendon behaviour.

Similarly, while the arm mechanism effectively demonstrates muscle contraction and extension, it lacks the size and complexity of a real human arm. Biological arms are intricately structured with multiple muscles, tendons, and ligaments working in synergy to produce varied and nuanced movements. In contrast, the mechanical setup simplifies these complexities for experimental purposes, focusing on basic replication rather than full anatomical fidelity.

To advance the design's capability in biomechanical studies, future iterations could explore methods to better emulate tendon connections and integrate more anatomically accurate arm structures. This enhancement would contribute to a more comprehensive understanding of muscle dynamics and their applications in both research and practical fields.

2.4 Electrical design

To effectively assess the performance of the origami-inspired sheet, integrating electrical components into the testing setup is crucial. Real-time data from these components provides valuable insights into the sheet's behaviour, enabling a better evaluation.

2.4.1 Requirements

In the integration of electronics into the testing setup, various aspects need to be considered to adequately evaluate the different sheets ultimately wrapped around the muscle. It is essential to determine which aspects of the sheets need to be tested to achieve the desired results.

- Given the integration of various structures into the sheets, understanding the exerted force is crucial. Therefore the system must accurately assess and test the exerted force on the sheets to ensure the effectiveness of the testing process.
- Additionally, the setup should include sensors to measure the arm's angle rotation. These measurements are essential for visually representing the effect of the sheet that is placed around the muscle. When combined with force data, they provide a comprehensive understanding of the interaction between the sheets and the system.
- Measuring the pressure and assessing a set pressure within the sheets is crucial for understanding their behaviour under pneumatic deformation and ensuring consistency across multiple tests. Therefore, the system must include a sensor capable of measuring this pressure and a mechanism to maintain a set pressure.

By maintaining consistent set pressure values, accurate comparisons between different sheet structures can be made ensuring consistency across multiple tests. Assessing a set pressure allows for precise monitoring of how each sheet responds determining their contraction force. These measurements should also be clearly displayed for thorough analysis over time.

- The system must provide clear visual representation of pressure, rotation, and force data to effectively assess the performance of the sheets and their interactions with the muscle model.
- Finally, all components must be calibrated to ensure accurate measurements and reliable testing outcomes. Adhering to these requirements will enable the testing setup to effectively evaluate the sheets' performance, ensuring reliable and consistent results across all tests.

By adhering to these requirements, the testing setup will be able to effectively evaluate the sheets' performance, ensuring reliable and consistent results across all tests.

2.4.2 Method

Measuring the force

Since the different structures influence the dynamics of the sheets, it is essential to measure these parameters accurately. Therefore, incorporating a force sensor becomes crucial in assessing the impact on the system and drawing conclusions regarding the different shapes and methods applied. Hence, a load cell is positioned at the beginning of the biceps brachii muscle.

To validate the load cell's performance, a defined weight of 500 grams was placed. This initial stage allowed the establishment of a reference point for future testing procedures. To study the load cell's behaviour under prolonged loading conditions, a steady weight was applied for 10 minutes. Additionally, the load cell was subjected to a repetitive loading and unloading cycle with an interval of 20 seconds to ascertain the repeatability of its measurements under varying conditions. Analysing the data from these tests provided insights into the load cell's long-term durability and performance consistency. In addition, another test was performed of continuous loading to evaluate the load cell's reaction after 5 minutes. This intermediate evaluation revealed information about any potential changes or drifts in the load cell's values across shorter time intervals, providing insights into its dynamic behaviour and response characteristics.

Measuring the angle

To measure the arm's angle rotation, a potentiometer is installed on the central pulley. By combining data from the force sensor and the potentiometer, it is possible to correlate the applied forces with the resulting movement.

In order to validate the values of the potentiometer were recorded when the arm mechanism was subjected to a 90-degree angle.

Measuring and controlling the pressure

in order to evaluate different pressure values and to establish a consistent pressure, a pressure sensor and a pneumatic pump were utilized.

Extraction, visualisation and calibration

To extract the data signals from the load cell, potentiometer and pressure pump these components are respectively connected to an Arduino Uno board, with the load cell being amplified for signal processing. The electrical schematic can be found in the appendix ([Appx. B, fig. 75](#)).

To convert and visualize the data from the load cell, potentiometer and pressure pump, MATLAB is utilized ([Appx. C, fig. 76-79](#)). Within the program the load cell and potentiometer are calibrated by correlating them with known reference values. This calibration process enables the translation of raw measurements into accurate physical units, ensuring precise data interpretation. Once calibrated, the acquired values are extracted and graphically represented to display the load and angle variations over time.

2.4.3 Results

During the experimental testing phase, observations were made regarding the behaviour of the load cell, potentiometer and pressure pump measurements.

Loadcell

A notable phenomenon observed in the load cell measurements (Fig. 14) was an initial upward movement upon the application of a constant weight. Despite prior calibration, this initial response can be attributed to the inherent characteristics of the load cell. Load cells often exhibit an adjustment period when subjected to sudden changes in load, during which they recalibrate and stabilize to the new load condition.

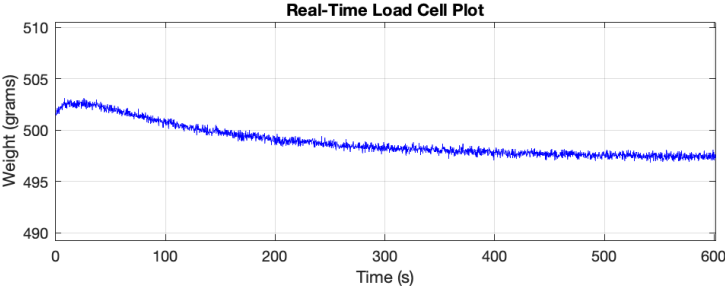


Figure 14: Real-Time plot of the loadcell with a reference value of 500 grams.

Subsequently, a gradual decline in the load cell readings was noted over time. This downward trend in the load cell measurements is indicative of a phenomenon known as "drift," where the measured values deviate from the true load. The observed decrease in load cell readings may be primarily attributed to warmup drift [32]. Warmup drift occurs when the load cell undergoes changes in its mechanical properties as the temperature increases. These changes affect the load cell's sensitivity and calibration, leading to lower readings over time. As the temperature stabilizes, the drift diminishes, resulting in a stabilized reading. After approximately 500 seconds, the line stabilizes around -2 grams of the placed weight. Additionally, noise is present in the signal, with peaks of roughly +1.6/-1.6 grammes.

Results from repeated placement and removal of the weight reveal minimal deviations apart from the previously described drift (Fig. 15). The weight decreases to zero when removed and returns to 500 grams when replaced. At certain points, the graph exhibits spikes, which can be attributed to the manual placement of the weight and the additional impact it introduces.

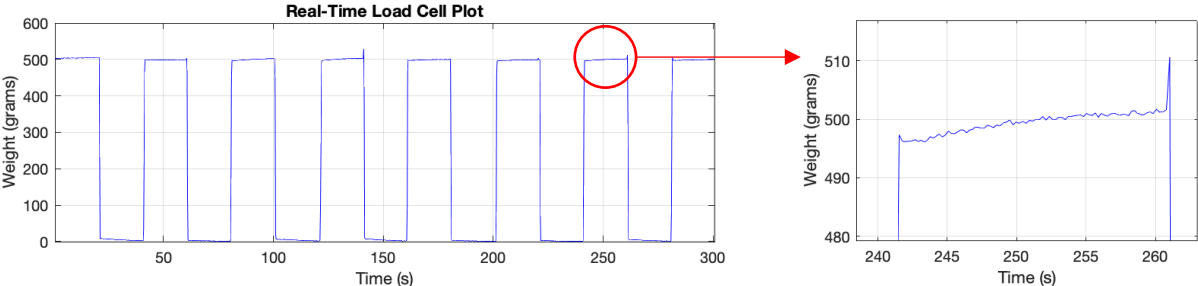


Figure 15: (a) Real-Time plot of the loadcell's placement and removal, (b) zoom-in plot on one of the peaks

Similar behaviour is observed over time (5 minutes), indicating the load cell's capability to accurately determine the weight during repeated placement and removal (Fig. 16).

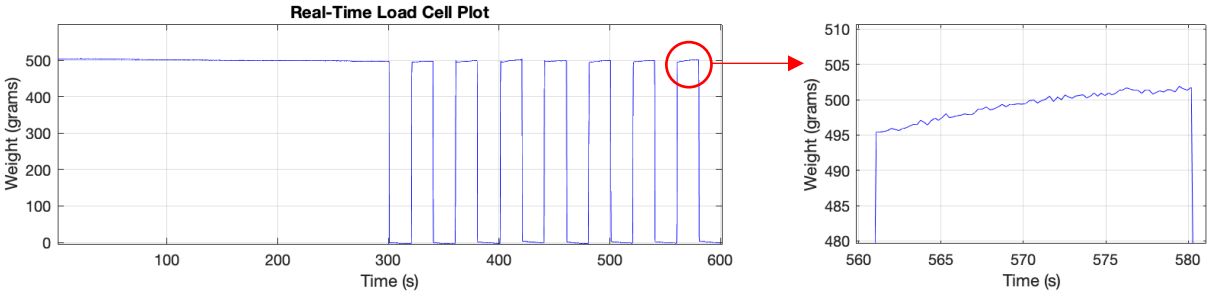


Figure 16: (a) Repeated placement and removal after 300s, (b) zoom-in plot on one of the peaks

Potentiometer

In parallel with load cell measurements, observations were made regarding the potentiometer readings (Fig. 17). The potentiometer consistently registered peaks at approximately +0.26/-0.26 and maintained a fluctuation around the 90-degree mark. This behaviour can be attributed to the inherent characteristics of the potentiometer itself and potential environmental factors. The peaks in the potentiometer readings may correspond to specific points in the potentiometer's range of motion or variations in its sensitivity, causing intermittent spikes in the readings.

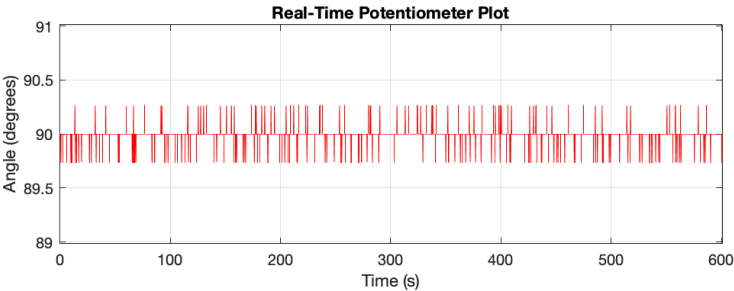


Figure 17: Real-Time plot of the Potentiometer with a reference value of 90 degrees

Pressure sensor and pump

the performance of the pressure sensor was assessed by subjecting it to a constant load of 2 bar pressure. The initial measurement revealed an average pressure reading of approximately 0.8 bar (Fig. 18), which did not align with the expected value of 2 bar. This discrepancy can be attributed to the assumption that 1 volt corresponds to 1 bar pressure. However, due to the voltage conversion process involving resistors and an Arduino board, the 1:1 correspondence was no longer valid. To address this, a conversion ratio of 2.5 times the output value was implemented in the program. Subsequent measurements, following this adjustment, showed average pressure readings that closely matched the expected 2 bar value.

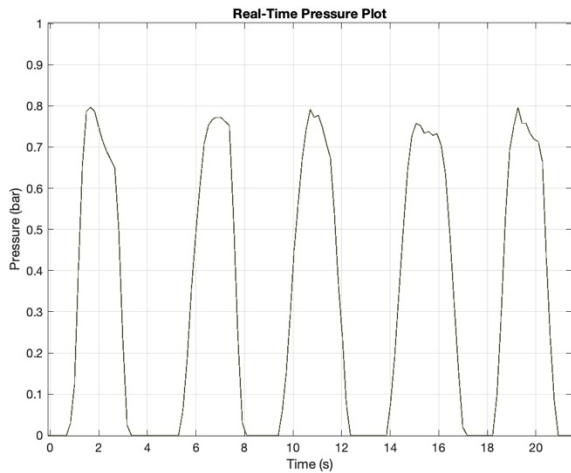


Figure 18: Real-Time plot of the Pressure sensor measuring approximately 0.8 bar

The results obtained from the pneumatic pump indicated a consistent and precise measurement of the applied pressure throughout the testing process, with maximum values ranging from approx. 1.69 to 1.72 with a mean of approx. 1.70 (Fig. 19). This demonstrates the reliability and accuracy of the pressure sensor in capturing variations in pressure levels. The narrow range of values suggests minimal fluctuations in the applied pressure, contributing to the stability of the setup up. Overall, these findings affirm the effectiveness of the pressure monitoring system in maintaining a constant and controlled pressure.

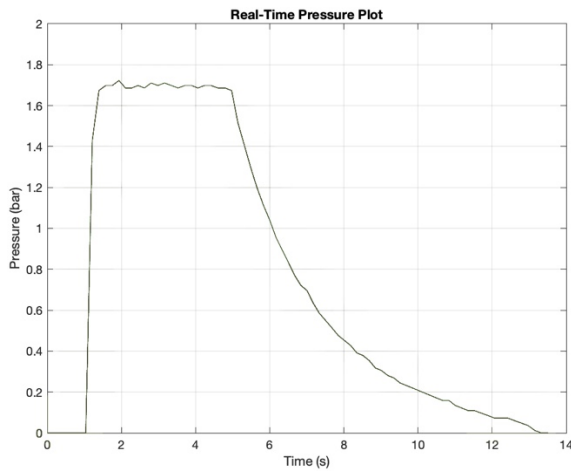


Figure 19: Real-Time plot of the pneumatic pump

In summary, the deviations observed in the load cell readings are primarily attributed to warm-up drift, which stabilizes at approximately 2 grams deviation from the target weight after about 500 seconds. Repeated placement and removal of the weight do not introduce additional errors in the test results. The potentiometer consistently indicates its angle, with peaks of +0.26 and -0.26 degrees. Additionally, the pressure sensor displays stable and accurate measurements throughout the testing process, with minimal fluctuations in the applied pressure, typically within a range of 0.05 to 0.1 bar.

2.4.4 Discussion

Loadcell

A load cell was used to measure the force applied to the system. To ensure the reliability and accuracy of the measurements, the load cell was calibrated and tested using known reference values. Graphical representations of the acquired data were generated to visualize weight variations over time. The load cell exhibited promising results, with the calibrated weight reflecting the chosen weight accurately. However, it's imperative to acknowledge the inherent limitations and sources of error associated with the measurements. One key observation was the presence of drift in the load cell readings, a phenomenon where the measured values deviate from the true load over time. This transient deviation introduces variations in data interpretation, emphasizing the need to conduct measurements after 500 seconds to allow for the stabilization of drift and minimize its influence on the results. Additionally, regular calibration checks of the load cell are recommended to ensure measurement accuracy and reliability. Considering the deviations caused by both drift and noise, it's prudent to establish a margin of approximately 2 grams. This margin was chosen based on the observation that even after the line stabilized, there was still a deviation of approximately 2 grams from the target weight.

Potentiometer

Potentiometers were used to measure the angle rotation of the system. A clear trend line in the angle rotation measurements was observed, indicating its stability and reliability. However, there were occasional short spikes in the readings, which could be further addressed by applying a low pass filter. The potentiometer was calibrated and tested with known reference values, and graphical representations of the acquired data were generated to visualize angle variations over time.

Pressure sensor and pump

A pressure sensor and pump were used to measure and maintain the applied pressure within the system, respectively.

Measuring the pressure and assessing a set pressure within the sheets is crucial for understanding their behaviour under pneumatic deformation and ensuring consistency across multiple tests. The pressure sensor ensured accurate monitoring of the applied pressure, while the pressure pump maintained a consistent pressure output throughout the testing process. Therefore, a pressure sensor must be implemented to accurately measure the pressure, and a pressure pump must be applied to establish and maintain a set pressure. This combination of instrumentation facilitated precise and reliable data collection, enabling thorough analysis of the sheet's response to pneumatic deformation.

The pressure sensor displayed stable and accurate measurements throughout the testing process, with minimal fluctuations in the applied pressure, typically within a range of 0.05 to 0.1 bar. Additionally, the pressure pump maintained a consistent pressure output, ensuring uniform conditions for testing the origami-inspired sheet's response to pneumatic deformation.

2.5 Conclusion

In conclusion, the integration of the biceps brachii muscle model within the test setup, incorporating both mechanical and electronic components, has resulted in a comprehensive framework for evaluating the performance of origami-inspired sheets. This study demonstrates that the silicone muscle model effectively replicates certain mechanical properties of the biceps brachii muscle, albeit with notable differences in size and stiffness when compared to biological muscles. Despite these disparities, the silicone muscle model proves valuable for biomechanical investigations, offering researchers a practical tool for studying muscle behaviour and performance.

Furthermore, the development and implementation of the mechanical system represent significant progress in biomechanical research, enabling more accurate simulations of muscle behaviour and arm movement. While the system showcases a nuanced understanding of biomechanical principles through its design and functionality, certain aspects, such as the emulation of tendon connections and the complexity of arm mechanics, warrant further refinement to better mirror real-world musculoskeletal dynamics.

Additionally, the utilization of load cells, potentiometers, pressure sensors, and pumps for real-time measurement of force, angle rotation, and pressure provides crucial insights into the behaviour of the test setup. Despite challenges such as drift, appropriate calibration enhance the reliability and accuracy of the measurements, thereby facilitating a more thorough understanding of the test setup's performance.

Combining those three aspects resulted in a test setup, capable of comprehensively evaluating the performance of origami-inspired sheets (Fig. 20).

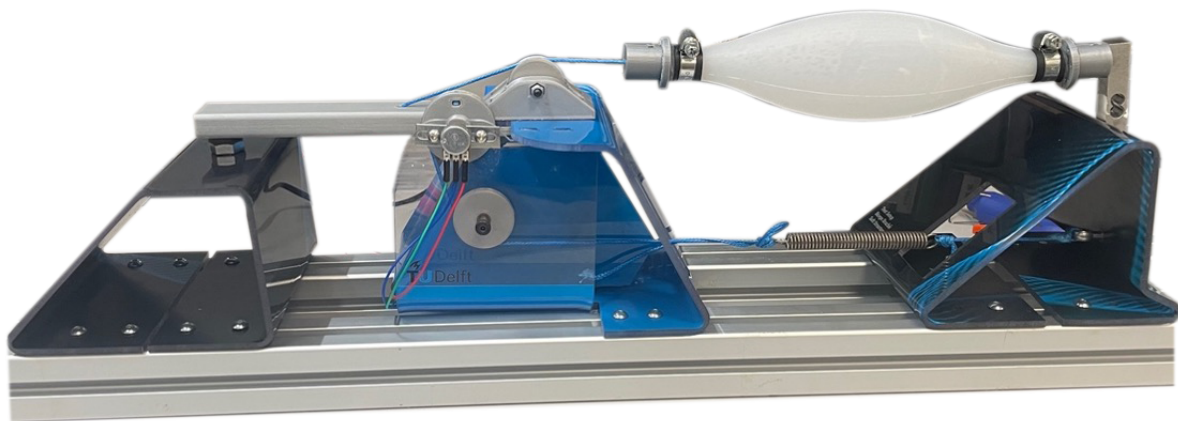


Figure 20: End result mechanical design

While it provides valuable insights into the potential effects on a biological muscle in terms of force and displacement, it's essential to acknowledge its current limitations. Despite its utility in mimicking certain aspects of muscle behaviour, the model may not fully replicate the complete range of complexities inherent in real biological systems.

Chapter 3

Exploration of the materials for the origami-inspired structured sheets.

Jeroen van de Kamp

This chapter entails an exploration of the most suitable materials for conforming to the contours of the muscle model and for designing different patterns. It begins with an overview of material selection, emphasizing their biocompatibility and flexibility for wrapping around the muscle model. The chapter then delves into the effects of temperature on material bonding, as well as the formation of patterns, and their responses to pneumatic pressure.

3.1 Introduction

Origami, an ancient Japanese art form, has gradually transcended its cultural roots, inspiring creativity and innovation throughout the world. It’s fascinating folds and complex patterns have captured imaginations for a long time, serving as a canvas for both creative expression and problem solutions. Where traditional paper is used in origami, for the origami-inspired structured sheet, various plastic layers can be used.

3.2 Materials

Specifically in this study, PVC-film (Polyvinyl chloride), TPU-film (Thermoplastic polyurethane), PET-film (Polyethylene terephthalate), and Nylon were chosen based on their availability and their prior use in the design of fluid-driven origami-inspired artificial muscles, as detailed in the publication by Li et al. [33]. These materials offer unique properties that make them suitable for the structured sheet intended (Table 1):

Material	Type	Advantages
PVC-film	Thermoplastic Polymer	Low cost, ease of processing
TPU-film	Thermoplastic Elastomer	High flexibility, high durability
PET-film	Thermoplastic Polymer	High tensile strength, high durability, resistance to stretching and shrinking
Nylon	Synthetic Polymer	High strength, high abrasion resistance, low friction properties

Table 1: Selected Materials, their types, and advantages

The thickness of the materials that was found in the literature [33] guided the selection process of the materials. Each of these materials, along with their, thickness and mass density are summarized below (Table 2):

Material	Literature Thickness (mm)	Selected Thickness (mm)	Mass density (g/cm ³)
PVC-film	~0.102	0.15	~1.343
TPU-film	0.04 - 0.24	0.2	~1.01
PET-film	~0.038	0.125	~1.3
Nylon	0.26 - 0.34	0.1	~0.857

Table 2: Material thickness based on literature [33], thickness and mass density of the selected materials

Although the chosen thicknesses may occasionally fall outside the ranges reported in the literature [33], the differences are minor. This selection process prioritizes practical considerations, particularly material availability.

These materials are tested to determine their effectiveness for inflatable structured sheets capable of wrapping around muscles. By evaluating their properties and performance, the aim is to identify the most suitable material for achieving optimal functionality in the design of the origami-inspired structured sheets.

3.2.1 Requirements

In order to create effective sheet that can be wrapped around the muscle, certain requirements must be met by the selected materials.

- Considering the future potential of origami-inspired artificial sheets to be wrapped around muscle tissue *in vitro*, it is crucial that these materials are suitable for implantation within the body without causing rejection.
- Flexibility is crucial, as the material needs to conform to the contours of the muscle it will encase, allowing for proper placement and movement. Considering the typical diameter of the biceps brachii muscle (approximately 3 cm), the sheet should wrap around it, ensuring that the bending radius is at least 180 degrees.
- The material's response to heat is significant, especially considering the structures that will be formed within it through heat bonding. Ease of patterning is also a key requirement. The material should allow for the creation of solderable patterns and the optimal temperature for this process needs to be identified to ensure proper bonding and functionality.
- The adhesive properties of the materials are critical. Strong adhesion is necessary to withstand the forces exerted during pneumatic deformation. Assessing how well the materials bond together is essential for determining their strength and durability.
- The ability of the material to deform pneumatically is essential for generating muscle contraction, mimicking natural muscle movements. The material's response to air pressure is evaluated to assess its flexibility in accommodating deformation.

3.2.2 Method

Biocompatibility

Ensuring biocompatibility is a crucial step for the materials intended to be wrapped around muscles to induce contraction. This includes assessing the material's cytotoxicity, which measures cell death or viability before and after exposure to the material. To evaluate this, existing literature on the cytotoxicity of the materials is reviewed.

Flexibility

To assess the flexibility of the materials, sheets measuring 30 cm by 20 cm were wrapped around a rod with a diameter of 30 mm, which is comparable to that of the biological biceps brachii muscle. The material was observed for its ability to conform to the shape of the rod and the bending angle was measured (Fig. 21). If the angle was less than 180 degrees, indicating that the sheet does not bend fully around the rod, it suggests that the sheet is not flexible enough to conform to the contours of the biceps brachii muscle.

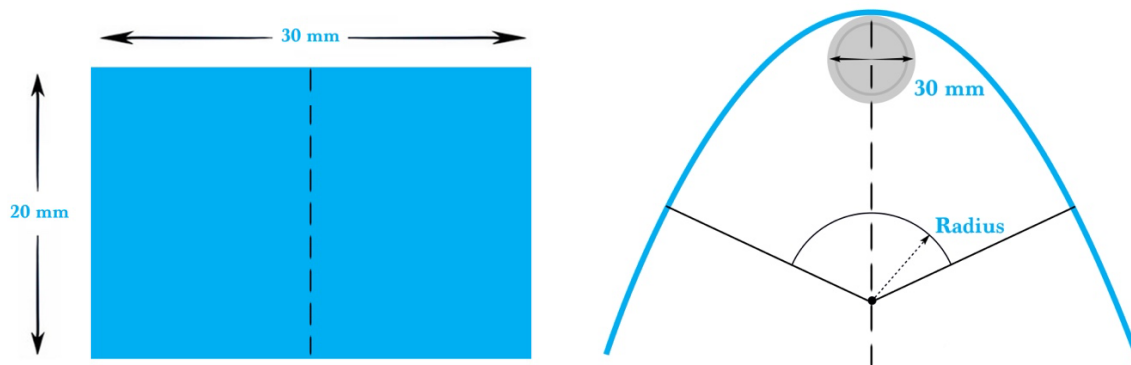


Figure 21: (a) dimensions of the sheets during the flexibility tests, (b) conceptual drawing of the flexibility tests

Temperature

To evaluate how the sheets responds to different temperatures and at what temperature two sheets bond together, a test was conducted where two sheets were overlapped and a line was drawn at a pace of 1 cm/s with a soldering iron to simulate the heat bonding process. The temperature was then gradually increased to observe the response of the sheets to different temperatures. This method was validated by comparing the bonding strength of the sheets at different temperature levels. Additionally, zigzag patterns were applied to the sheets at each temperature to assess the ease of creating patterns on the sheets. This process was validated by examining the clarity and consistency of the patterns created at different temperature settings.

To assess the material's sensitivity and corresponding temperature, a test was conducted to measure the time it took for a soldering iron to penetrate through the material (Fig. 22). This test provides insights into how quickly the soldering iron should move and the material's response to heat, aiding in determining optimal temperature.

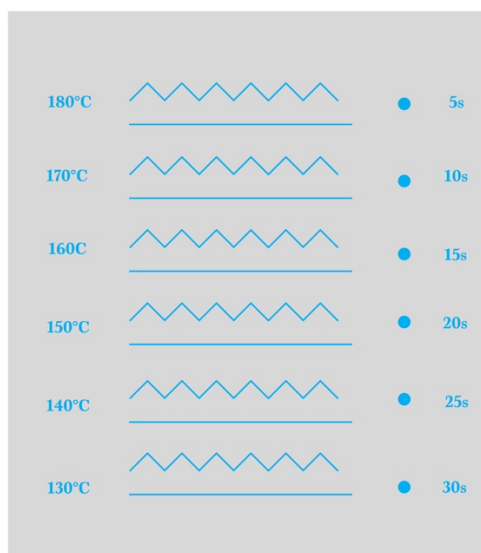


Figure 22: Conceptual drawing to test the material response to temperature, including patterns and heat sensitivity

Adhesion

In order to evaluate the sheets' adhesion and its ability to withstand the forces exerted during pneumatic deformation two sheets were heat bonded together at the optimal temperature determined from previous tests. first, a observational test was conducted to observe how the sheets respond to inflation with air and whether they are flexible enough to deform under pneumatic pressure.

Subsequently, a controlled amount of air pressure will be applied to the sheets using the pressure sensor to measure the pressure in bars. The sheets will be gradually subjected to increasing levels of air pressure until they reach their breaking point, at which the maximum pressure they can withstand will be recorded. This test will provide valuable insights into the sheets' ability to withstand pneumatic forces and their overall durability under pressure.

3.2.3 Results

Biocompatibility

Ensuring biocompatibility involves assessing cytotoxicity which measures cell death or viability before and after exposure to a material. [34], Cytotoxicity tests are essential as they evaluate the potential of the material to cause cell damage, thereby ensuring that the materials are safe when in contact with human tissues.

- Polyvinylchloride (PVC), plays a pivotal role in the medical plastics industry due to its exceptional properties and versatility. According to Zhao et al. [35] PVC is an excellent biocompatible material, citing its low toxicity and chemical stability. Zhao et al. provide in vitro evidence supporting the biocompatibility of PVC in their study.
- Thermoplastic Polyurethane (TPU) is a versatile polymer that finds extensive use in various industries, including medical applications. For example they are used for vascular grafts [36]. This material highly versatile synthetic polymer widely used in medical applications due to its structural adaptability and excellent mechanical properties. According to Butnaru et al. [37], TPU shows significant biocompatibility, primarily assessed through in vitro cytotoxicity evaluations.
- Polyethylene terephthalate (PET), is widely used in medical applications, for instance, in vascular grafts [38]. According to recent studies [39], PET demonstrates good biocompatibility, maintaining high cell viability rates in vitro, consistently above 70%, affirming its low toxicity under the conditions tested. Despite its good chemical resistance, PET can degrade when exposed to high temperatures or prolonged sunlight, which can lead to the release of small amounts of chemicals.
- Nylon, a versatile thermoplastic material, used in various forms such as fibers, moulded plastic, and flexible tubing. According to research, nylon exhibits excellent biocompatibility, attributed to the presence of amide groups in its chemical structure. These amide groups mimic natural peptides, which helps in preventing a foreign body response from the immune system. Notably, nylon 6 and nylon 66 are widely used for permanent sutures due to their stable interaction with tissues [40].

Flexibility

The results of the flexibility test (Fig. 23), shows that the PET-film does not wrap well around the axis due to its stiffness. This material exhibited a bending radius of 115° rendering it unsuitable for wrapping around the biceps brachii. Conversely, PVC, nylon, and TPU sheets exhibit sufficient flexibility to wrap around the axis smoothly and securely. These materials achieved a bending radius of 180° , indicating their ability to conform the contours of the bicep brachii muscle.



Figure 23: Flexibility test, left to right, top to bottom: (a) PVC-film, TPU-film, PET-film and Nylon

Temperature

In order to find the optimal bonding temperatures for the materials, a series of tests were conducted using varying temperature ranges for each material. (Fig. 24).

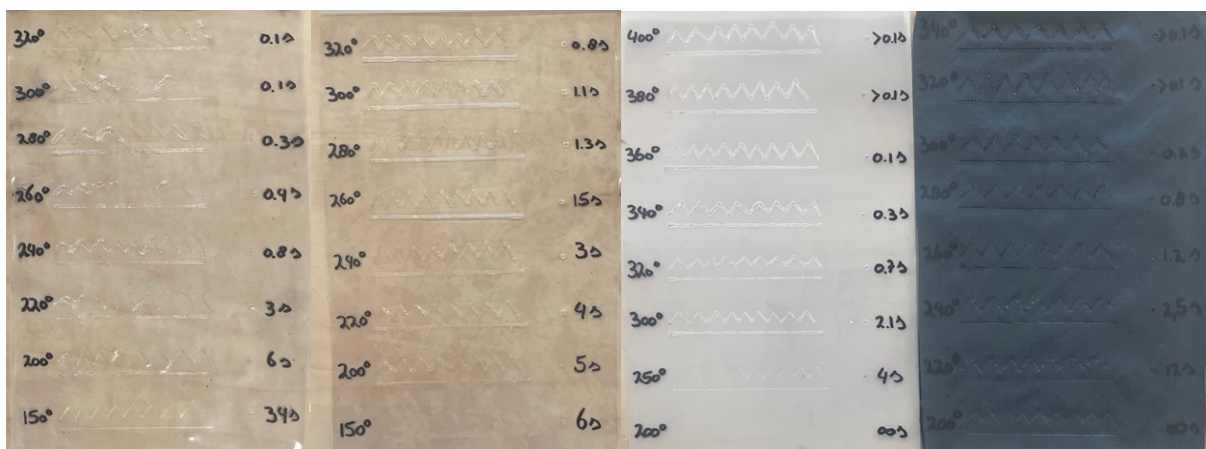


Figure 24: Temperature test. (a) PVC-film, (b) TPU-film, (c) PET-film, (d) Nylon

During these tests, a good result was defined as a temperature range that ensures adequate bonding and smooth lines without cutting into the material. The findings of these tests are summarized in a table (Table 3) highlighting the optimal temperature ranges for each material and the corresponding times to penetrate through the material.

Material	Best Temperature Range (°C)	Penetration Time (at optimal range)
PVC-film	230 - 260	3.5s - <1.5s (≈)
TPU-film	220 - 275	3s - <0.35s (≈)
PET-film	340 - 370	0.3s - <0.1s (≈)
Nylon	275 - 300	1s - <0.2s (≈)

Table 3: Optimal temperature ranges and penetration times

The PVC-film shows that within the optimal temperature range, the bonding is adequate, and the material remains intact. Structures formed within this range exhibit the most consistency, with smooth patterns and without significant deviations.

TPU-film exhibits a wider effective temperature range, and the soldering iron does not penetrate the TPU-film as quickly compared to other materials. Structures formed within this range display smooth zigzag patterns, making TPU a preferable option for this application.

The PET-film, being somewhat stiffer, requires higher temperatures and necessitates careful handling due to the tendency to penetrate through the material quickly.

Nylon requires swift movements to avoid penetration into the material. The patterns formed within the optimal temperature range show smooth results.

Deformation

During the observational test, the response of the bonded sheets to air inflation and their flexibility under pneumatic pressure were evaluated (Fig. 25). The test results reveal that only the polyester film exhibits minimal deformation in response to pneumatic pressure. This is primarily attributed to the relatively rigid nature of the material, which renders it less flexible and resistant to deformation. In contrast, the other materials demonstrate deformation patterns consistent with expectations under pneumatic pressure.

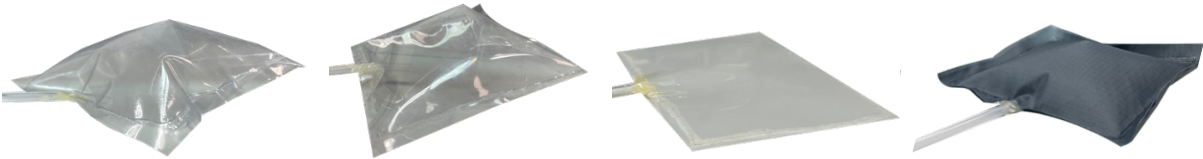


Figure 25: Inflation test, left to right, top to bottom: (a) PVC-film, (b) TPU-film, (c) PET-film, (d) Nylon

Adhesion

In order to determine how much pressure the sheets can withstand and to evaluate the adhesion strength, pneumatic pressure resistance tests were conducted (Fig. 26). These tests revealed notable differences in the materials' capacity to withstand pneumatic forces. The average temperature from the optimal ranges identified in the previous test was used for these evaluations.

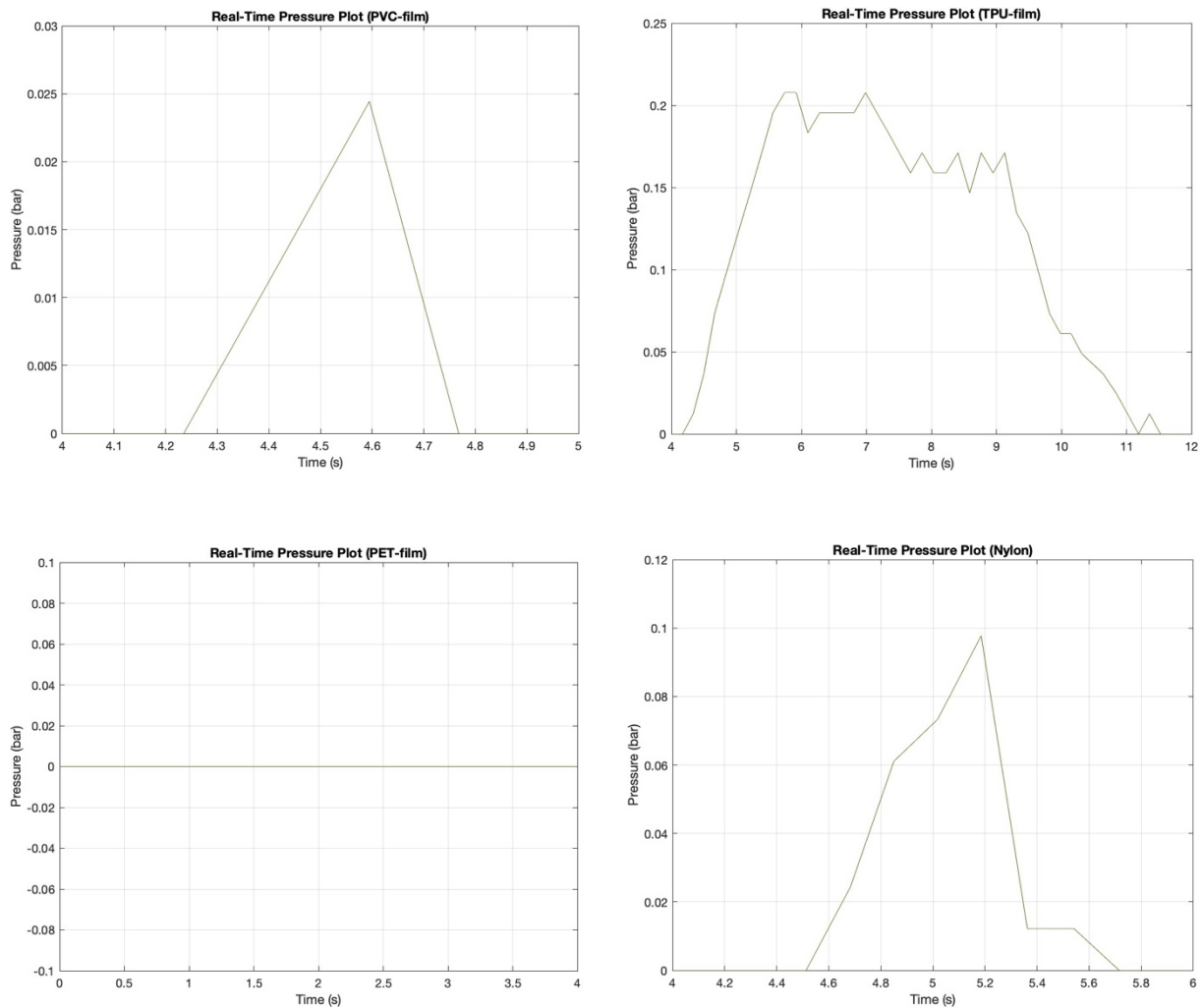


Figure 26: Pressure tests, left to right, top to bottom: (a) PVC-film, (b) TPU-film, (c) PET-film, (d) Nylon

PVC film exhibited the lowest pressure resistance, reaching a breaking point at 0.024 bar before adhesion failure. In contrast, TPU exhibited the highest pressure resistance, successfully enduring pressures up to 0.21 bar before rupturing. PET film, however, showed no measurable pressure values and immediately reached a breaking point. This is due to the rigid structure of PET material, which prevents deformation under air pressure. Nylon demonstrated slightly higher resistance, withstanding a maximum pressure of 0.10 bar before rupturing.

3.2.4 Conclusion

The materials chosen for this study PVC-film, TPU-film, PET-film and Nylon, offer distinct properties that contribute to their suitability for the origami inspired artificial muscle sheets. The findings from the flexibility, temperature sensitivity, and adhesion tests provide valuable insights into the performance characteristics of the selected materials.

PVC-film exhibits limitations in adhesion strength, making it less ideal for applications requiring robust bonding under pressure.

TPU-film emerges as the best option due to its ability to withstand higher forces than the other materials while maintaining adhesive characteristics under pressure. Its wide effective temperature range increases its versatility, making it a great option.

PET film possesses high tensile strength but demonstrates minimal deformation under pneumatic pressure, highlighting its limitations in flexibility and adaptability.

Nylon presents a balance between strength and flexibility; however, its adhesion strength may not match that of TPU.

Material	Flexibility		Deformability		Biocompatibility		Adhesive strength (bar)
PVC-film		++		++		++	0.024
TPU-film		++		++		++	0.10
PET-film	--		--			+	0
Nylon		++		++		++	0.21

Table 4: Overview of the materials, including flexibility, deformability, biocompatibility and adhesive strength

Consequently, future chapters will exclusively use TPU at a temperature of 250 degrees for further testing and development of origami-inspired artificial muscle sheets.

3.2.5 Discussion

Despite the valuable insights gained, it's important to acknowledge the study's limitations. One limitation is the focus on a limited set of materials, potentially overlooking other viable options. Furthermore, the selection of material thickness was based on availability, which may not represent all possible thicknesses and could yield different results. Finally, while the tests provide insights into individual material properties, they do not consider potential interactions or synergies between different materials when used together. In practical applications, materials are often combined or coated, and their combined behaviour may differ.

Chapter 4

Towards the design of origami-inspired structured sheets

Jeroen van de Kamp

In this chapter, the impact of various structures on the deformation of the sheets under air pressure will be examined to determine the most effective design for this purpose. First, the effects of different structural patterns on the sheet's behaviour when subjected to air pressure will be analysed. Subsequently, the knowledge gained from these various structural designs will be utilized to design and evaluate sheets that can be wrapped around a muscle model. This will involve examining how effectively the sheets can induce muscle contraction.

4.1 Introduction

Through the application of air pressure and strategically designed structures within the sheet, deformation can be achieved. These structures create air pockets that play a crucial role in the deformation process, enabling the sheet to expand and contract in response to pneumatic pressure. By carefully designing these patterns, the air pockets can be optimized to produce controlled and precise movements, facilitating natural muscle contractions (Fig. 27).

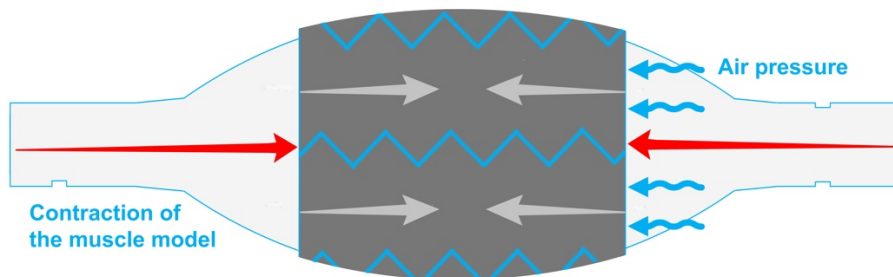


Figure 27: Concept drawing demonstrating the sheet (grey) wrapped around a muscle model, inducing muscle contraction (red) through air pressure (blue).

In order to seal the sheets and create the structures, heat is applied using a soldering iron. Previous tests identified Thermoplastic Polyurethane (TPU) as the most suitable material among the four tested materials. Therefore, the sheets used in this study are made exclusively of TPU.

4.2 Preliminary study

A preliminary study is conducted to observe how the sheets respond to different structural patterns before testing them on the muscle. This initial phase involves evaluating the deformation capabilities and air pocket formation under pneumatic pressure for the following structural designs (Fig. 28):

- Horizontal lines pattern at the centre
- Horizontal lines pattern with side constraints
- Zig-zag pattern
- Yoshimura pattern
- Miura ori pattern

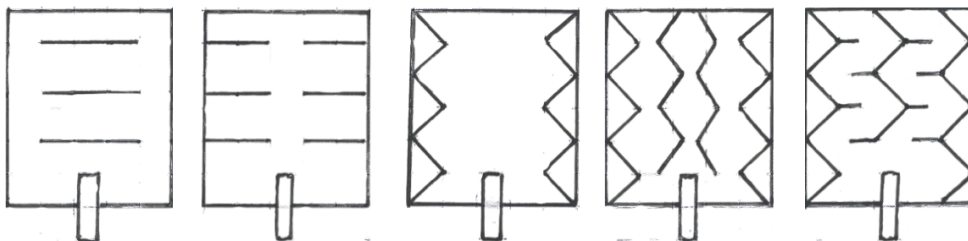


Figure 28: Conceptual drawings of the preliminary study: (a) horizontal line pattern at the centre, (b) horizontal line pattern with side constraints, (c) zig-zag pattern, (d) Yoshimura pattern, (e) Miura-ori pattern

During the test, a sheet with a fixed format was used. Each sheet measures approximately 130 in length and 110 mm in width. The soldering iron operates at a temperature of approximately 250 degrees Celsius, which is ideal for sealing TPU and forming the required patterns without damaging the material. It seals the TPU material with a thickness of approximately 1.5 mm (Fig 29).

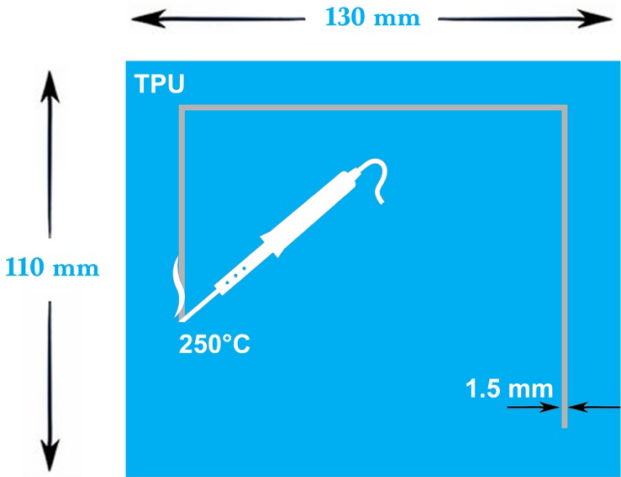


Figure 29: Dimensions of TPU sheets used in the tests for the structures and the temperature (approx.. 250 degrees Celsius) applied by a soldering iron for sealing

Initially, a sheet devoid of any structural modifications was tested (Fig. 29). This approach served as a fundamental reference point for evaluating the impact of subsequent structural additions. The initial observation revealed that while the sheet inflated under pneumatic pressure, it did not exhibit a significant contraction mimicking the shortening of the muscle length. Approx. 7 mm of contraction was observed, suggesting the need for structural modifications to achieve the desired muscle-like actuation.

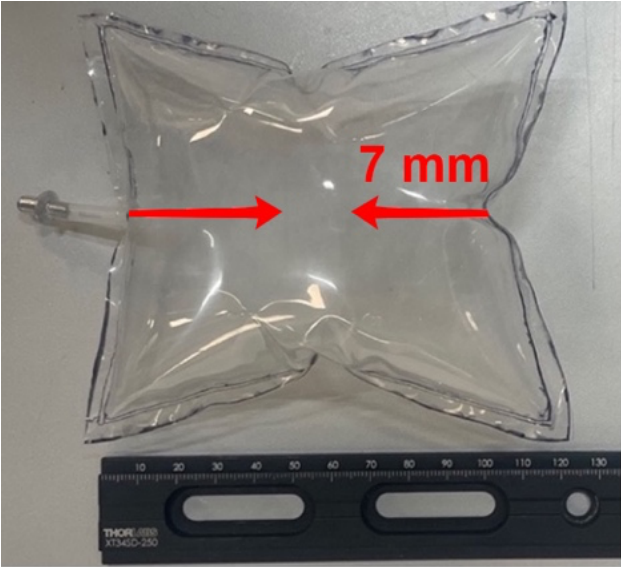


Figure 30: TPU-film without a structure inflated, resulting in a contraction of approx. 7mm.

Horizontal line pattern at the centre

Parallel lines were chosen as the structural pattern because they inherently facilitate the formation of air pockets when inflated. This ability to manipulate air pockets effectively is key to achieving controlled deformation.

The design incorporates a linear structure at the centre. This configuration allows for controlled inflation through the formation of air pockets. As air is pumped into the sheet, the material between the parallel lines acts as a barrier, restricting airflow and causing pockets to inflate. These air pockets accumulate between the lines, leading to a localized pressure increase. The pressure buildup within the air pockets creates a pushing force on the material between the lines. This force pushes the material outward, causing the parallel lines to be drawn closer together. This inward movement of the lines, akin to squeezing a balloon, translates into a contraction effect along the length of the sheet, mimicking the shortening of a muscle (Fig. 31).

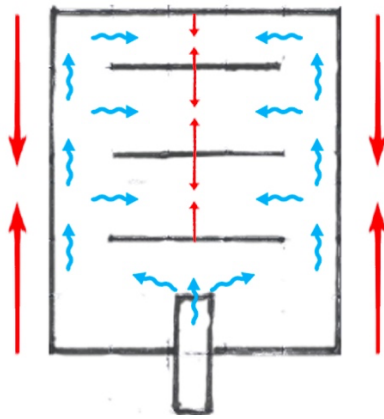


Figure 31: Conceptual drawing horizontal line structure at the centre: hypotheses on the deformation of the sheet

The implementation of parallel lines resulted in noticeable changes in the sheet's behaviour under pneumatic pressure (Fig. 32). Observations revealed that the parallel lines induced a pulling effect, causing the sheet to bulge and contract in length by approximately 55 mm. This contraction is indicative of the successful activation of muscle-like behaviour within the sheet.



Figure 32: Inflated TPU sheet, horizontal line structure at the centre

Horizontal line pattern with side constraints

Similar to the central linear structure, parallel lines can also be placed on both sides of the sheet, leaving the central region open for airflow. By positioning the parallel lines on the sides, the air pockets form between the lines but allow for a larger pressure surface, as there are more constraints on the sheet and fewer air leakage points (Fig. 33).

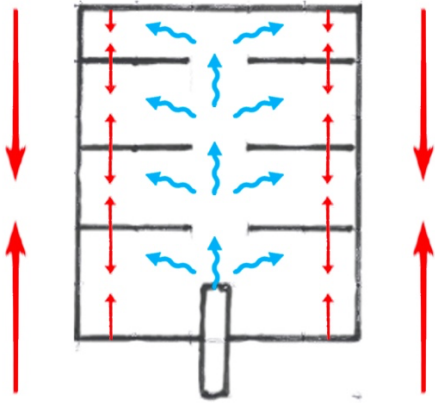


Figure 33: Conceptual drawing horizontal line structure with side constraints: hypotheses on the deformation of the sheet

The larger pressure surface created by the side constraint of the parallel lines, the contraction effect becomes more pronounced (Fig. 31). This results in a greater overall contraction along the length of the sheet, effectively mimicking the shortening of a muscle even more effectively than with a central linear structure alone. This design achieves a contraction of approximately 63 mm.

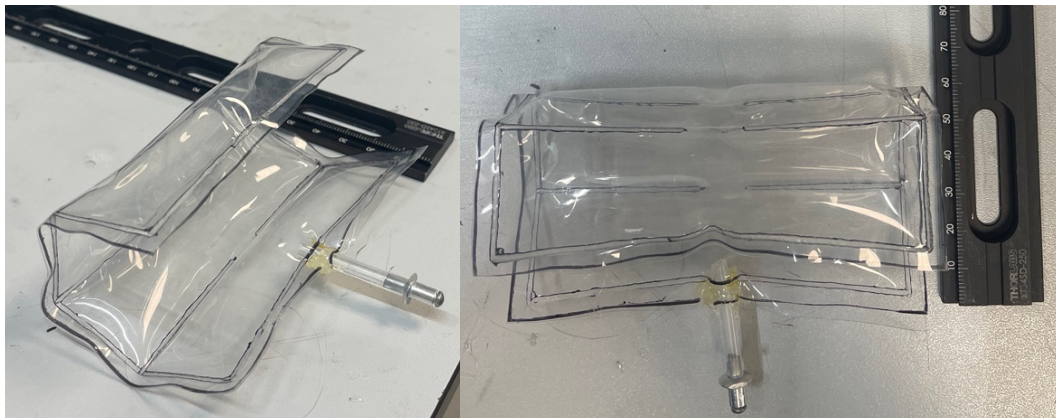


Figure 34: Inflated TPU sheet, horizontal line structure with side constraint

Zig-zag pattern

Following the exploration of parallel lines, the implementation of zigzag patterns within the sheet was considered. Zigzag lines were chosen for their potential to induce controlled deformation and contraction due to the alternating directions of the lines. The hypothesis is that the alternating angles of the lines create a crimping effect when inflated, causing the sheet to buckle and shorten in length. This mimics the accordion-like shortening principle observed in biological muscles (Fig. 35).

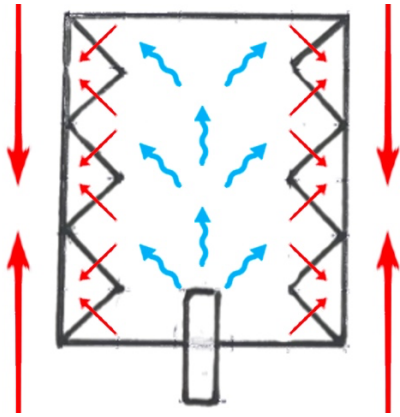


Figure 35: Conceptual drawing zig-zag pattern: hypotheses on the deformation of the sheet

The results indicate that the zigzag pattern yields less favourable outcomes compared to the parallel lines, with approximately 15 mm of contraction observed (Fig. 36). However, this outcome provides valuable insights into the behaviour of the sheet and identifies its limitations.



Figure 36: Inflated TPU sheet, zigzag structure

Specifically, the straight segments at the edges of the zigzag pattern introduce a constraint effect, restricting deformation (Fig. 37). Consequently, the subsequent step involves exploring modifications to the zigzag structure to mitigate this constraint effect and further optimize the sheet's contraction potential.

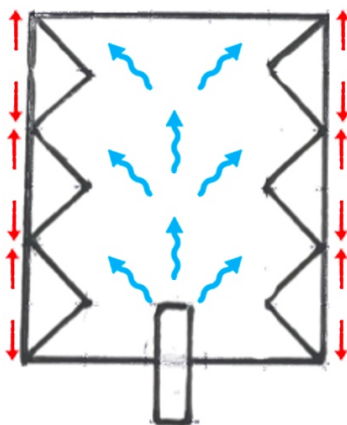


Figure 37: Conceptual drawing zigzag pattern with constraint effects on deformation

Addressing the constraint

The constraint effect introduced by the straight segments at the edges of the zig-zag pattern was addressed by reconceptualizing the sheet's design. Rather than considering the sheet as a singular square, it was reimagined as a holistic zig-zag structure (Fig. 38a). This modification aimed to distribute the constraint more evenly across the sheet, thereby allowing for a more uniform deformation and enhancing the overall contraction potential.

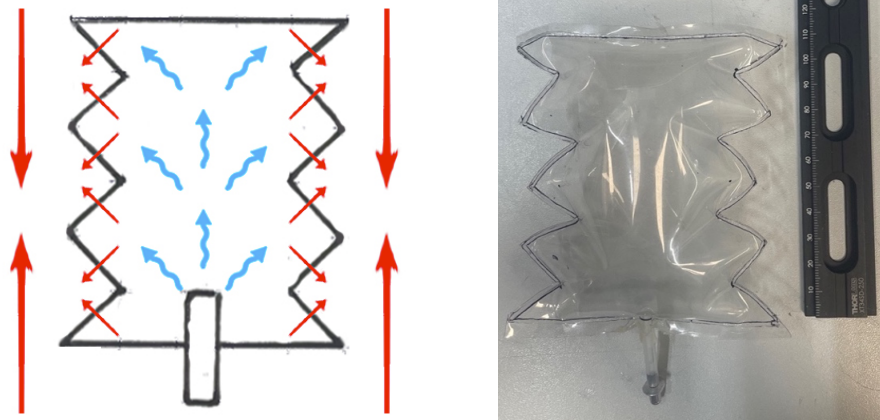


Figure 38: (a) Conceptual drawing: zig-zag cutouts addressing the structural constraint, (b) Inflated TPU sheet, zigzag cutout

Although the results indicate an improvement in contraction by alleviating constraints through the implementation of a zigzag structure, the extent of contraction achieved falls short of that observed with parallel lines, approx. 20 mm (Fig. 38b).

In order to minimize constraints while maximizing the contraction effect, a hybrid approach combining elements from various structures, including line structures, Yoshimura patterns, and Miura-ori folds, were explored (Fig. 39). By integrating these structural patterns, the sheet can benefit from the reduced constraint effect of the zigzag design while leveraging the potentially enhanced contraction offered by parallel lines, Yoshimura and Miura-ori patterns. This strategic combination offers a more balanced solution, potentially optimizing the sheet's performance for effective muscle wrapping and contraction simulation.

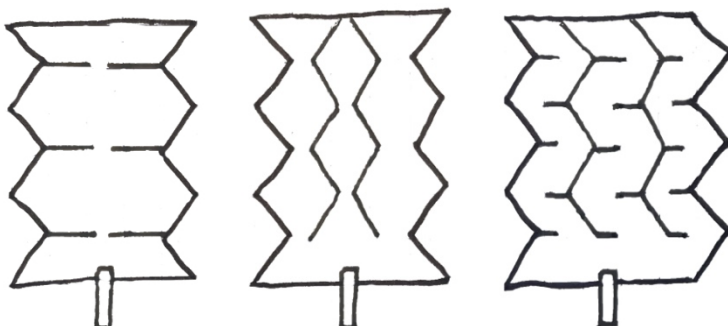


Figure 39: Conceptual drawing of the preliminary study: (a) zig-zag pattern in combination with the horizontal lines with side constraints, (b) zig-zag pattern in combination with the Yoshimura pattern, (c) zig-zag pattern in combination with the Miura-ori pattern.

Zig-zag pattern and horizontal line pattern with side constraints

The zigzag pattern was combined with horizontal lines at the side constraints. Previous results have identified that placing horizontal lines at the side constraints yielded better results than placing them at the center.

When placing the horizontal lines, two options are considered: on the inward and outward facing corners.

By placing the horizontal lines on the outward-facing corners, air pressure distribution would occur where the zigzag lines are already inclined towards each other, leading to inefficient utilization of pressure and disruption of the desired contraction effect (Fig. 40).

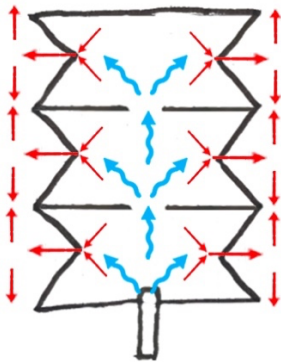


Figure 40: Conceptual drawing: zig-zag pattern in combination with the horizontal lines with side constraints on the outward facing corners

By positioning the horizontal lines on the inward-facing corners of the zigzag structure, a mechanism is created where air pressure is utilized to achieve controlled contraction (Fig. 41). When the sheet is inflated, air pockets form between the zigzag lines and the horizontal lines, ensuring even distribution of air pressure. This arrangement pushes the zigzag lines towards each other at desired points, optimizing the natural movement of the structure. As a result, a controlled and uniform contraction of the sheet occurs, resembling the unfolding of an accordion

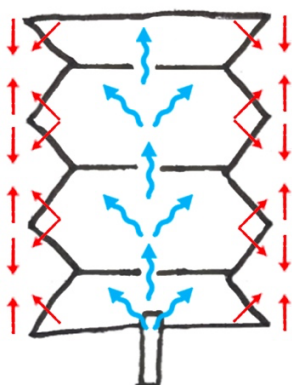


Figure 41: Conceptual drawing: zig-zag pattern in combination with the horizontal lines with side constraints on the inward facing corners,

The results of combining the zigzag and parallel line structures yielded an approximate contraction of 66 mm (Fig. 42). This outcome signifies a notable improvement

compared to the individual implementations of each structural pattern. By integrating both designs, the sheet demonstrated enhanced deformation capabilities, achieving a more significant contraction effect. The combination effectively minimized constraints while maximizing the sheet's responsiveness to pneumatic pressure.

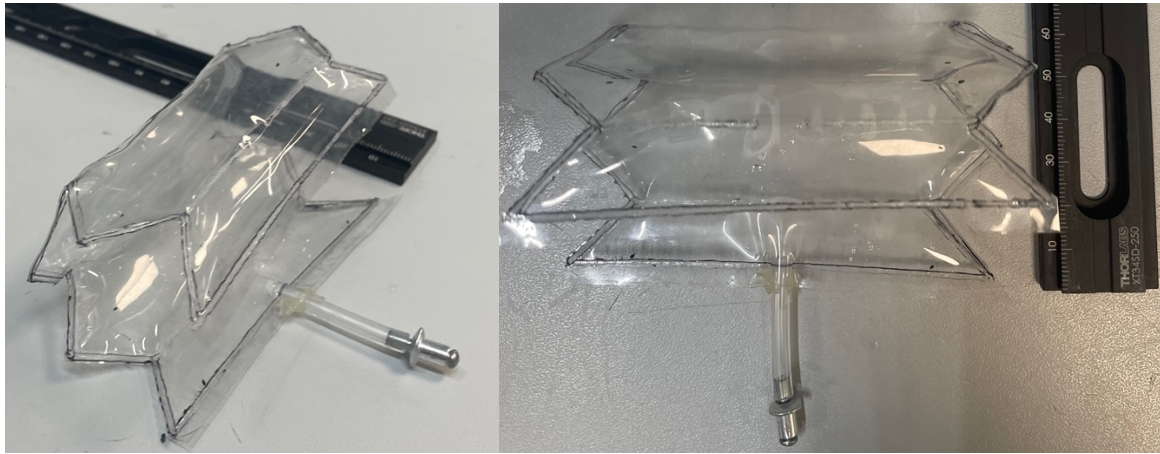


Figure 42: Inflated TPU sheet, zig-zag pattern in combination with the horizontal lines with side constraints on the inward facing corners

Yoshimura pattern

The Yoshimura pattern [41] is a well-known origami-inspired structure with unique geometric configurations that have demonstrated remarkable deformation properties in various applications. The pattern, with its alternating mountain and valley folds arranged in a grid-like fashion, offers a promising approach to distributing deformation more evenly across the sheet (Fig. 43). This distribution could potentially facilitate a more uniform contraction, thereby enhancing the effectiveness of the muscle wrapping process.

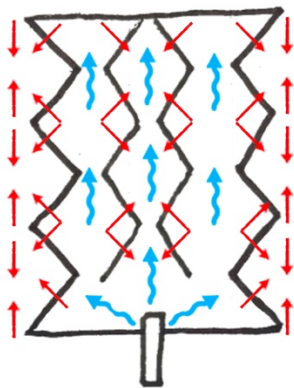


Figure 43: Conceptual drawing zig-zag pattern and Yoshimura pattern: hypotheses on the deformation of the sheet through air pressure

However, the observed results indicate that the Yoshimura pattern does not respond significantly when subjected to pneumatic pressure and does not show a contraction like the parallel horizontal lines (Fig. 44).

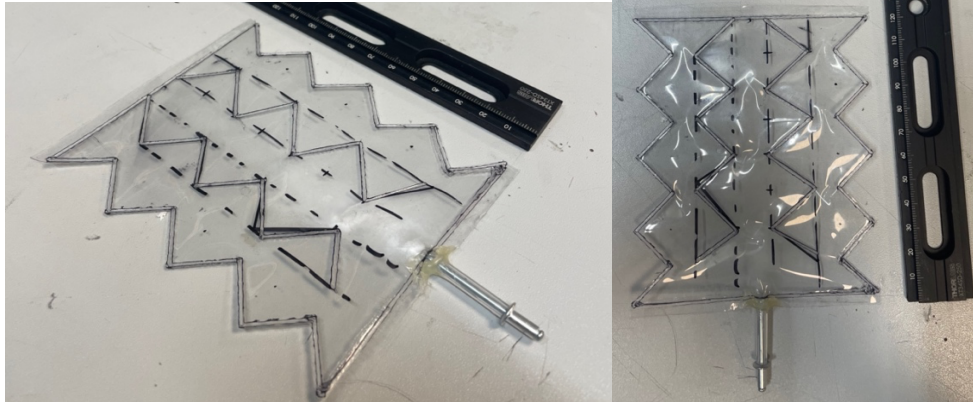


Figure 44: Inflated TPU sheet, Yoshimura structure (zigzag cutout)

The force distribution within the Yoshimura pattern does not facilitate the formation of air pockets necessary for effective contraction. In the center, air pockets are formed, which cause the forces to cancel each other out, preventing contraction (Fig. 45).

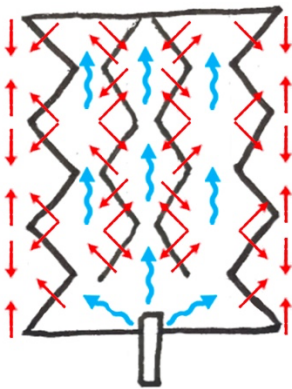


Figure 45: Conceptual drawing zig-zag pattern and Yoshimura pattern: force distribution prevents contraction

Miura-ori pattern

The Miura-ori pattern, renowned for its ability to fold and unfold [42] offers intriguing possibilities for enhancing the sheet's deformability.

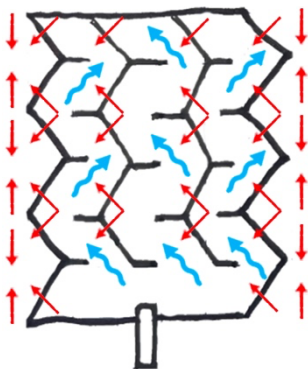


Figure 46: Conceptual drawing zig-zag pattern and Miura-ori pattern: hypotheses on the deformation of the sheet through air pressure

However, the observed results from testing reveal minimal deformation when subjected to pneumatic pressure (Fig. 47).

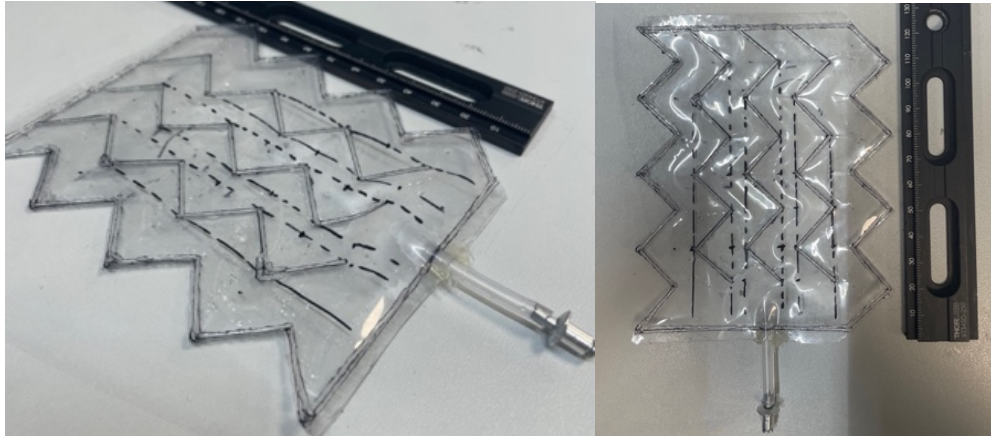


Figure 47: Inflated TPU sheet, Miura-ori structure (zigzag cutout)

This limited response can be attributed to the geometry of the Miura-ori pattern, which hinders the formation of localized air pockets necessary for effective deformation under pneumatic pressure. The forces within the sheet cancel each other out due to the distribution of airflow in the central path, resulting in deformation perpendicular to the sheet rather than parallel to it (Fig. 48)

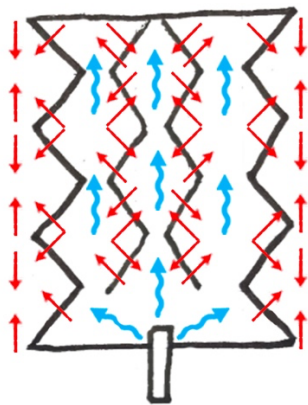


Figure 48: Conceptual drawing zig-zag pattern and Miura-ori pattern: force distribution prevents contraction

4.2.1 Conclusion

During the preliminary phase, parallel lines initially showed promise for facilitating air pocket formation and deformation. However, testing revealed constraints, which affected the sheet's ability to deform effectively under pneumatic pressure.

To address these limitations, a hybrid approach combining zigzag with parallel lines, Miura-ori, and Yoshimura structures was devised. While Miura-ori and Yoshimura patterns were examined for their deformation capabilities, they did not exhibit significant contraction under pneumatic pressure due to their intricate geometries dispersing forces unevenly.

Integration of parallel lines with zigzag structures proved most effective among the tested patterns. This configuration demonstrated substantial contraction and deformation capabilities, making it the preferred choice for designing sheets intended for muscle wrapping tests.

4.3 Implementation around the muscle model

The combination of the Zig-zag pattern and horizontal line pattern with side constraints is applied in the design of the origami-inspired sheet intended to wrap around and contract the muscle.

4.3.1 Requirements

To effectively design the sheet for muscle contraction, several critical requirements must be met. The primary goal is for the sheet to deform under air pressure, simulating a contraction that shortens the length of the biceps brachii muscle.

- First, The sheet must be able to wrap around the biceps brachii muscle smoothly, conforming to its contours, without restricting the airflow.
- The sheet must be capable of significant deformation under pneumatic pressure, enabling it to shorten in length and thereby generate enough contraction when wrapped around the biceps brachii muscle model to induce a contraction force of at least 153.55 N, which is necessary for minimal flexion of the biological forearm.
- The sheets must be completely airtight, ensuring secure seals at the points where air enters the sheet, and ensuring that the patterns within the sheet are free from any leaks that could compromise its integrity.
- The sheets used for testing must be uniform in length and width to minimize deviations and ensure consistent results. Consistency in sheet dimensions helps in comparing performance across various designs and iterations.

4.3.2 Method

Conforming the contours of the muscle model

The sheet must accurately conform to the muscle contours to achieve optimal muscle contraction. To accomplish this, the sheet requires dimensions tailored to accommodate the muscle's curvature. Specifically, the sheet measures 21 cm in length and 12 cm in width (Fig. 49). These dimensions were maintained during the tests of the sheets.

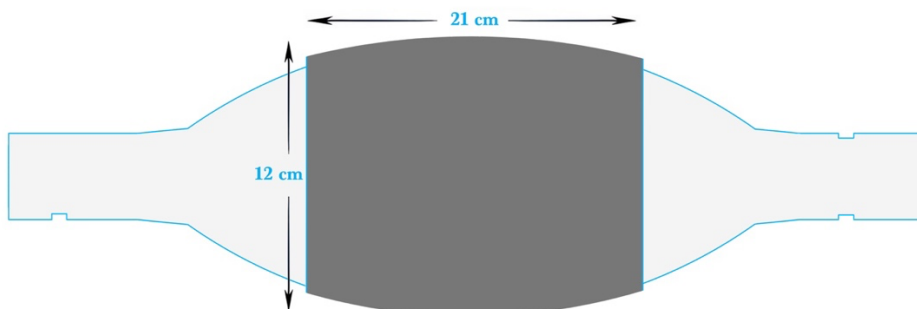


Figure 49: Dimensions of the sheet, wrapped around the muscle

Muscle contraction

To achieve contraction of the muscle, the sheet must exert a force equivalent to that of the spring. Calculations revealed that the spring exerts a force of 43.4 N. Based on the forces and dimensions outlined in the free body diagram (Fig. 50), the amount of force the sheet must exert to affect the muscle can be determined.

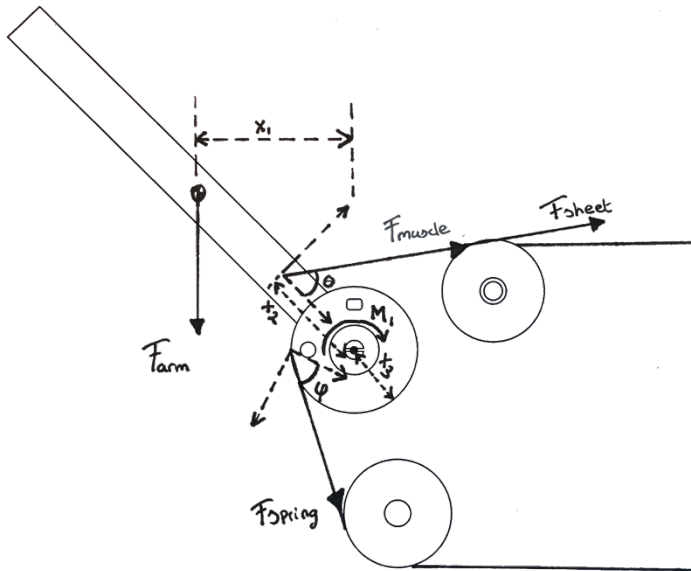


Figure 50: Free body diagram, test setup

By calculation, the sheet must exert a minimum force of 15.96 N in order to lift the arm.

$$M = (F_{muscle} + F_{sheet}) \cdot (\sin(\theta) \cdot x_2) - F_{spring} \cdot \sin(\varphi) \cdot x_3 - F_{arm} \cdot x_1 = 0$$

$$F_{sheet} = \frac{F_{spring} \cdot \sin(\varphi) \cdot x_3 + F_{arm} \cdot x_1 - F_{muscle} \cdot \sin(\theta) \cdot x_2}{\sin(\theta) \cdot x_2}$$

$$x_1 = 0.076 \text{ m}$$

$$x_2 = 0.038 \text{ m}$$

$$x_3 = 0.018 \text{ m}$$

$$\theta = 21.8^\circ$$

$$\varphi = 72.1^\circ$$

$$F_{muscle} = 38.4 \text{ N}$$

$$F_{arm} = 0.3 \text{ N}$$

$$F_{spring} = 43.4 \text{ N}$$

$$F_{sheet} = \frac{43.4 \cdot \sin(72.1^\circ) \cdot 0.018 + 0.3 \cdot 0.076 - 38.4 \cdot \sin(21.8^\circ) \cdot 0.038}{\sin(21.8^\circ) \cdot 0.038}$$

$$F_{sheet} \approx 15.96 \text{ N}$$

Horizontal line pattern with side constraint

Regarding the internal structure of the sheet, the horizontal lines with side constraints as identified in the preliminary study are initially applied. These lines must be placed perpendicular to the muscle model along the entire length of the sheet to ensure that contraction occurs in the direction parallel to the muscle model (Fig. 51). Regarding the zigzag structure, an additional consideration is required because the sheet is placed around the muscle and thus has no outer edge in the direction of the muscle fibers. Due to the absence of an outer edge, the necessity of applying a zigzag structure is reduced as there are minimal constraints in that direction.



Figure 51: (a) TPU sheet with the horizontal line pattern with side constraint, (b) deformation of the sheet during inflation

The use of parallel lines for the structure of the sheet has shown to yield undesired results given the specific circumstances in which the sheet is placed. This is primarily due to the restriction of airflow caused by the sheet being wrapped around the muscle (Fig. 52).

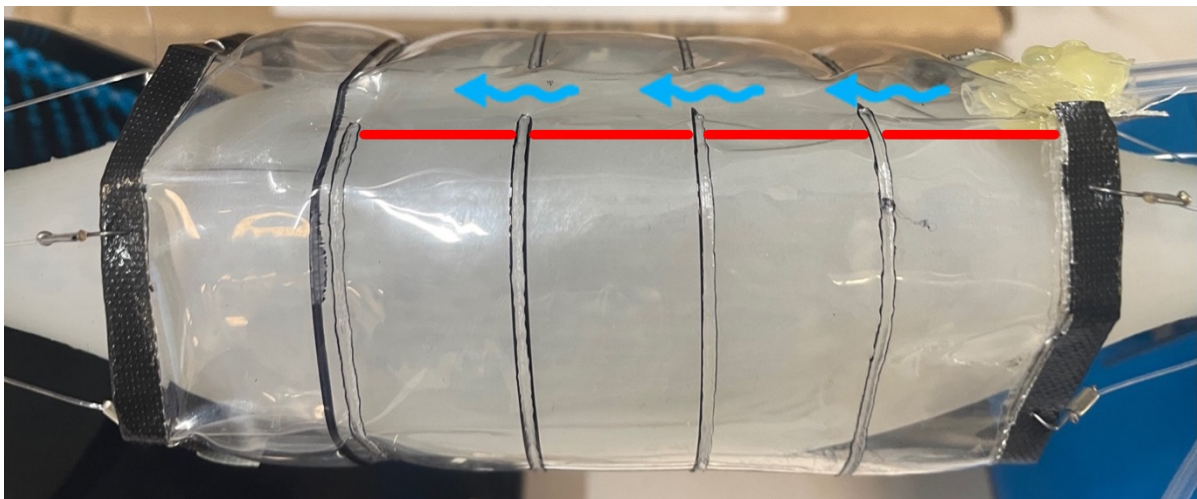


Figure 52: restriction air flow

Chambered structures

To address this issue, introducing air pockets into various sections of the sheet, similar to enlarging nodes in a circular mesh structure. This entails dividing the parallel lines on the sheet, thereby creating chambers to facilitate this division. Each chamber would then experience its own deformation when air is introduced, promoting a more uniform and efficient contraction of the sheet.

To provide each chamber with pneumatic pressure, various design solutions were considered and analysed. One option was to use individual air channels leading to each chamber. However, this could result in complications such as inconsistencies in pressure between the chambers and an increased risk of leaks. Another option considered was to use a single air duct that branches from one of the chambers to each subsequent chamber. However, this could pose problems with the even distribution of air across the chambers, especially for those farther from the central duct.

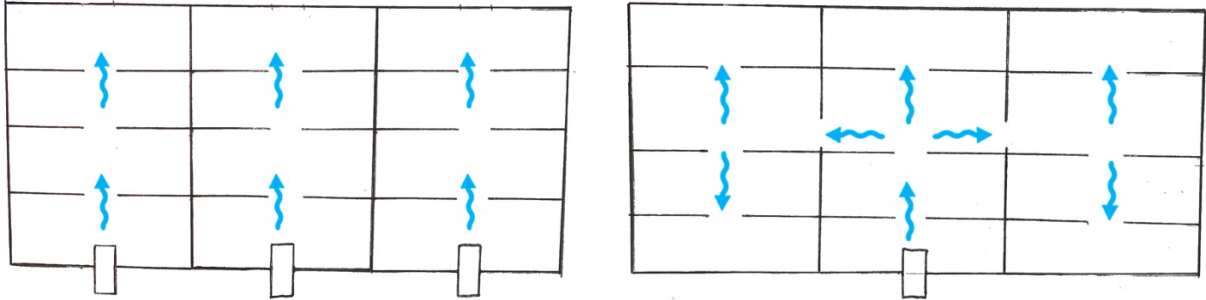


Figure 53: Conceptual drawings chamber orientation for pneumatic pressure: (a) individual air channels, (b) single air duct that branches from one of the chambers to each subsequent chamber.

Ultimately, a single air duct that branches out to each chamber was chosen as the best option. This approach involves a main pipeline that uniformly transports air to all chambers, ensuring consistent pneumatic pressure and offering operational simplicity.

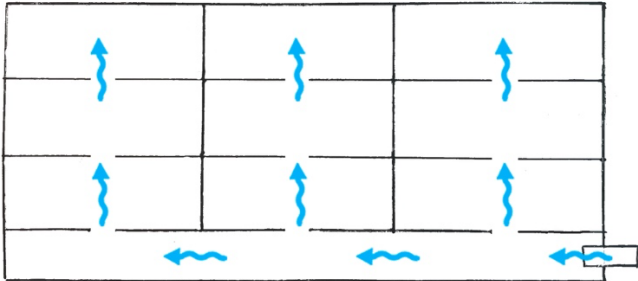


Figure 54: Conceptual drawings chamber orientation for pneumatic pressure: single air duct that branches out to each chamber

The introduction of these chambers creates a new constraint parallel to the expected line of contraction necessitating the application of a zigzag structure again (Fig. 55).

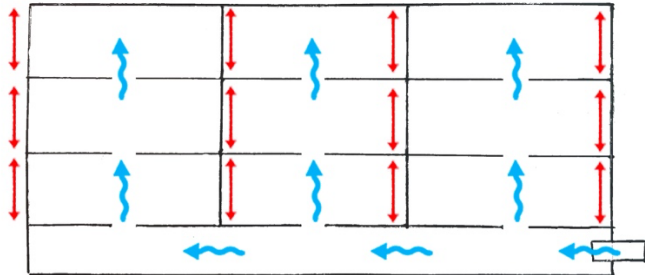


Figure 55: Conceptual drawings: constraint effects on deformation

Addressing the constraint

Yet, incorporating a zigzag pattern presents an additional consideration. Since the sheet is wrapped around the muscle and lacks an outer edge in the direction of the muscle fibers, careful attention must be paid to the design of the zigzag pattern. This pattern must be strategically positioned to effectively stimulate the desired muscle contraction without the constraints. To address this, a zigzag pattern has been implemented between the chambers, forming a diamond-shaped cutout (Fig. 56).

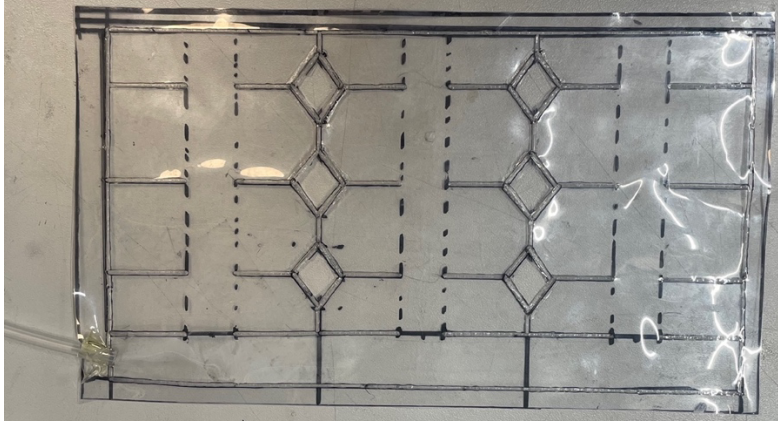


Figure 56: TPU sheet with the horizontal line pattern with side constraints on the inward facing zig-zag pattern

However, testing did not show the same effect as observed in the preliminary study of the zigzag patterns. Initially, it was found that lines on the inward-facing corners gave the best results. However, when subjected to pneumatic pressure, the sheet did not contract. Instead, the deformation appeared perpendicular to the sheet (Fig. 57).

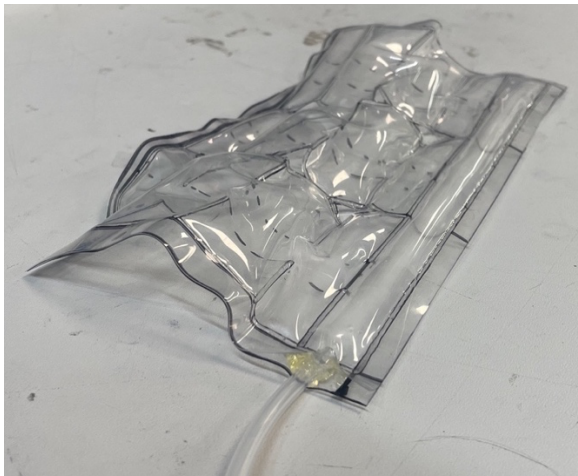


Figure 57: Deformation of the sheet with the horizontal line pattern with side constraints on the inward facing zig-zag pattern during inflation

This discrepancy can be attributed to the introduction of chambers in the design, which creates a diamond-shaped zigzag structure between the chambers. When pressure is applied, the zigzag structure expands outward, creating a counteractive force against the intended contraction, effectively acting as a constraint. Additionally, the presence of an adhesion line, parallel to the direction of contraction between the diamond shapes further contributes to this constraint.

To address this issue, the design was re-evaluated with the lines positioned on the outward-facing corners of the zigzag pattern. This adjustment ensures that the diamond-shaped structures between the chambers move inward rather than outward when air pressure is applied. By positioning the lines outward, the diamond shapes fold inward, promoting a more effective contraction.

This inward folding of the diamond shapes allows the air pockets to form more effectively, facilitating uniform contraction. The natural movement of the structure is optimized, and the air pressure is utilized more efficiently (Fig. 58).

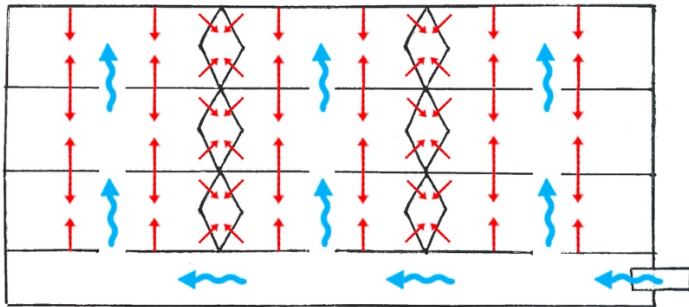


Figure 58: Conceptual drawings: horizontal line pattern with side constraints on the outward facing zig-zag pattern during inflation

As a result, this configuration achieves controlled and significant contraction of the sheet, as the inward movement of the diamond shapes eliminates the previously observed constraint effect (Fig. 59).

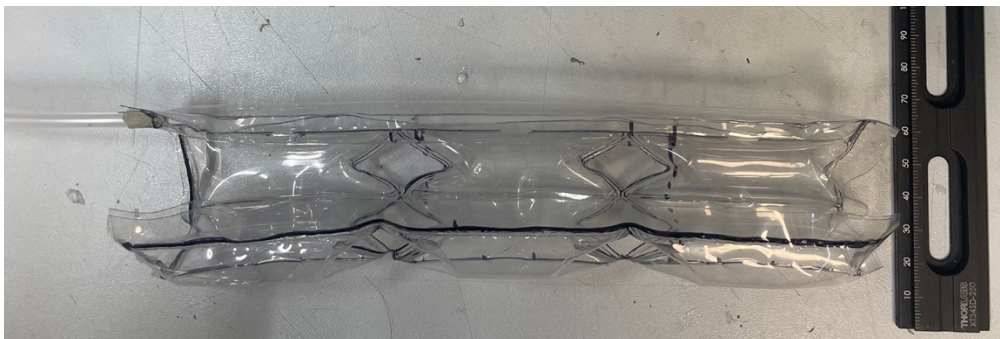


Figure 59: Deformation of the sheet with the horizontal line pattern with side constraints on the outward-facing zig-zag pattern during inflation

This design was implemented around the biceps brachii muscle model to test its ability to effectively contract the muscle, thereby inducing rotational movement in the arm mechanism.

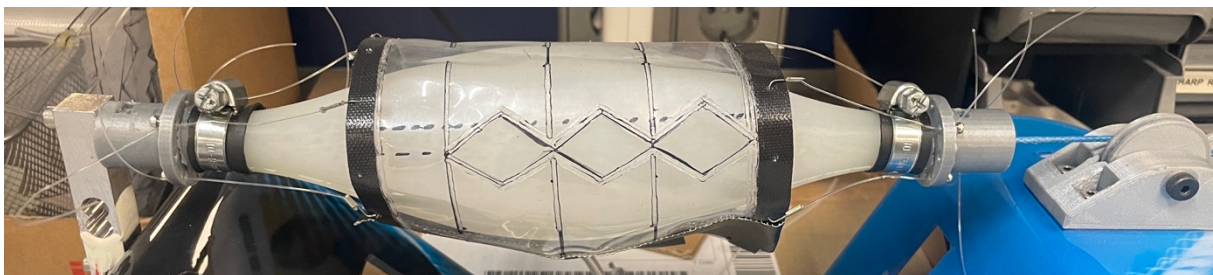


Figure 60: Implementation of the final design around the biceps brachii muscle model

4.3.3 Results

The designed sheet is placed around the muscle for evaluation by employing the load cell, potentiometer, and pressure sensor. A pneumatic pressure with a maximum value of approximately 1.7 bar, is applied to the sheet, and the ensuing results are graphically represented for analysis (Fig. 59)

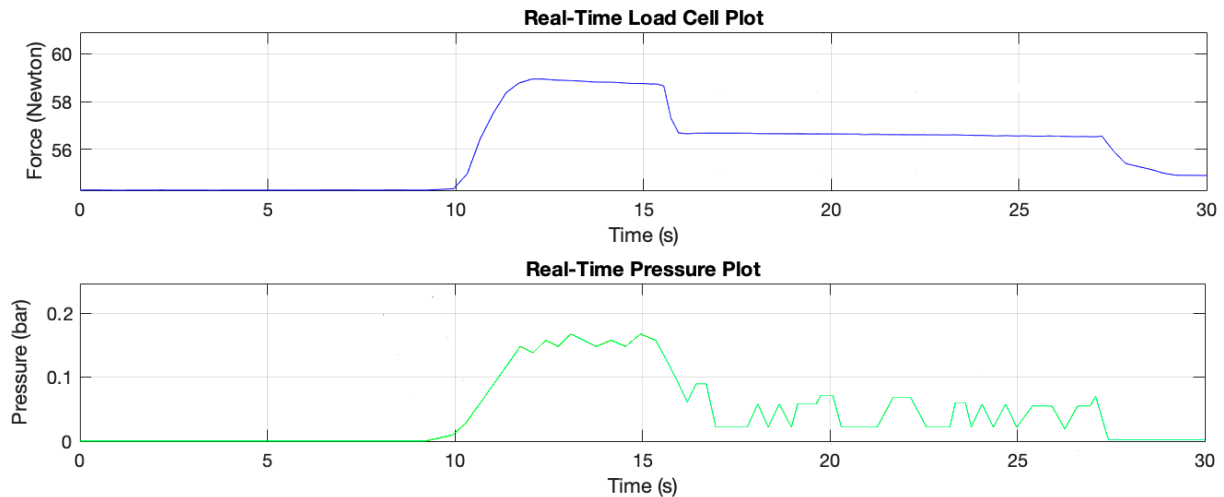


Figure 61: Real-time plot of the load cell- and pressure sensor (chambers and zigzag cutouts)

In the load cell plot, the activation of the sheet by the pressure pump is depicted, revealing a force measurement of 59N. This value represents a notable increase of 5N from the calibrated baseline of approximately 54N, indicative of the muscle's elongated state. Concurrently, the pressure sensor records an approximate pressure of 0.15 bar, resulting in an deformation and a subtle contraction of the sheet. However, after 5s, both the load cell and pressure sensor readings experience a rapid decline, with the load cell value decreasing to 57N.

This reduction coincides with a diminishing pressure level, suggesting that the sheet has reached its maximum pressure threshold, due to a leakage, resulting in inadequate contraction.

Despite the load cell detecting some force increase, the potentiometer data presents no significant results, indicating insufficient force to rotate the arm effectively (Fig. 60).

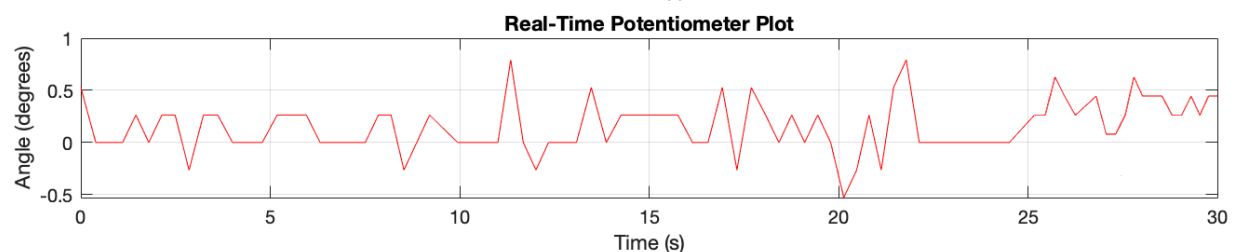


Figure 62: Real-time plot of the potentiometer (chambers and zigzag cutouts)

Conclusively, the sheet's maximum sustainable pressure appears to be around 0.2 bar, which proves insufficient for significant muscle contraction.

4.3.4 Conclusion

The exploration of structures delved into a comprehensive investigation into the potential of structured sheets to induce muscle contraction through pneumatic pressure.

In the preliminary study, various structural patterns were tested to identify designs capable of producing significant deformation and contraction. These included horizontal lines, zigzag patterns, and complex origami structures like the Yoshimura and Miura-ori patterns. Among the tested patterns, a combination of parallel lines with a zigzag pattern emerged as the most promising choice due to their facilitation of air pocket formation and subsequent controlled deformation. The incorporation of the zigzag pattern aimed to alleviate constraints and enhance performance.

In the practical application, a specific design was chosen incorporating chambers, a zigzag pattern and a single air duct,. Chambers were integrated to enhance pressure distribution, ensuring uniform muscle activation across the sheet. The zigzag pattern facilitated controlled deformation and contraction, optimizing muscle movement. Additionally, the single air duct allowed for precise airflow regulation, contributing to consistent pressure maintenance within the sheet.

The sheet designed with this configuration was applied around the muscle model and tested to observe its effect. During these tests, a load cell, potentiometer, and pressure sensor were utilized for evaluation. At a pneumatic pressure of approximately 1.7 bar, the load cell recorded a force increase of 5N and the arm mechanism did not exhibit rotational movement despite the force exerted by the sheet.

4.3.5 Discussion

The aim of this study was to explore the potential of a specially designed sheet to induce muscle contraction by analysing its structural deformation under pneumatic pressure. The objective was to create a sheet capable of effectively mimicking natural muscle activation and contraction, thereby facilitating arm flexion through strategic structural designs and controlled pneumatic pressure.

Under a pneumatic pressure of approximately 1.7 bar, the load cell recorded a force increase of 5N, indicating a relatively small level of muscle activation. From a simplified force calculation of the forearm and upper arm, it appears that the biceps should deliver approximately 153.8N to lift the forearm. force generated was insufficient for achieving effective muscle contraction, indicating the need for further refinement.

Additionally, pressure sensor readings declined rapidly after 5 seconds, suggesting leakage and a failure to maintain necessary pressure for sustained contraction. Moreover, the potentiometer data showed no significant arm movement, indicating insufficient force generated for effective muscle contraction.

Leakage issues significantly impacted the sheet's ability to maintain necessary pressure for sustained contraction. The thin adhesion lines, at approximately 1 mm thickness, were insufficient for optimal adhesion and pressure retention. Thicker adhesion lines would enable better adhesion, accommodating higher pressures and generating greater force.

Moreover, the manual application of adhesion lines using a soldering iron introduced inconsistencies and potential errors, leading to variations in performance and limiting overall reliability.

The study revealed that while certain structural patterns, particularly the combination of parallel lines and zigzag patterns, could facilitate significant deformation and mimic muscle contraction, practical application revealed limitations. The sheet's maximum sustainable pressure of around 0.2 bar was insufficient for significant muscle contraction. Future research should focus on optimizing the structural design further, exploring materials and configurations capable of maintaining higher pressures without leaking. Additionally, integrating more advanced pressure management systems could enhance the sheet's ability to simulate natural muscle behaviour effectively.

Chapter 5

Conclusion, recommendations and future work

Jeroen van de Kamp

This chapter reflects on the approach, process, and execution of the graduation project. First, the most important conclusions of this thesis are listed, addressing the main question of whether inflatable structures are suitable for restoring the functionality of biological muscles in individuals with muscle impairments. Subsequently, the recommendations and suggestions for future research are proposed

5.1 Conclusion

In this thesis, the suitability of inflatable structures for restoring the functionality of biological muscles in individuals with muscle impairments was analysed. The research aimed to determine whether an origami-inspired sheet, when wrapped around a muscle, could induce muscle contraction and flexion. To achieve this, a test setup mimicking the biceps brachii was designed, and various materials and structural designs were evaluated.

Regarding the material selection, out of various materials (Polyester, TPU, Nylon and PVC) TPU emerged as the most promising option due to its superior performance in withstanding high forces while maintaining adhesive characteristics under pressure. Its wide effective temperature range and versatility make it well-suited.

The exploration of structural designs revealed promising results, particularly with the combination of parallel lines and zigzag patterns, which minimized constraints and maximized responsiveness to pneumatic pressure. However, practical application exposed limitations, such as leakage issues and therefore insufficient pressure retention, hindering effective muscle contraction.

The key findings of this study suggest that the origami-inspired sheet, in its current form, is not effective for restoring the functionality of biological muscles in individuals with muscle impairments. The load cell recorded a force increase of only 5N, which was insufficient to activate the muscle and induce flexion. Despite these challenges, the study underscores the potential of origami-inspired sheets for muscle assistance. While certain structural patterns showed promise in inducing muscle contraction, further optimization is required to overcome practical limitations and enhance performance.

In conclusion, while the exploration of inflatable structures and origami-inspired designs has provided valuable insights, further research is essential to overcome practical limitations and optimize performance. By addressing challenges such as leakage, origami-inspired sheets have the potential to enhance muscle movement and consequently improve the quality of life for individuals with muscle impairments. This underscores the necessity for ongoing research and development to discover effective solutions for restoring muscle functionality in individuals with muscle impairments.

5.2 Recommendations and Future Work

The study's conclusion offers important suggestions and directions for further research.

A critical aspect that emerged from the testing phase is the importance of adhesion lines in ensuring the proper functionality of origami-inspired sheets. Throughout the study, leakage issues were a persistent challenge, often attributed to insufficient bonding between the sheets. To address this, future research should prioritize the exploration of thicker adhesion lines. By testing various thicknesses and compositions, the optimal configuration can be identified to ensure optimal bonding while maintaining the necessary flexibility for muscle movement.

Furthermore, exploring advancements in methods to bond the sheets together through heat bonding could lead to improved outcomes. Currently, all bonding is done manually, which is time-consuming, prone to human error, and lacks precision. This lack of precision can result in inconsistencies and variations in performance. Moreover, the transition from manual to automated technologies such as laser cutting, 3D printing, or CNC machining represents a significant opportunity for improving the consistency and scalability of origami-inspired sheet production.

While certain structural patterns showed promise in inducing muscle contraction, there remains room for optimization and innovation. Future research should prioritize the exploration of advanced structural designs that leverage the principles of origami to maximize performance. This could involve experimenting with novel geometries, fold patterns, skeletal structures within the sheet or material compositions to enhance the sheet's ability to mimic natural muscle activation and contraction. Additionally, computational modelling and simulation techniques can be employed to predict the behaviour of complex origami structures and guide the design optimization process.

In parallel, while pneumatic pressure has primarily driven origami-inspired muscle assistance devices, exploring alternative actuation methods could offer unique advantages and expanded capabilities. Future research should investigate not only the continued use of pneumatic pressure but also the potential of pneumatic vacuum systems, which bring different design considerations and opportunities. Additionally, hydraulic systems present another promising way for inducing muscle contraction. Each of these methods—pneumatic pressure, pneumatic vacuum, and hydraulic systems can offer distinct benefits in terms of force output and control precision, which could broaden the applications and functionalities of origami-inspired muscle sheets.

Another option to consider for future work is the selection of materials, which plays a crucial role in determining the performance and functionality of origami-inspired sheets. Future research should focus on exploring advanced materials with enhanced properties, such as greater flexibility, durability, pressure resistance and biocompatibility. Furthermore, with the integration of smart materials with responsive properties, such as shape memory alloys or hydrogels, the sheet holds the potential to create a hybrid origami structures capable of dynamic shape change in response to external stimuli.

Also the integration of mechatronic components presents a promising way for enhancing the capabilities of origami-inspired sheets for muscle assistance. By incorporating sensors, actuators, and feedback control systems into the design, researchers can develop intelligent and responsive devices that adapt to the user's movements and provide personalized assistance. For example, the integration of force sensors on the sheet itself can enable real-time monitoring of muscle activity and adjustment of pneumatic pressure to optimize performance. Additionally, the incorporation of wearable electronics can facilitate seamless interaction between the user and the device, enhancing user experience and usability (Fig. 63).



Figure 63: Concept drawing, real-time monitoring of the origami inspired sheet with wearable electronics

In addition to the integration of mechatronics, incorporating springs and dampers into the design of origami-inspired muscle assistance devices presents significant opportunities for enhancing functionality and addressing clinical needs. These components can be integral to improving muscle contraction efficiency, stability, and overall control.

The integration of springs into the sheet design can facilitate more effective muscle contraction by augmenting the pneumatic actuation mechanisms. Springs can provide a force that enhances and restore the contraction of the sheet, similar to the McKibben muscle sleeve, which uses the elastic properties of its sleeve material to enhance movement [43].

Adding contractile elements such as small springs, shape memory alloys or elastic bands, at both ends of the sheet can enhance the sheet's ability to contract. By incorporating extension springs, renowned for their capacity to withstand tensile forces and elongate when pulled apart, present a novel method to augment muscle contraction in origami-inspired sheets. By strategically integrating extension springs at both ends of the sheet, between the caps, or along the horizontal lines, they can complement the natural movement of the chambers towards each other (Fig. 64).

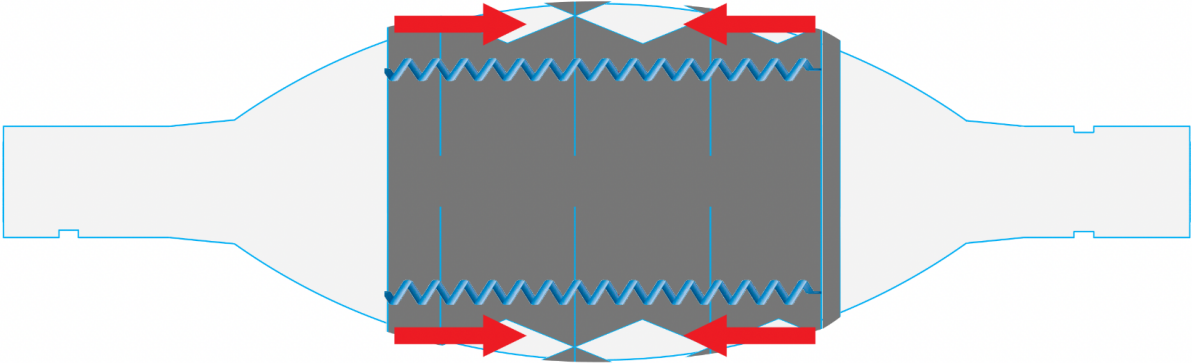


Figure 64: Concept drawing, integration of extension springs

Another approach to enhance the functionality of origami-inspired muscle sheets is by incorporating compression springs at the end caps. These compression springs can exert force from the end caps onto the sheet, serving as a replacement for the currently placed wires between the end caps and the sheet. By strategically positioning compression springs at the end caps, the springs can apply consistent pressure to the sheet, promoting controlled muscle contraction and movement (Fig. 65). This alternative configuration offers the advantage of simplifying the design by eliminating the need for separate wires, while also potentially providing more uniform and reliable force distribution throughout the sheet.

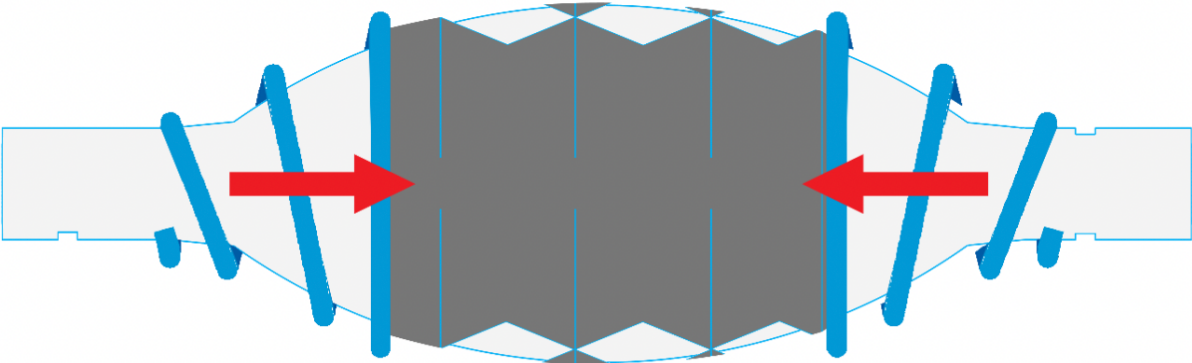


Figure 65: Concept drawing, integration of compression springs

In addition to traditional coil springs, the integration of elastic mesh springs can significantly enhance the mechanical integrity and performance of origami-inspired sheets. Drawing inspiration from the design principles of the McKibben muscle sleeve, composed of interconnected strands of elastomeric material, can be incorporated into the outer structure of the sheet to distributed more evenly across the surface, aiding in muscle contraction (Fig. 66).

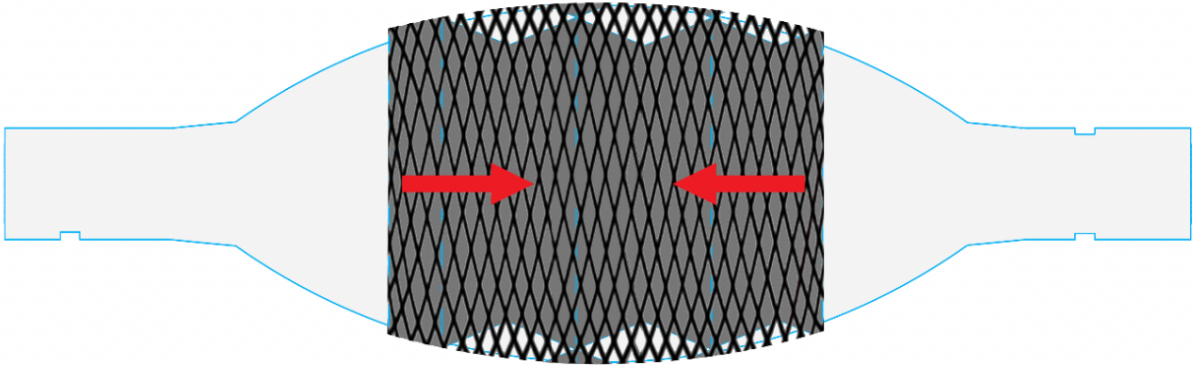


Figure 66: Concept drawing, integration of mesh springs

Another way for enhancing the functionality of origami-inspired muscle assistance devices lies in the exploration of advanced damping mechanisms. Dampers can play a crucial role in stabilizing movements and controlling unwanted vibrations, which is particularly beneficial for conditions such as tremors or Parkinson's disease. Integrating various types of dampers can mitigate the effects of these involuntary movements, providing smoother and more controlled muscle activity.

Conventional dampers, such as foam dampers present an effective solution for mitigating vibrations in the origami inspired sheets . These dampers, when integrated between, for example, the diamond shape cutouts, can absorb vibrations and tremors by compressing and releasing foam material (Fig. 67). By distributing the energy of erratic movements, foam dampers contribute to smoother muscle activity and enhanced stability.

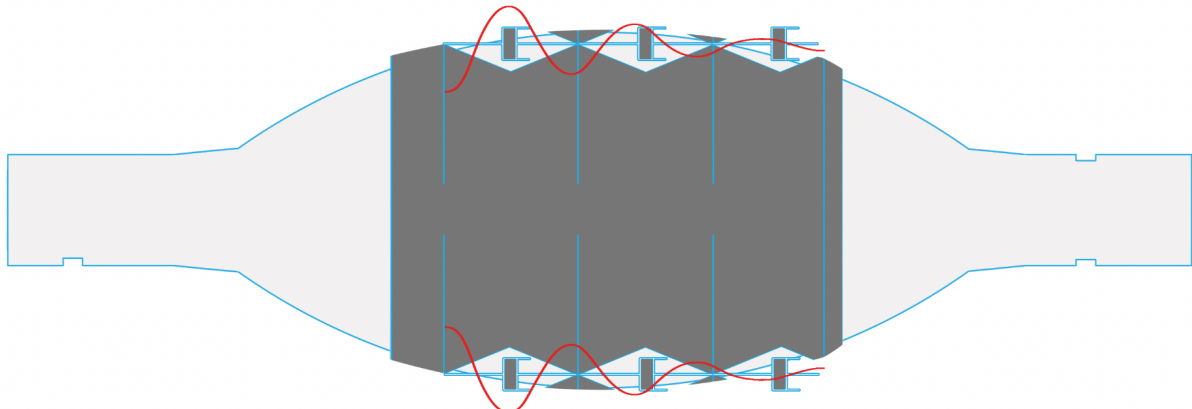


Figure 67: Concept drawing, integration of foam dampers

Another damper that could be integrated are fluid dampers. Fluid dampers offer dynamic damping capabilities by utilizing fluid properties to resist motion. Integrating water-based or viscous fluids within the sheet allows for adjustable damping levels, accommodating varying levels of muscle contractions. This adaptability ensures consistent damping across different movement intensities, providing precise control over muscle assistance.

Magnetorheological dampers present an innovative approach to damping by utilizing magnetic fields to control fluid viscosity (Fig. 68). By embedding magnetorheological fluids within the origami-inspired sheet and applying magnetic fields, the viscosity of the fluid can be adjusted in real-time. This enables customizable damping characteristics tailored to the user's specific muscle assistance needs.

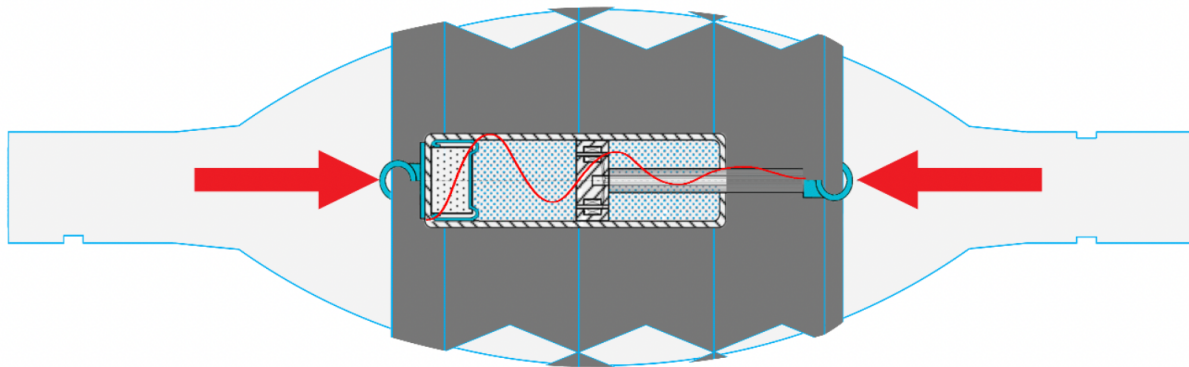


Figure 68: Concept drawing, integration of magnetorheological dampers

Finally, as intention of the origami-inspired sheets to move towards more practical applications in clinical settings, ensuring biocompatibility and compatibility with invasive procedures becomes important. Future research should focus the comprehensive evaluation of the biocompatibility of materials utilized in origami-inspired sheets. This entails conducting thorough assessments to identify any potential risks of adverse reactions or tissue rejection, ensuring that the materials are safe and suitable for long-term use within the human body.

Additionally, studies should investigate invasive techniques for implanting origami-inspired sheets on muscle tissue, enabling more direct and targeted muscle assistance. This could involve the development of minimally invasive surgical procedures or implantation techniques that minimize tissue trauma and promote rapid healing. By addressing these challenges, researchers can pave the way for the clinical translation of origami-inspired muscle assistance devices and ultimately improve the quality of life for individuals with muscle impairments.

In conclusion, by addressing the challenges and recommendations outlined for future exploration, origami-inspired technology holds the potential to advance the state-of-the-art in muscle assistance technology. Through these advancements, there is the promise of ultimately improving the quality of life for individuals with muscle impairments, offering enhanced mobility and functionality.

Acknowledgements

First of all, I would like to thank my supervisor, Arno Stienen, for the opportunity to work on this project under his guidance. His clear communication and our weekly meetings greatly contributed to the focus of my thesis and my motivation. The bi-weekly meetings with the graduation group were also incredibly beneficial, providing insights into others' work and helping me realize that I was not the only one facing difficulties during my thesis.

Additionally, I want to extend my gratitude to Thijs Blad for his time and effort, always being ready to help when I encountered challenges. His clear explanations and guidance on technical aspects have been invaluable to my progress and understanding.

Finally, I would also like to thank my family for their unwavering support throughout my studies. Peter, Annemieke, Marit and Elies, your patience, love, and advice have been invaluable to me, helping me through difficult times and providing constant encouragement.

References

- [1] A. F. Ruiz, A. Forner-Cordero, E. Rocon, and J. L. Pons, "Exoskeletons for rehabilitation and motor control," *Proc. First IEEE/RAS-EMBS Int. Conf. Biomed. Robot. Biomechatronics, 2006, BioRob 2006*, vol. 2006, pp. 601–606, 2006, doi: 10.1109/BIOROB.2006.1639155.
- [2] M. Cardona, K. S. Solanki, and C. E. García Cena, *Springer Briefs In Applied Sciences And Technology: Exoskeleton Robots for Rehabilitation and Healthcare Devices*. 2020.
- [3] J. L. Contreras-Vidal *et al.*, "Powered exoskeletons for bipedal locomotion after spinal cord injury," *J. Neural Eng.*, vol. 13, no. 3, 2016, doi: 10.1088/1741-2560/13/3/031001.
- [4] N. Jurassé, M. Maestrutti, G. Morel, and A. Roby-Brami, "Robotic Prosthetics : Moving Beyond Technical Performance," *IEEE Technol. Soc. Mag.*, vol. 34, no. 2, pp. 71–79, 2015, doi: 10.1109/MTS.2015.2425813.
- [5] K. A. Shorter, J. Xia, E. T. Hsiao-Wecksler, W. K. Durfee, and G. F. Kogler, "Technologies for powered ankle-foot orthotic systems: Possibilities and challenges," *IEEE/ASME Trans. Mechatronics*, vol. 18, no. 1, pp. 337–347, 2013, doi: 10.1109/TMECH.2011.2174799.
- [6] J. H. Hsiao, J. Y. Chang, and C. M. Cheng, "Soft medical robotics: clinical and biomedical applications, challenges, and future directions," *Adv. Robot.*, vol. 33, no. 21, pp. 1099–1111, 2019, doi: 10.1080/01691864.2019.1679251.
- [7] M. Craddock, E. Augustine, S. Konerman, and M. Shin, "Biorobotics: An Overview of Recent Innovations in Artificial Muscles," *Actuators*, vol. 11, no. 6, 2022, doi: 10.3390/act11060168.
- [8] B. Kalita, A. Leonessa, and S. K. Dwivedy, "A Review on the Development of Pneumatic Artificial Muscle Actuators: Force Model and Application," *Actuators*, vol. 11, no. 10, pp. 1–28, 2022, doi: 10.3390/act11100288.
- [9] R. Tiwari, M. A. Meller, K. B. Wajcs, C. Moses, I. Reveles, and E. Garcia, "Hydraulic artificial muscles," *J. Intell. Mater. Syst. Struct.*, vol. 23, no. 3, pp. 301–312, 2012, doi: 10.1177/1045389X12438627.
- [10] C. Naresh, P. S. C. Bose, and C. S. P. Rao, "Shape memory alloys: A state of art review," *IOP Conf. Ser. Mater. Sci. Eng.*, vol. 149, no. 1, 2016, doi: 10.1088/1757-899X/149/1/012054.
- [11] Y. Bar-cohen and J. P. L. Caltech, "Artificial Muscles using Electroactive Polymers (EAP): Capabilities , Challenges and Potential," pp. 1–14, 2005.
- [12] L. M. Fonseca, G. V. Rodrigues, and M. A. Savi, "An overview of the mechanical description of origami-inspired systems and structures," *Int. J. Mech. Sci.*, vol. 223, no. August 2021, p. 107316, 2022, doi: 10.1016/j.ijmecsci.2022.107316.
- [13] A. Zaghoul and G. M. Bone, "Origami-Inspired Soft Pneumatic Actuators: Generalization and Design Optimization," *Actuators*, vol. 12, no. 2. 2023, doi: 10.3390/act12020072.
- [14] S. Li, D. M. Vogt, D. Rus, and R. J. Wood, "Fluid-driven origami-inspired artificial muscles," *Proc. Natl. Acad. Sci. U. S. A.*, vol. 114, no. 50, pp. 13132–13137, 2017, doi: 10.1073/pnas.1713450114.
- [15] S. Li *et al.*, "A Vacuum-driven Origami ' Magic-ball ' Soft Gripper," pp. 7401–7408, 2019.

- [16] M. Hoehn, *Anatomy and Physiology*, 11th editi. Pearson, 2018.
- [17] S. Hyland and M. Varacallo, "Anatomy, Shoulder and Upper Limb, Clavicle," *StatPearls*, no. December, 2019, [Online]. Available: <http://www.ncbi.nlm.nih.gov/pubmed/30252246>.
- [18] C. M. Nelson, J. P. A. Dewald, and W. M. Murray, "In vivo measurements of biceps brachii and triceps brachii fascicle lengths using extended field-of-view ultrasound," *J. Biomech.*, vol. 49, no. 9, pp. 1948–1952, 2016, doi: 10.1016/j.jbiomech.2016.03.040.
- [19] M. Szewczyk, Bartłomiej; Sanudo, Jose Ramon; Podgórski, "A Proposal for a New Classification of the Supernumerary Heads of the Biceps Brachii Muscle," *Hindawi*, 2022.
- [20] R. Khan, K. S. Satyapal, N. Naidoo, and L. Lazarus, "Long head of biceps brachii tendon and transverse humeral ligament morphometry and their associated pathology," *Folia Morphol.*, vol. 79, no. 2, pp. 359–365, 2020, doi: 10.5603/FM.a2019.0075.
- [21] E. Nygaard, M. Houston, Y. Suzuki, K. Jørgensen, and B. Saltin, "Morphology of the brachial biceps muscle and elbow flexion in man," *Acta Physiol. Scand.*, vol. 117, no. 2, pp. 287–292, 1983, doi: 10.1111/j.1748-1716.1983.tb07208.x.
- [22] S. D. Joshi, S. S. Joshi, Y. A. Sontakke, and P. S. Mittal, "Some details of morphology of biceps brachii and its functional relevance," *J. Anat. Soc. India*, vol. 63, no. 1, pp. 24–29, 2014, doi: 10.1016/j.jasi.2014.03.001.
- [23] T. Matta, R. Simão, B. F. De Salles, J. Spinetti, and L. F. Oliveira, "Strength training's chronic effects on muscle architecture parameters of different arm sites," *J. Strength Cond. Res.*, vol. 25, no. 6, pp. 1711–1717, 2011, doi: 10.1519/JSC.0b013e3181dba162.
- [24] S. J. Fellows and P. M. Rack, "Changes in the length of the human biceps brachii muscle during elbow movements.," *J. Physiol.*, vol. 383, no. 1, pp. 405–412, 1987, doi: 10.1113/jphysiol.1987.sp016416.
- [25] G. S. Athwal, S. P. Steinmann, and D. M. Rispoli, "The Distal Biceps Tendon: Footprint and Relevant Clinical Anatomy," *J. Hand Surg. Am.*, vol. 32, no. 8, pp. 1225–1229, 2007, doi: 10.1016/j.jhsa.2007.05.027.
- [26] R. Drillis, "Body Segment Parameters," *Electron. Commun. Eng. J.*, vol. 1, no. 2, pp. 61–70, 1989, doi: 10.1049/ecej:19890011.
- [27] X. Zhang, L. Zhang, Y. Sun, T. Li, and M. Zhou, "Quantitative assessment of biceps brachii muscle stiffness by using Young's modulus–Angle curve during passive stretching in stroke patients," *Front. Physiol.*, vol. 14, no. March, pp. 1–10, 2023, doi: 10.3389/fphys.2023.907337.
- [28] R. Bott, "Mechanical Properties and Durability of Natural Rubber Compounds and Composites," *Igarss 2014*, no. 1, pp. 1–5, 2014.
- [29] D. Ahirwar, A. Telang, R. Purohit, and A. Namdev, "A short review on polyurethane polymer composite," *Mater. Today Proc.*, vol. 62, pp. 3804–3810, 2022, doi: 10.1016/j.matpr.2022.04.481.
- [30] Polytek, "PlatSil® Silicone Gels." pp. 1–2.
- [31] H. Dsm, H. P. F. Eisterweg, P. N. Heerlen, and N. L. The, "Performance improvement of Dyneema in ropes."
- [32] Epsilon Technology Corporation, "Tech Understanding Warmup Drift Tech," 2017. <https://www.epsilontech.com/understanding-extensometer-warmup-drift/>.
- [33] D. E. Mortenson *et al.*, "Fluid-driven origami-inspired artificial muscles supporting materials: Appendix," *Proc. Natl. Acad. Sci.*, vol. 1, pp. 1–18, 2017.
- [34] M. Assad and N. Jackson, "Biocompatibility Evaluation of Orthopedic Biomaterials and

- Medical Devices: A Review of Safety and Efficacy Models," *Encycl. Biomed. Eng.*, vol. 1–3, pp. 281–309, Jan. 2019, doi: 10.1016/B978-0-12-801238-3.11104-3.
- [35] J. M. C. Zhao, Xiaobin, *Update on Medical Plasticised PVC*. 2009.
- [36] H. Bergmeister *et al.*, "Biodegradable, thermoplastic polyurethane grafts for small diameter vascular replacements," *Acta Biomater.*, vol. 11, no. 1, pp. 104–113, Jan. 2015, doi: 10.1016/J.ACTBIO.2014.09.003.
- [37] V. Butnaru, Mario; Macocinsch Doina; Harabagiu, *Polyurethane*. .
- [38] S. Dimitrievska *et al.*, "Effect of Sterilization on Non-woven Polyethylene Terephthalate Fiber Structures for Vascular Grafts," *Macromol. Biosci.*, vol. 11, no. 1, pp. 13–21, 2011, doi: 10.1002/mabi.201000268.
- [39] I. L. Lo, C. Y. Kao, T. H. Huang, C. Te Ho, and C. T. Kao, "The cytotoxicity assessment of different clear aligner materials," *J. Dent. Sci.*, no. xxxx, 2024, doi: 10.1016/j.jds.2024.05.025.
- [40] M. Shakiba *et al.*, "Nylon—A material introduction and overview for biomedical applications," *Polym. Adv. Technol.*, vol. 32, no. 9, pp. 3368–3383, 2021, doi: 10.1002/pat.5372.
- [41] Q. Zhang, H. Fang, and J. Xu, "Tunable dynamics in Yoshimura origami by harnessing pneumatic pressure," *J. Sound Vib.*, vol. 544, no. October 2022, p. 117407, 2023, doi: 10.1016/j.jsv.2022.117407.
- [42] S. Liu, G. Lu, Y. Chen, and Y. W. Leong, "Deformation of the Miura-ori patterned sheet," *Int. J. Mech. Sci.*, vol. 99, pp. 130–142, 2015, doi: 10.1016/j.ijmecsci.2015.05.009.
- [43] S. Kuriyama, M. Ding, Y. Kurita, T. Ogasawara, and J. Ueda, "Flexible sensor for McKibben pneumatic actuator," *Proc. IEEE Sensors*, vol. 3, no. 6, pp. 520–525, 2009, doi: 10.1109/ICSENS.2009.5398292.

Appendices

Appendix A
Technical drawings

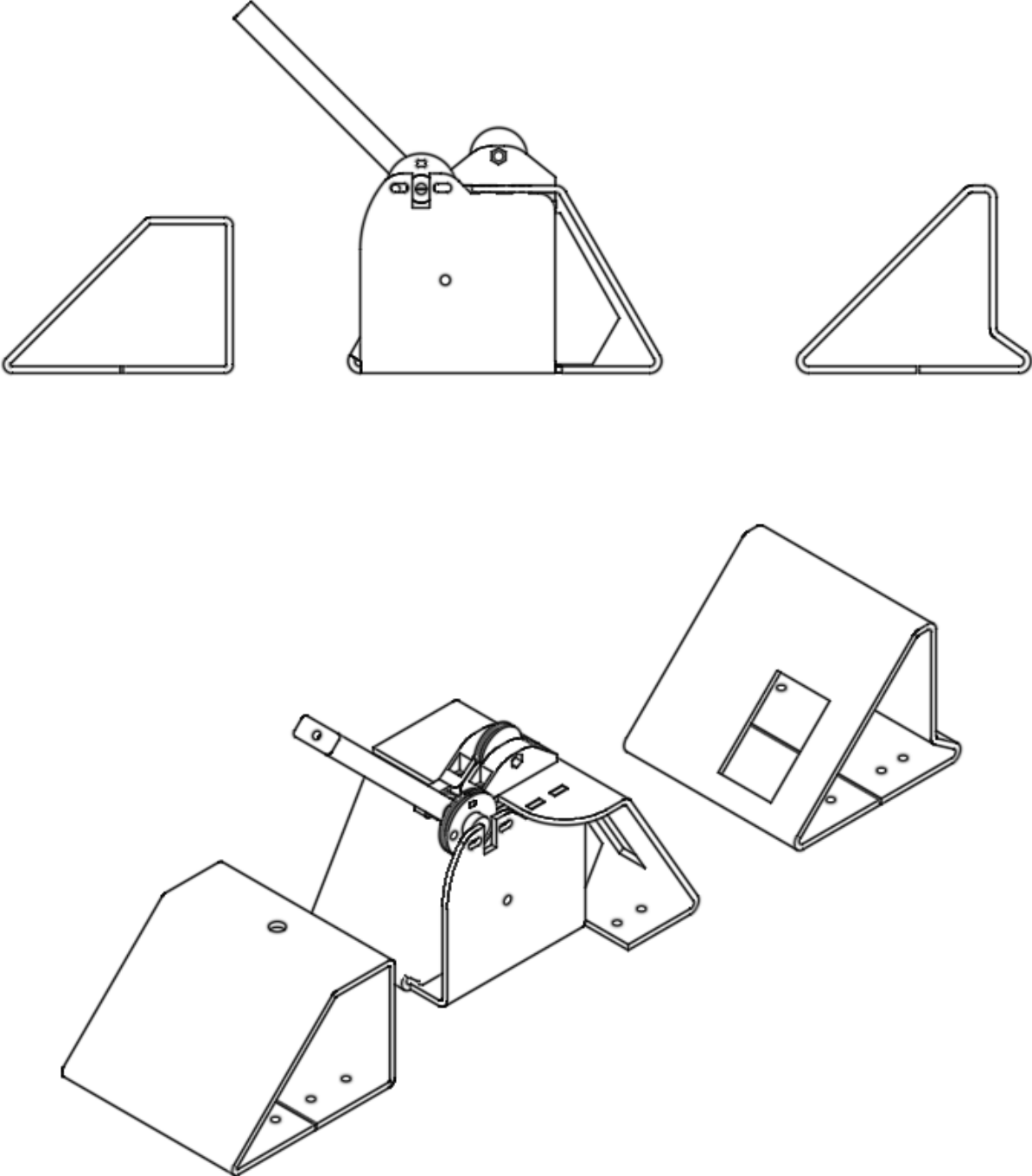


Figure 69: Overview test setup assembly

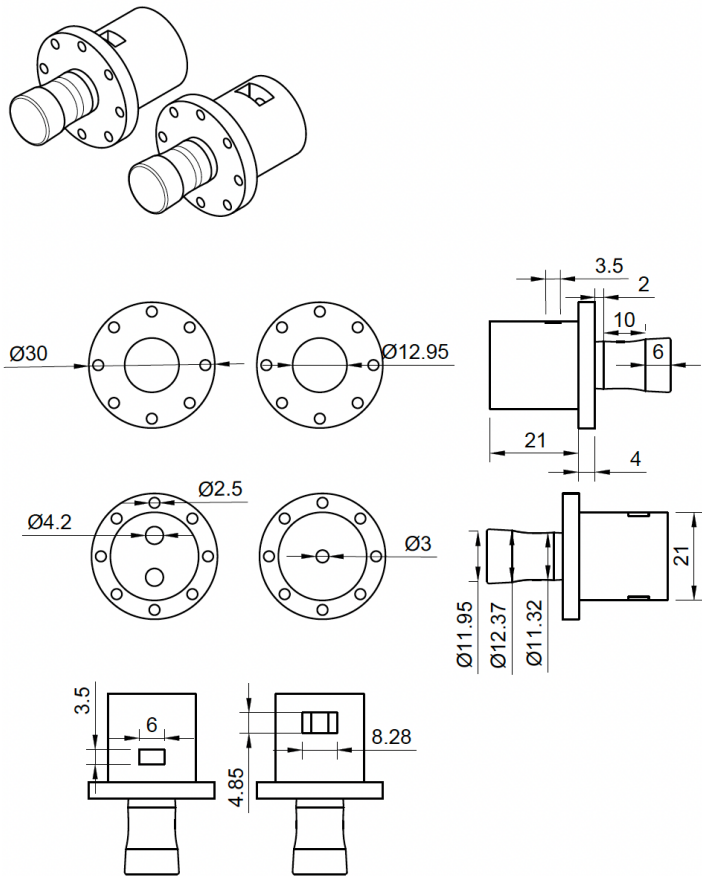


Figure 69: Technical drawing and measures of the end caps

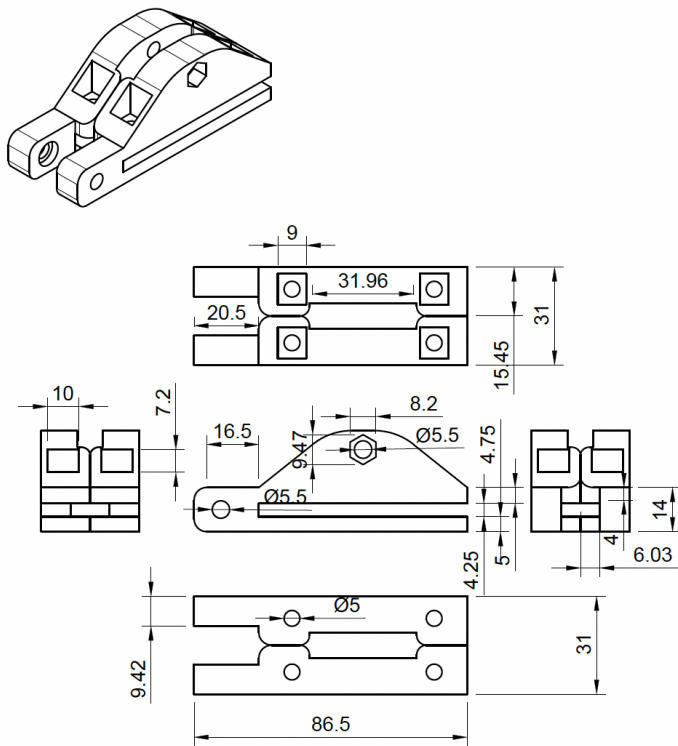


Figure 70: Technical drawing and measures of the pulley bracket

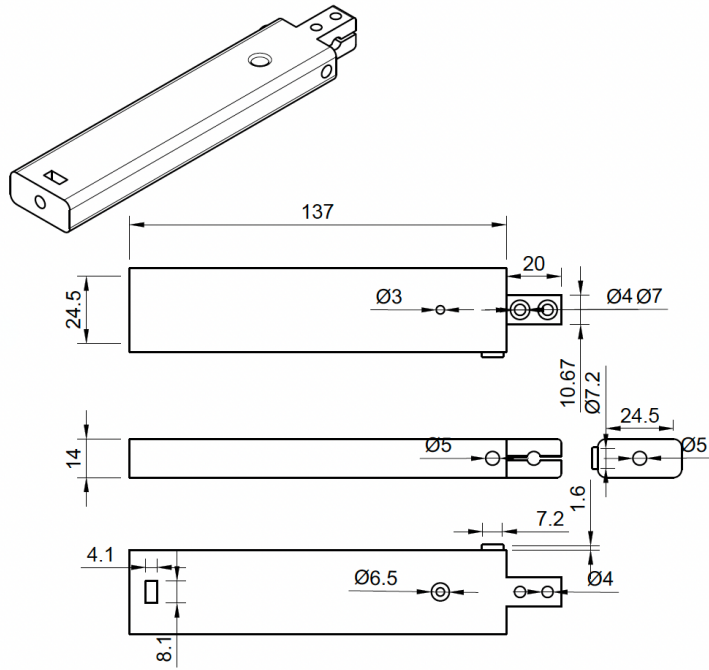


Figure 72: Technical drawing and measures of the arm

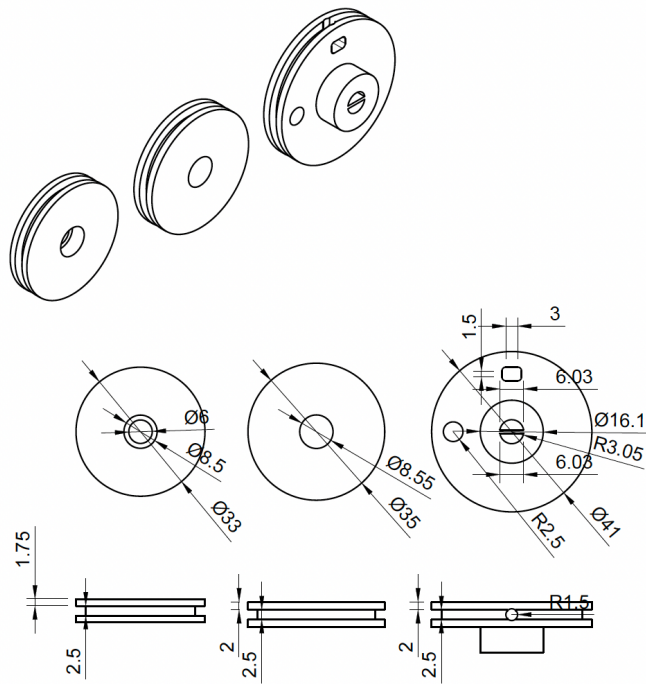


Figure 71: Technical drawing and measures of the pulley's

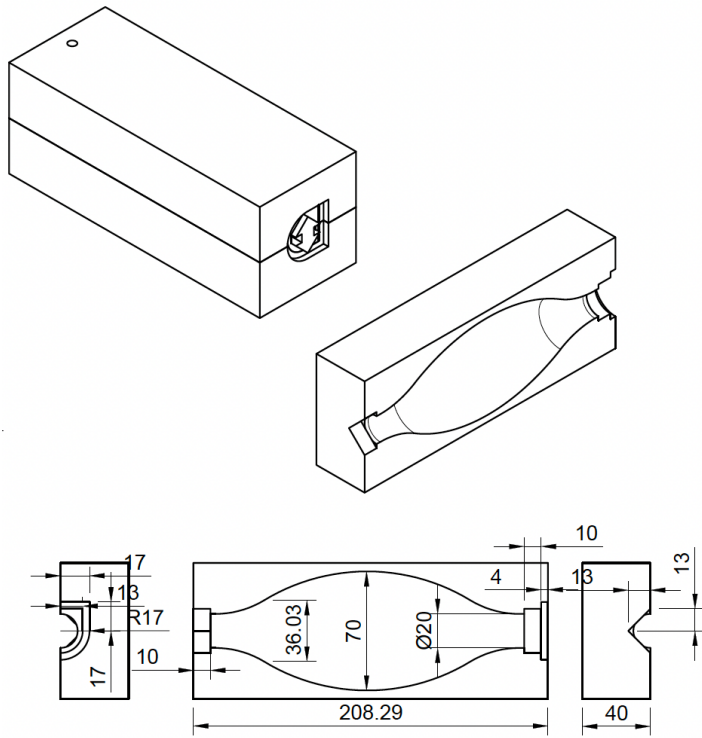


Figure 74: Technical drawing and measures of the silicon muscle moulding

Appendix B
Electrical diagram

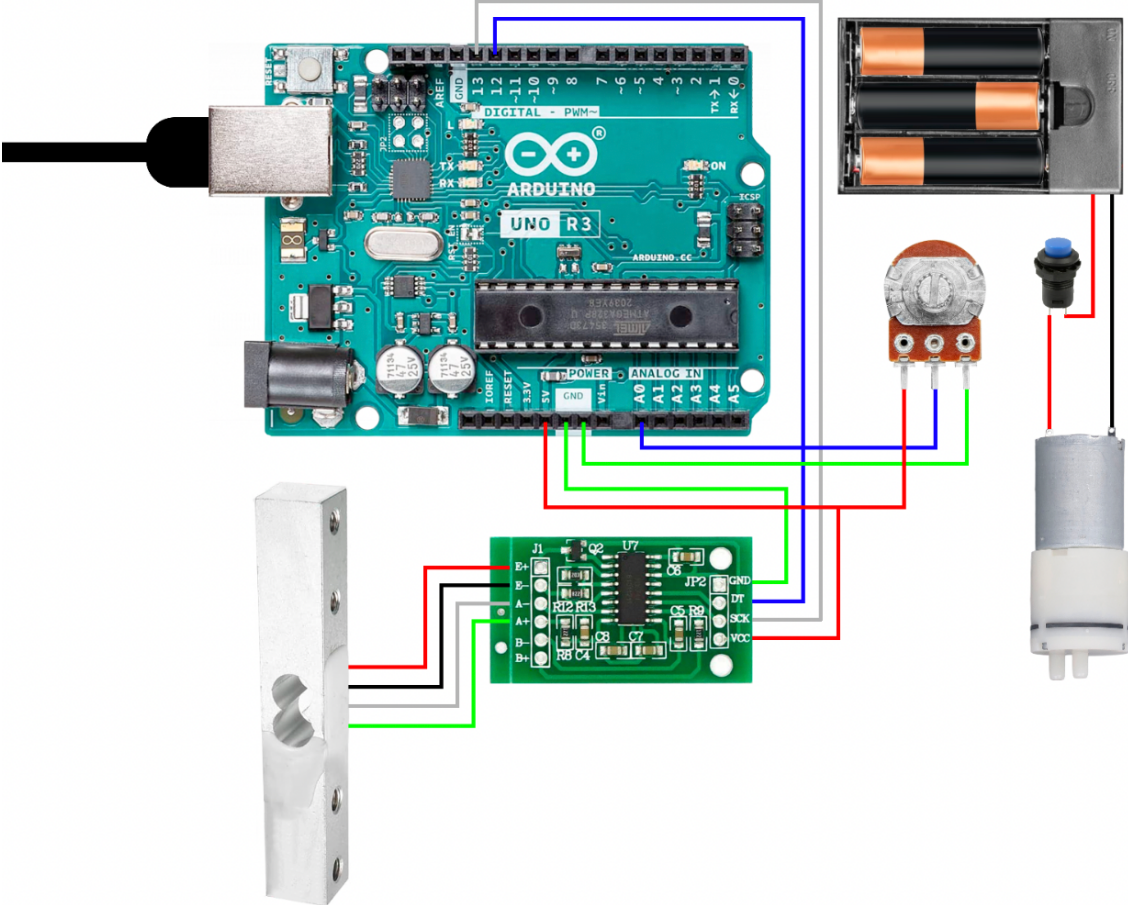


Figure 75: Electrical diagram, Arduino, loadcell, potentiometer and vacuum pump

Appendix C

Matlab Program

Calibration class

```
%% Calibration Class
classdef calibration < dynamicprops
    properties(Access = public)
        n = [] % Number of readings
        known_weight = [] % Calibration weight
    end
    properties(Access = private)
        tare_weight = 0
        scale_factor = 1
    end
    methods(Access = public)
        %% Calibration Function
        function cal = calibration(varargin)
            % Check the number of inputs
            if nargin < 1
                error('Not enough input arguments.');
            elseif nargin > 1
                error('Too many input arguments.');
            end
            % Check the inputs
            if varargin{1} < 0
                error('The number of readings must be positive');
            elseif ~isnumeric(varargin{1}) || ~isscalar(varargin{1})
                error('Incorrect type');
            end
            cal.n = varargin{1};
        end
        %% Tare Function
        function value = tare(obj, HX711_obj)
            value = 1:1:obj.n;
            for i = 1:1:obj.n
                value(i) = read_HX711(HX711_obj);
                if check_conversion(obj, value(i))
                    value(i) = NaN;
                end
            end
            value = mean(value, 'omitnan');
            obj.tare_weight = value;
        end
        %% Scale Function
        function value = scale(obj, HX711_obj, weight_for_calibration)
            if isempty(weight_for_calibration)
                error('No weight specified for calibration.');
            end
            value = 1:1:obj.n;
            for i = 1:1:obj.n
                value(i) = read_HX711(HX711_obj);
                if check_conversion(obj, value(i))
                    value(i) = NaN;
                end
            end
            ev_value = mean(value, 'omitnan');
            % Use the provided weight for calibration
            obj.known_weight = weight_for_calibration;
            value = (ev_value - obj.tare_weight) / obj.known_weight;
            obj.scale_factor = value;
        end
        %% Weight Function
        function weight = get_weight(obj, HX711_obj, varargin)
```

Figure 76: page 1 of calibration class

```

if nargin < 2
    error('MyComponent:incorrectType',...
        'Not enough input arguments:\nprovide *calibration* and *HX711* %<
s',...
        'class objects in this order.');
```

```

elseif nargin > 3
    error('MyComponent:incorrectType',...
        'Too many input arguments:\nprovide *calibration* and *HX711* %<
s',...
        'class objects in this order. You can also provide the number of<
readings');
```

```

end
if ~isempty(varargin)
    if ~isnumeric(varargin{1}) || ~isscalar(varargin{1})
        error('Incorrect type');
    end
end
if isempty(varargin)

    % Raw Reading
    val = read_HX711(HX711_obj);
    if check_conversion(obj,val)
        weight = NaN;
    else
        weight = (val - obj.tare_weight)/obj.scale_factor;
    end
else

    % Average of multiple readings
    k = varargin{1};
    value = 1:1:k;
    for i=1:1:k
        value(i) = read_HX711(HX711_obj);
        if check_conversion(obj,value(i))
            value(i) = NaN;
        end
    end
    ev_value = mean(value,'omitnan');
    weight = (ev_value - obj.tare_weight)/obj.scale_factor;
end
end

%% Statistical Function
function [Av,Std] = stat(obj,HX711_obj,k)
    if nargin < 3
        error('MyComponent:incorrectType',...
            'Not enough input arguments:\nprovide *calibration* and *HX711* %<
s',...
            'class objects in this order then the number of readings.');
```

```

    elseif nargin > 3
        error('MyComponent:incorrectType',...
            'Too many input arguments:\nprovide *calibration* and *HX711* %<
s',...
            'class objects in this order then the number of readings');
```

```

    end
    if ~isnumeric(k) || ~isscalar(k)
        error('Incorrect type');
    end
    weight = 1:1:k;
    for i=1:1:k
        val = read_HX711(HX711_obj);
        weight(i) = (val - obj.tare_weight)/obj.scale_factor;

        if check_conversion(obj,val)
            weight(i) = NaN;
        end
    end
    Av = mean(weight,'omitnan');
    Std = std(weight,'omitnan');
end
end

%% Check HX711 Data
function incorrect = check_conversion(~,val)
    if (val == hex2dec('800000') || val == hex2dec('7FFFFFFF'))
        incorrect = true;
    else
        incorrect = false;
    end
end
end
end
end
```

Figure 77: page 2 of calibration class

Calibration main

```
%% Init
% Pins
potPin = 'A0';
pressurePin = 'A1';
Dout = 'D12';
sck = 'D13';

%Arrays for real-time plotting
timeValues = [];
weightValues = [];
potentiometerValues = [];
pressureValues = [];

%% LoadCell Calibration
performCalibrationLoadCell = input('Wil je een nieuwe kalibratie voor de load cell
uitvoeren? (y/n): ', 's');

if lower(performCalibrationLoadCell) == 'y'

    %Init
    clear a loadCell;
    a = arduino('/dev/cu.usbmodem14601');
    loadCell = addon(a, 'advancedHX711/advanced_HX711', 'Pins', {Dout, sck},
'Interrupt', true);

    % Calibration object
    iteraties = 100;
    cal = calibration(iteraties); % aantal metingen voor kalibratie, het bekende
gewicht zal later gespecificeerd

    % Tare
    disp('Maak de loadcell vrij van gewicht');
    input('Druk op Enter als je klaar bent om te taren...');
    cal.tare(loadCell);

    % scale
    weight_for_calibration = input('Voer het gewicht (in gram) voor kalibratie in: ');
    cal.scale(loadCell, weight_for_calibration);
else
    disp('Gebruikt de laatst gebruikte kalibratie');
end

%% Potentiometer Calibration
performCalibrationPotentiometer = input('Wil je een nieuwe kalibratie voor de
potentiometer uitvoeren? (y/n): ', 's');

if lower(performCalibrationPotentiometer) == 'y'
    % Automatische potentiometer kalibratie
    initialPotValue = readVoltage(a, potPin);
else
    % Gebruik de laatst bekende kalibratie voor de potentiometer
    disp('Gebruik de laatst bekende kalibratie voor de potentiometer.');
```

```
end

%% Figure Init
% Create subplot for real-time plot
figure;
subplot(3, 1, 1); % Verander naar 3 subplots
loadCellPlot = plot(NaN, NaN, '-b');
xlabel('Time');
ylabel('Weight (grams)');
title('Real-Time Load Cell Plot');
```

Figure 78: page 1 of calibration main

```

grid on;
hold on;

subplot(3, 1, 2);
potentiometerPlot = plot(NaN, NaN, '-r');
xlabel('Time');
ylabel('Angle (degrees)');
title('Real-Time Potentiometer Plot');
grid on;
hold on;

subplot(3, 1, 3); % Voeg een subplot toe voor de druksensor
pressurePlot = plot(NaN, NaN, '-g');
xlabel('Time');
ylabel('Pressure (bar)');
title('Real-Time Pressure Plot');
grid on;
hold on;

%% Resultaten
while true
    % Voeg een korte vertraging toe voor elke meting
    pause(0.1); % Pas de vertraging aan indien nodig

    % Ontvang gewicht
    currentWeight = cal.get_weight(loadCell);

    % Lees potentiometerwaarde en corrigeer met initiële waarde
    potVoltage = readVoltage(a, potPin) - initialPotValue;

    % Converteer de potentiometerwaarde naar graden
    potDegrees = (potVoltage / 5) * 270;

    % Lees de drukwaarde van de druksensor
    pressureVoltage = readVoltage(a, pressurePin);
    pressure = pressureVoltage; % 1V komt overeen met 1 bar

    % Weergeef het resultaat
    disp(['Gewicht: ' num2str(currentWeight) ' gram, Potentiometer: ' num2str(
potDegrees) ' graden, Druk: ' num2str(pressure) ' bar']);

    % Store current time, weight, potentiometer, and pressure value for real-time
plotting
    currentTime = datetime('now');

    % Update timeValues, weightValues, potentiometerValues, and pressureValues arrays
    timeValues = [timeValues, currentTime];
    weightValues = [weightValues, currentWeight];
    potentiometerValues = [potentiometerValues, potDegrees];
    pressureValues = [pressureValues, pressure];

    % Convert datetime values to seconds
    timeSeconds = seconds(timeValues - timeValues(1));

    % Update real-time load cell plot
    subplot(3, 1, 1);
    set(loadCellPlot, 'XData', timeSeconds, 'YData', weightValues);
    xlabel('Time (s)');
    drawnow; % Update the load cell plot

    % Update real-time potentiometer plot
    subplot(3, 1, 2);

    set(potentiometerPlot, 'XData', timeSeconds, 'YData', potentiometerValues);
    xlabel('Time (s)');
    drawnow; % Update the potentiometer plot

    % Update real-time pressure plot
    subplot(3, 1, 3);
    set(pressurePlot, 'XData', timeSeconds, 'YData', pressureValues);
    xlabel('Time (s)');
    drawnow; % Update the pressure plot
    ylim([0 1]);
end

```

Figure 79: page 2 of calibration main

Origami inspired sheet main

```
%% Init
% Pins
potPin = 'A0';
pressurePin = 'A1';
Dout = 'D12';
sck = 'D13';

% Arrays for real-time plotting
timeValues = [];
weightValues = [];
forceValues = []; % Changed to store force in Newton
potentiometerValues = [];
pressureValues = [];

%% LoadCell Calibration
performCalibrationLoadCell = input('Wil je een nieuwe kalibratie voor de load cell
uitvoeren? (y/n): ', 's');

if lower(performCalibrationLoadCell) == 'y'

    % Init
    clear a loadCell;
    a = arduino('/dev/cu.usbmodem14601');
    loadCell = addon(a, 'advancedHX711/advanced_HX711', 'Pins', {Dout, sck},
'Interrupt', true);

    % Calibration object
    iteraties = 100;
    cal = calibration(iteraties); % aantal metingen voor kalibratie

    % Tare
    disp('Maak de loadcell vrij van gewicht');
    input('Druk op Enter als je klaar bent om te taren..');
    cal.tare(loadCell);

    % scale
    weight_for_calibration = input('Voer het gewicht (in gram) voor kalibratie in: ');
    cal.scale(loadCell, weight_for_calibration);
else
    disp('Gebruikt de laatst gebruikte kalibratie');
end

%% Potentiometer Calibration
performCalibrationPotentiometer = input('Wil je een nieuwe kalibratie voor de
potentiometer uitvoeren? (y/n): ', 's');

if lower(performCalibrationPotentiometer) == 'y'
    % Automatische potentiometer kalibratie
    initialPotValue = readVoltage(a, potPin);
else
    % Gebruik de laatst bekende kalibratie voor de potentiometer
    disp('Gebruik de laatst bekende kalibratie voor de potentiometer.');
```

```
end

%% Figure Init
% Create subplot for real-time plot
figure;
subplot(3, 1, 1); % Verander naar 3 subplots
loadCellPlot = plot(NaN, NaN, '-b');
xlabel('Time');
ylabel('Force (Newton)'); % Changed to Newton
title('Real-Time Load Cell Plot');
```

Figure 80: page 1 of Origami inspired sheet main


```

grid on;
hold on;

subplot(3, 1, 2);
potentiometerPlot = plot(NaN, NaN, '-r');
xlabel('Time');
ylabel('Angle (degrees)');
title('Real-Time Potentiometer Plot');
grid on;
hold on;

subplot(3, 1, 3); % Voeg een subplot toe voor de druksensor
pressurePlot = plot(NaN, NaN, '-g');
xlabel('Time');
ylabel('Pressure (bar)');
title('Real-Time Pressure Plot');
grid on;
hold on;

%% Resultaten
while true
    % Voeg een korte vertraging toe voor elke meting
    pause(0.1); % Pas de vertraging aan indien nodig

    % Ontvang gewicht in gram
    currentWeight = cal.get_weight(loadCell);

    % Converteer gewicht naar kracht (N) zonder zwaartekracht correctie
    currentForce = currentWeight * 9.81 / 1000; % Van gram naar kg (1 kgf ≈ 9.81 N,
    maar hier direct 1:1 verhouding)

    % Lees potentiometerwaarde en corrigeer met initiële waarde
    potVoltage = readVoltage(a, potPin) - initialPotValue;

    % Converteer de potentiometerwaarde naar graden
    potDegrees = (potVoltage / 5) * 270;

    % Lees de drukwaarde van de druksensor
    pressureVoltage = readVoltage(a, pressurePin);
    pressure = pressureVoltage; % 1V komt overeen met 1 bar

    % Weergeef het resultaat
    disp(['Kracht: ' num2str(currentForce) ' Newton, Potentiometer: ' num2str(
    potDegrees) ' graden, Druk: ' num2str(pressure) ' bar']);

    % Store current time, weight, force, potentiometer, and pressure value for real-
time plotting
    currentTime = datetime('now');

    % Update timeValues, weightValues, forceValues, potentiometerValues, and
pressureValues arrays
    timeValues = [timeValues, currentTime];
    weightValues = [weightValues, currentWeight]; % Store weight in grams
    forceValues = [forceValues, currentForce]; % Store force in Newton
    potentiometerValues = [potentiometerValues, potDegrees];
    pressureValues = [pressureValues, pressure];

    % Convert datetime values to seconds
    timeSeconds = seconds(timeValues - timeValues(1));

    % Update real-time load cell plot
    subplot(3, 1, 1);
    set(loadCellPlot, 'XData', timeSeconds, 'YData', forceValues); % Plot force in
Newton
    xlabel('Time (s)');
    drawnow; % Update the load cell plot

    % Update real-time potentiometer plot
    subplot(3, 1, 2);
    set(potentiometerPlot, 'XData', timeSeconds, 'YData', potentiometerValues);
    xlabel('Time (s)');
    drawnow; % Update the potentiometer plot

    % Update real-time pressure plot
    subplot(3, 1, 3);
    set(pressurePlot, 'XData', timeSeconds, 'YData', pressureValues);
    xlabel('Time (s)');
    drawnow; % Update the pressure plot
    ylim([0 1]);
end

```

Figure 81: page 2 of Origami inspired sheet main

Appendix D

Literature study

Classification and review of mechatronics that are suitable for implantation to facilitate skeletal movement

Systematic literature review

By

J.P.G. van de Kamp

Student number: 4975588
Supervisor: Dr. ir. A.H.A. Stienen

Abstract

This paper presents an evaluation of techniques for facilitating skeletal movement through implantable actuators, dampers, and springs. The aim of the study is to classify and assess the feasibility of these techniques for implantation in the human body by evaluating their advantages and disadvantages compared to criteria for implantation. Based on the assessment, it can be concluded that McKibben actuators, carbon nanotube actuators, Yoshimura-, Miura-ori-, and Kresling pattern origami actuators, magnetorheological fluid dampers, rotary magnetorheological fluid dampers with limited angle, leaf springs, and shape memory alloy springs are the most suitable techniques for implantation to facilitate skeletal movement.

Although this study identifies areas for further research, this study provides valuable insights into the suitability of these techniques for implantation to guide the development of new implantable devices for skeletal movement, which can contribute to the development for artificial muscles.

Table of contents

Abstract	ii
Introduction	1
Method	2
2.1 Eligibility Criteria	2
2.2 Information Sources	3
2.3 Search Strategy	3
2.4 Selection Process	4
2.5 Data collection Process	4
2.6 Data Items	4
2.7 Study Risk of bias assessment	5
2.8 Effect measures	6
2.9 Synthesis methods	6
2.10 Reporting bias assessment	6
Results	7
3.1 Study selection	7
3.2 Results of studies	8
3.2.1 Actuators for skeletal movement	8
3.2.2 Dampers for skeletal movement	27
3.2.3 Springs for skeletal movement	33
3.3 Implantability	36
3.3.1 Implantability criteria for actuators	36
3.3.2 Implantability criteria for dampers	37
3.3.3 Implantability criteria for springs	38
3.3.4 Assessment of implantability criteria	38
3.4 Suitability of mechatronic techniques for implantation	39
Discussion	40
Limitations	41
Conclusion	42
Bibliography	43
7.1 Articles	43
7.2 Other	47
7.3 ChatGPT	48
Appendix	49
A1 Characteristics actuators	49
A2 Characteristics dampers	52
A3 Characteristics springs	53
B1 Implantability assessment actuators	54
B2 Implantability assessment dampers	55
B3 Implantability assessment springs	56

Introduction

Artificial muscles are of great interest in various fields of biomechanics, bioelectronics and materials science. The technique is used to mimic muscular movement such as replicating the expansion, contraction and rotation [1]. Although the development of artificial muscles is still in its early stages, this technology offers promising results in the medical sector. For instance, the design of prosthetics can be improved with artificial muscles by making them more resembling normal limbs and therefore easier to use [2] [3] [4].

One of the most promising types of artificial muscles are implantable artificial muscles, which can be implanted in the human body to provide mechanical assistance or to replace lost or damaged tissue. People with paralysis or neuromuscular diseases can both benefit from artificial muscles. For example, someone with facial paralysis can be helped by placing an implantable artificial muscle around the eye, enabling them to close the eye again [5] [6].

In recent years, research has been conducted in many different fields of engineering on various types of artificial muscles and ways to control them. For example, there are artificial muscles that can be controlled pneumatically [7] or hydraulically [8]. There are materials, Shape memory alloys (SMA), that can return to their original state after stretching by heating (usually by electric current), just like a muscle contracts and relaxes [9]. Significant progress has also been made in controlling artificial muscles using electroactive polymers (EAP). EAP's are polymers that deform under electric current [10] and allow for many different types due to the wide range of materials available [11].

As there has already been extensive research into various materials and concentrating exclusively on artificial muscles could be too specific and might lead to the exclusion of potential solutions for other types of skeletal movement. Therefore, this literature review will focus on mechatronic solutions that can facilitate skeletal movement, including artificial muscles, exoskeletons, orthotics and prosthetics.

Mechatronics combines mechanical, electrical, and computer engineering to create autonomous systems that respond to environmental changes and perform tasks independently. This integration includes sensors, actuators, controllers, springs, and dampers.

The overall objective of this literature is to define and classify the different types of mechatronic techniques that can be implanted in order to facilitate skeletal movement. For the mechatronics, this literature review will solely focus on actuators, dampers, and springs used in exoskeletons, artificial muscles, orthotics, and prosthetics. These techniques will be described, along with their application, advantages and disadvantages. The following chapter focuses on implantability criteria for actuators, dampers and springs. Then, the previously described techniques are evaluated for their potential as an implantable technique to be used for skeletal movement. Finally, the conclusion and discussion are presented.

2

Method

In this literature review, the PRISMA checklist [12] was used as a guide for ensuring the completeness and transparency of the process. The PRISMA (Preferred Reporting Items for Systematic Reviews and Meta-Analyses) checklist is a tool used to ensure a transparent and comprehensive reporting of systematic reviews and meta-analyses. However, due to the checklist's focus on clinical research, some of its items were not applicable to the topic of this literature review. As such, adjustments to the checklist items were made to better suit the objectives and to ensure that it remained relevant to the topic. This approach helped to identify relevant studies and to synthesize their findings in a comprehensive and meaningful way. In adherence to the PRISMA structure, the certainty assessment was excluded from the review. This decision was made because assessing the certainty of evidence for an outcome is a complex and elaborate process that is more applicable for clinical research studies.

2.1 Eligibility Criteria

The PICO framework [13] was used to define eligibility criteria. The PICO framework is a tool typically used to structure a clinical research. It consists of four components:

- Population/ patient: The group of individuals or patients being studied.
- Intervention/ treatment: The treatment or intervention being studied.
- Comparison: The comparison of alternative interventions.
- Outcome: The desired outcome or effect of the intervention being studied.

As the research topic is non-clinical and related to mechatronics, adjustments to the PICO framework have been made in order to suit this literature review. The population and comparison part are not applicable; therefore, the focus will be on the intervention, exclusion- and inclusion criteria and outcome.

For the intervention, studies will discuss the development, applications, design and operation of mechatronics that may facilitate skeletal movement or that are capable of functioning as artificial muscles.

This literature review will only include actuators, dampers and springs and will exclude electrical components and embedded systems (computers and control).

The outcome of interest is an overview of traditional, new, and potential mechatronics, with a focus on whether they are implantable or not.

2.2 Information Sources

The online database Google Scholar was used to find relevant information about journal articles, books and conference papers. The search dates were determined based on the specific section of the review. Studies before 2003 contained significant information that was also provided in studies after 2003. Since the studies before 2003 do not reflect the newest trends in the field, only studies published between 2003 and 2023 were included for the section.

2.3 Search Strategy

To identify relevant keywords, the snowball method was initially used. Through this method, it became clear that there is a wide variety of actuators, dampers, and springs present in the categories of orthotics, prosthetics and exoskeletons, alongside artificial muscles.

To further refine the search, a Boolean search strategy was used. The search queries were separated with 'OR', combined with 'AND' and excluded with 'NOT' to generate the full Boolean search query. Furthermore, review papers should only be considered if the search results are excessively numerous.

The five concepts used in the search were:

- One of the mechatronic techniques (actuators, dampers and springs)
- Artificial muscles
- Orthotics
- Prosthetics
- Exoskeletons

The following search terms were included:

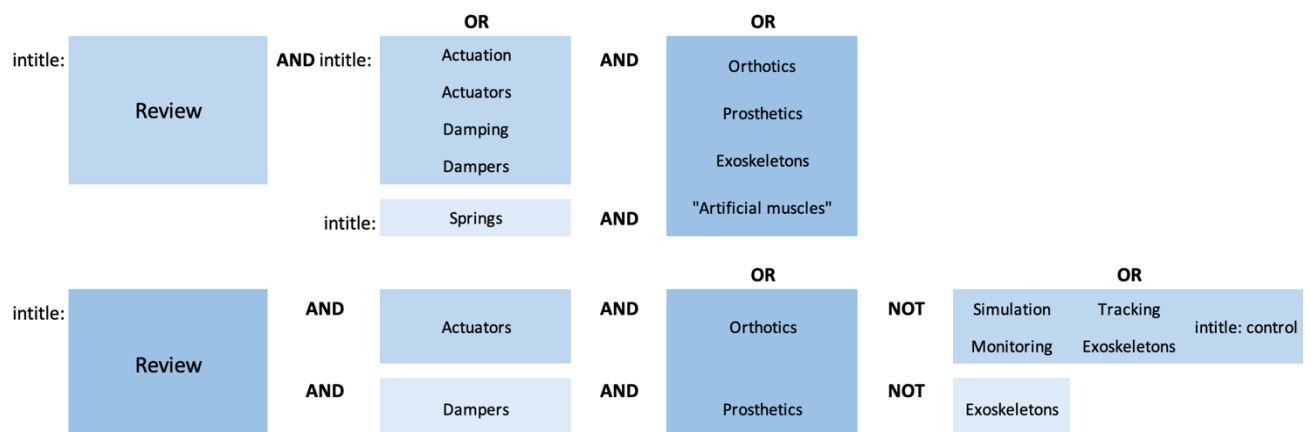


Figure 1: Search terms using Boolean operators

2.4 Selection Process

The selection process involved three stages:

- First, only books, journal articles, conference papers and grey literature were included. While grey literature can provide valuable insights and perspectives, journal articles, books and conference papers provide information in a more comprehensive and detailed manner. Therefore, before including grey literature, studies that discuss the information provided by the grey literature were reviewed.
- Second, the titles and abstracts of the studies obtained through the search strategy were screened for relevance to the concerned subject. Any article that was off topic was excluded. The studies were exported to a reference manager program to exclude any duplicates. Subsequently, the full text of the remaining studies was reviewed for eligibility. Any study that did not meet the previous described criteria was excluded.
- Third, all remaining studies were screened for any additional relevant studies that may have been missed in the initial search. Any uncertainties throughout the selection process were discussed with my supervisor.

2.5 Data collection Process

For the data collection process, the reference manager program Mendeley was used to organize and store all relevant studies.

Once the studies were organized, the full text of each article was read, and relevant data was documented in a table. This table included information such as: name and type of the article, type of technology, advantages, disadvantages and applications. This enabled a systematic comparison and overview of the techniques and possibilities across all included studies. The studies used in this literature study were sorted in various folders belonging to the relevant chapters.

Any uncertainties during the data collection process were discussed with my supervisor.

2.6 Data Items

The data items used in this review were organized into five different categories to ensure that all relevant information was collected:

- The first category aimed to classify the mechatronic techniques for skeletal movement that could advance skeletal movement. This classification was on the data items such as the application, level of development and the year the article was published.
- The second category focused on the specific type of technology being examined. Data items for mechatronic components were based on the function, design and types of aids in actuators, dampers and springs.

- The third category involved the examination of the characteristics of each type of mechatronics. This included advantages and disadvantages, such as power source, force output, response time, durability, biocompatibility, complexity and voltage requirements.
- The fourth category examined the implantability criteria for actuators, dampers and springs. This included the data items of the criteria that was gathered by using ChatGPT (OpenAI, 2021). These criteria included: biocompatibility, size and shape, weight, flexibility, range of motion, durability, response time, actuator force output, actuator voltage requirements, damping force, damping flexibility, spring strength and spring stiffness.
- The fifth category assessed the implantability of the mechatronic technologies. This included the data items of the previous category and additional information that was gathered from the mechatronic technologies.

2.7 Study Risk of bias assessment

A risk of bias assessment focused on the quality and reliability of the studies that was used. The assessment consisted of three steps:

- The first step was to evaluate the selection of studies. As the sole reviewer, only I assessed whether the studies were relevant and unbiased for this literature review. This involved a clear search strategy with multiple criteria. However, there is a possibility that some relevant studies may have been missed due to the exclusion of possible other databases or non-English language studies since the search strategy is completely English oriented.
- The second step involved evaluating the studies' quality, which was done by evaluating the risk of bias across various domains, including publication year, citation count, reputable publishers, country of origin, and the form and location of publication.
- The third step was to ensure that the data presented in the studies were sufficient and consistent. This involved checking that the study protocols were adequately described that the data presented were complete and accurate, and that the conclusions drawn were supported by the data.

While efforts were made to minimize bias in the systematic review, some degree of bias cannot be completely ruled out. Any studies that were deemed to have a high risk of bias were excluded from the analysis or their findings were interpreted with caution.

2.8 Effect measures

Effect measures are used to quantify and measure the outcomes of the intervention or exposure being studied. The effect measures were adjusted in a manner that does not strictly adhere to the PRISMA checklist [12], as this literature is non-clinical.

First a performance scheme was made to assess the effectiveness and efficiency of the technologies. These measures include type of technology, advantages, disadvantages, applications and the location where the technology was applied (Appendix A1, A2, A3).

Then a comparative analysis was conducted to compare and contrast the different types of technologies with the criteria for implantation (Appendix B1, B2, B3).

Finally, a classification scheme was developed (table 1) to categorize the different various types of mechatronics based on their suitability for implantation.

2.9 Synthesis methods

To ensure that the research generates new information, a synthesis method was developed, and the synthesis methods were adjusted to accommodate the non-clinical literature, deviating from the PRISMA checklist [12].

The first step is a descriptive analysis of the studies to identify and characterize the included studies. The screening process then determines the eligible studies by first screening the titles and abstracts, followed by reading the full text. The included studies will undergo a critical evaluation using the certainty assessment. The data extracted from the included studies will be synthesized using a narrative approach that primarily focuses on the experiments conducted, the degree of agreement among the studies, and the potential limitations. The final step is presenting the findings in a clear and transparent manner using tables, figures, and text, along with a discussion of limitations and recommendations for future research.

2.10 Reporting bias assessment

To reduce the risk of publication bias, a comprehensive search will be conducted utilizing one database, as well as searches of grey literature, books, journal articles, and conference papers. In cases where there is doubt or inconsistency in the reported data, The authors of the studies will be contacted for any missing data or for clarifications. Any discrepancies or inconsistencies in the reported data will be documented.

To ensure a transparent and comprehensive reporting, relevant reporting guidelines such as the Preferred Reporting Items for Systematic Reviews and Meta-Analyses (PRISMA) [12] was adjusted for a non-clinical literature review and subsequently was used as a checklist to guide the reporting of the methods and results.

3.1 Study selection

The study selection process involves several steps to identify and select relevant studies from Google Scholar. The search yielded a total of [n=3625] results of which [n=3177] studies being excluded due to their ineligibility marked by automation tools. After screening the title and abstract [n=109] articles remained. These articles consisted of [n=3] books, [n=92] journal articles, [n=7] conference papers, [n=1] grey literature and [n=6] from ChatGPT (OpenAI, 2021). The full texts of these articles were then screened, resulting in [n=80] articles being included in the final review.

The selected articles for the following chapters and subchapters were:

- Method: [n=2]
- Actuators for skeletal movement: [n=29]
- Dampers for skeletal movement: [n=8]
- Springs for skeletal movement: [n=22]
- Implantability: [n=3]

A flowchart of the study selection process has been displayed in figure 2:

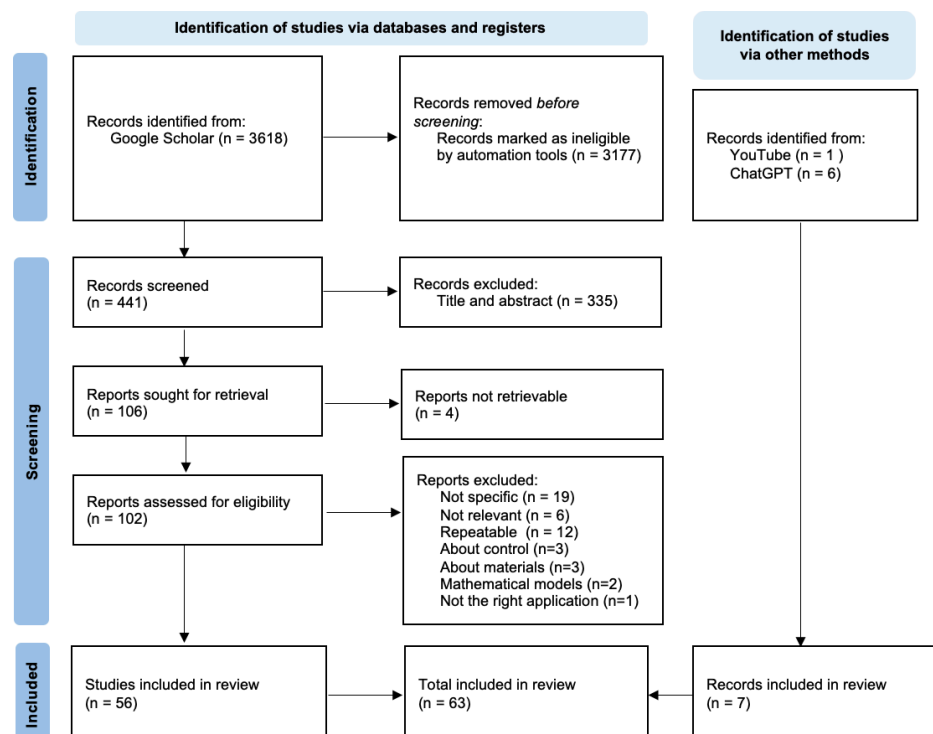


Figure 2: Study selection flowchart

3.2 Results of studies

3.2.1 Actuators for skeletal movement

Extensive study has been done on many types of actuators for skeletal movement. During this literature review, actuators were found in the following categories: electromechanical actuators, vacuum actuators, pneumatic actuators, hydraulic actuators, magnetic actuators, electroactive actuators, ionic electroactive polymer actuators, electronic electroactive polymer actuators, thermal actuators and variable stiffness actuators. A comprehensive overview can be found in the appendix (Appendix A1, table 2a,b,c).

3.2.1.1 Electromechanical actuators

Electromechanical actuators use an electric motor to generate mechanical movement. Two mechanical actuators were found in the literature, a servo motor and a DC brushless motor.

- A servo motor is an actuator that is designed for precise positioning, velocity, and acceleration [14]. It can be either a linear or rotary actuator and is widely used in soft robotics [15] and medical applications, such as ankle-foot orthotics, where precise control of movement is crucial [14]. Servo motors offer high speed and torque [14] but can be bulky and have limited flexibility [15]. Additionally, the actuators were found not suitable for precision control of rotation and when there is vibration [14].
- A DC brushless motor [16][17] is a type of actuator that uses electronic commutation to control the movement of the rotor. It consists of a permanent magnet rotor and a stator with electronically controlled windings to generate rotational motion [OpenAI, 2021]. These motors are commonly used in knee exoskeletons and ankle and foot prosthetics [16], where they offer precise and efficient motion control [17]. DC brushless motors offer large drive and auxiliary torque, but may have defects in weight and drive flexibility [16].

Bowden cables are often used in exoskeletons and soft robotics to extend the range of motion of the previously described motors [18][19]. The cable is affixed to a point on a device or structure, is routed along a specific path and fed to a motor which, when activated, winds the cables to apply a tensile force to the anchor point to mimic the musculoskeletal behaviours of specified joint or area. [19]. Motors with Bowden cables have advantages such as better alignment with the human body [18], high force output and adaptability [19], but may have difficulty with low-level position and torque control [18], add a lot of weight and have anchor points that can slip as well as potential frictions from moving cables [19].

3.2.1.2 Vacuum actuators

Vacuum actuators use a vacuum to generate movement. In general the actuators are compact, robust and have a fast response [20]. Within the field of vacuum actuators, there were two primary types of skin structures found to be used in soft robotics [20]: convoluted and pleated skin type actuators.

- Convoluted skin actuators represents a unique structure made of multiple convolutions periodically arranged along the vertical direction of the structure [20] (figure 3a).
- Pleated skin actuators [20][21] are designed in such a way that parallel stress is made zero in the actuator membrane. This is achieved by introducing folds or pleats in the membrane parallel to the axis of the actuator [21] (figure 3b).

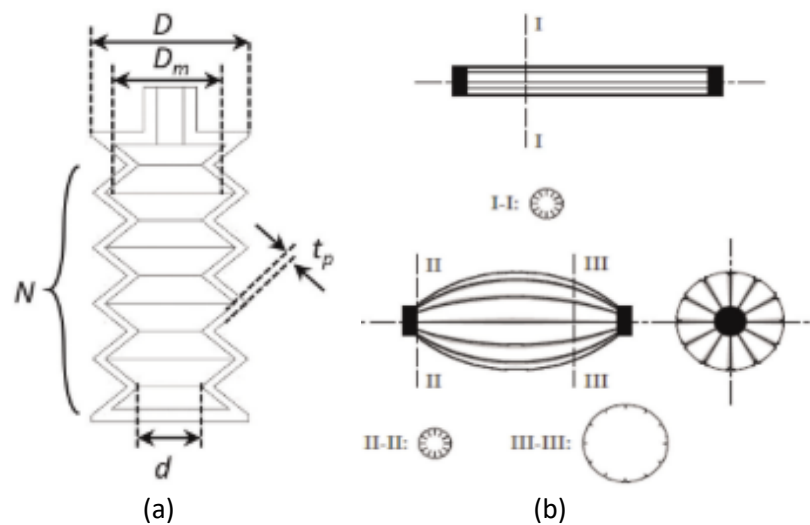


Figure 3: Skin type vacuum actuators [20]: (a) convoluted skin and (b) pleated skin

Another type of vacuum actuators are origami-based actuators. This type of vacuum actuators uses folding techniques to create structures that can be actuated by vacuum pressure. Joe Seongun et al. [20] describes three types of origami-based actuators: Yoshimura, Miura-ori and Kresling pattern origami actuators.

- The Yoshimura pattern is a pleated skin type actuator that consists of identical isosceles triangles symmetrically connected in each row (figure 4a) and enables high axial stiffness and high deformability [20].
- The Miura-ori pattern origami actuator is a pleated type that uses a folding technique consisting of congruent parallelograms forming a zigzag configuration in two directions (figure 4b). It has high stiffness, compressibility, and extensibility. Lastly, the Kresling pattern consist of a series of parallel diagonal creases defined by triangular facets [20].
- The Kresling pattern origami actuator uses convolutions (figure 4c) that enables axial and torsional movements and exhibits bistable movements (i.e., contraction and elongation). However, the Kresling pattern origami actuator has an unbalanced deployment [20].

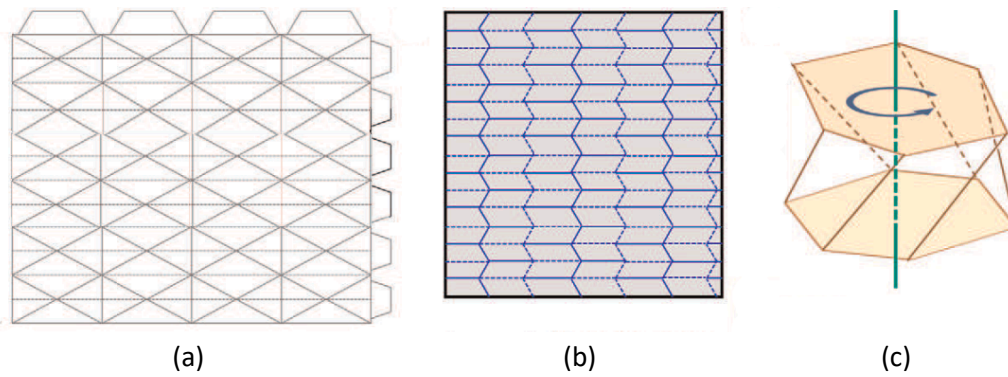


Figure 4: Origami-based actuators [20]: (a) Yoshimura pattern, (b) Miura-ori pattern and (c) Kresling pattern

3.2.1.3 Pneumatic actuators

Another type of actuator that uses air are pneumatic actuators. While in vacuum actuators, force is generated by removing air, pneumatic actuators use compressed air to generate movement. They can be classified into two main categories: linear pneumatic actuators, that generate linear motion and rotary pneumatic actuators that enable rotational movement.

- Linear pneumatic actuators are one of the most commonly used types of pneumatic actuators and are mainly used in exoskeletons designed for the knee [16]. This device includes a cylinder and piston that move linearly through the control of a pneumatic system with compressed air. The air flow direction changes to move the piston in the opposite direction. Linear pneumatic actuators are advantageous due to their easy controllability, however, they suffer from poor human-machine interaction [16].
- Rotary pneumatic actuators are another type of pneumatic actuator. De Greef et al. [22] describes a pneumatic rotary soft actuator used in hand prosthetics. These actuators use side plates, a sector circular arc, and a pneumatic tube to achieve rotation. Pressurization causes expansion solely in the circumferential direction. Pneumatic rotary actuators are compliant, lightweight and can have self-sensing capabilities [22]. However, they require bulky equipment such as pumps, valves, and pipes, and can be prone to leakage [22].

More specific pneumatic actuators for hand prosthetics include HASEL actuators [23].

- HASEL actuators use flexible polymer films filled with liquid dielectric and electrodes on either side to create a rectangular shell (figure 5). Opposing charges cause HASEL actuator electrodes to zip together via electrostatic force. This motion makes the fluid squeeze into the shell volume, resulting in linear contraction. HASEL actuators have the advantage of fast and precise linear motion and have self-sensing capabilities [23].

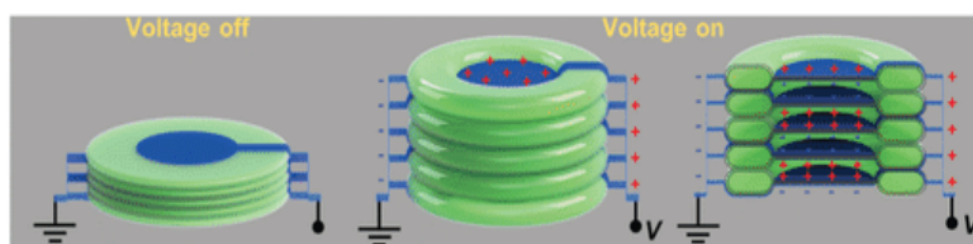


Figure 5: HASEL actuator (voltage off and voltage on) [23]

pneumatically-driven microcage actuators [22], pneumatic balloon actuator [22] and flexible rubber micro actuators [22] are also used for hand prosthetics and share the same advantages and disadvantages. They are compliant and lightweight but require bulky components and can be prone to leakages [22].

- Pneumatically-driven microcage actuators use the deformation of an elastic membrane to achieve the displacement of rigid parts fastened to it [22] (figure 6a).
- Pneumatic balloon actuators consist of two flexible films: a silicon rubber membrane and a polyimide substrate. Pressurized air inflates the membrane, while tensile forces in the membrane cause the substrate to bend and produce significant vertical and horizontal displacement [22] (figure 6b).

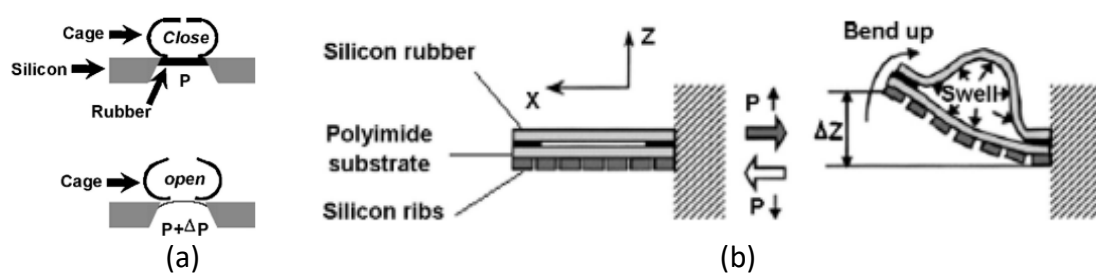


Figure 6: (a) pneumatically-driven microcage actuator, (b) pneumatic balloon actuator [22]

- Flexible rubber micro actuators are composed of silicone rubber reinforced with nylon fibers disposed in a circular direction. When a chamber is pressurized, the cylinder bends in the direction opposite this chamber, creating motion [22] (figure 7).

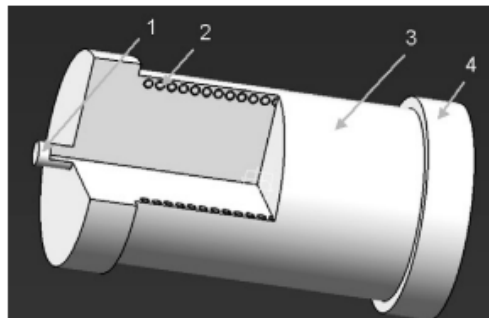


Figure 7: Flexible rubber micro actuator [22]: 1) air feeding tube. 2) spiral fibers. 3) rubber cylinder. 4) cover

Pneumatic actuators, specific for artificial muscle applications, can be further categorized into pleated-, braided-, netted- and embedded muscle actuators [7].

- Pleated muscle actuators are, beside a type of vacuum actuators, also a type of pneumatic actuators. The pneumatic type of the actuator is commonly used in a variety of applications such as for artificial muscles [7]. It consists of multiple pleats in axial direction and inflates by unfolding the pleats [7] (figure 8a). Pleated pneumatic actuators have the advantage of having no strain or friction when inflated, resulting in no hysteresis [7].

- A variation of pleated pneumatic actuators is the antagonistic pleated pneumatic muscle actuator. This type of pneumatic actuator, commonly used in knee exoskeletons [16], consists of two opposing pleated pneumatic muscle actuators that work together to create movement (figure 8b). One of the actuator contracts while the other one expands [16]. Antagonistic pleated pneumatic actuators have a simple structure, making them easy to manufacture. However, they have a slow response time [16].

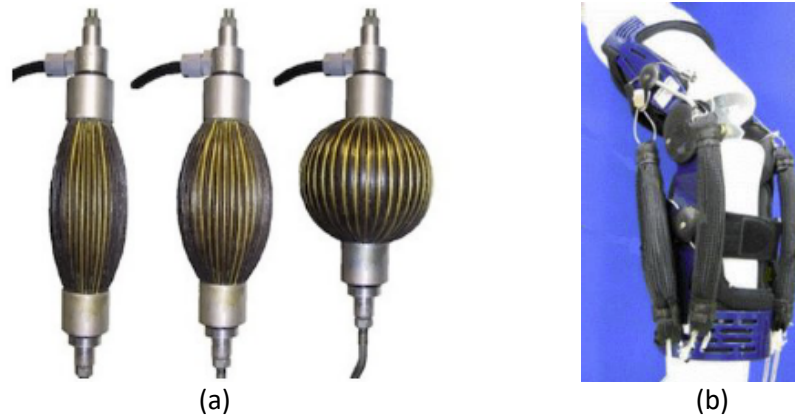


Figure 8: (a) pleated muscle actuator, (b) antagonistic pleated muscle actuator for the knee [16]

Braided muscle actuators are made out of a bladder surrounded by a braided netting which is wrapped helically around the long axis of the muscle [7].

- McKibben pneumatic muscle [16][7][19] actuator is one of the most common braided muscle [7]. This type of actuator is used in a wide range of applications throughout the body, such as in exoskeletons [16], orthotics [7], artificial muscles [7] and soft robotics [19]. McKibben pneumatic actuators are made out of a flexible, braided sleeve that is filled with compressed air (figure 9a). Pumping air into the sleeve causes the braided sleeve to contract and generate linear motion [7]. They are compliant [16], have a high force-to-weight ratio, are flexible, and durable [19]. However, they have a fixed movement [16], can be bulky, and must be securely fixed to function as intended [19].
- Another braided type used for artificial muscles is the sleeved bladder actuator [7]. This type of actuator has only the braid connected to end fittings and in which the inner tube is an unattached bladder [7] (figure 9b). These actuators are easy to assemble, making them a convenient choice for certain applications [7].

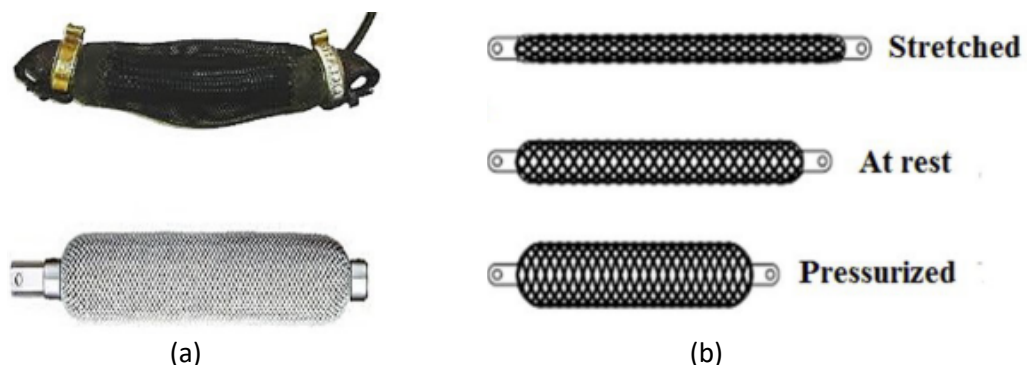


Figure 9: Braided muscle actuators [7]: (a) McKibben pneumatic actuator, (b) sleeved bladder actuator

A netted muscle is almost similar as a braided muscle but has a smaller grid density surrounding the membrane [7].

- The Kukolj netted muscle actuator for example is a modification of the standard McKibben muscle (figure 10a). The main difference between the muscles is the sleeve, where the McKibben muscles have a tightly woven braid, the Kukolj design uses an open-meshed net [7].
- The Yarlott muscle actuator is another netted pneumatic actuator. It includes an elastomeric bladder of a prolate spheroidal shape that is netted by a series of cords or strands (figure 10b). The actuator initially inflates into a spheroid bladder shape, but as it elongates, the axial strands straighten out and cause the bladder to transform into a shape with distinct ridges and valleys [7].

However there is a major disadvantage for both actuators, both can only withstand low pressures due to their mesh with large holes, limiting their use in certain applications [7].

- The ROMAC actuator is a netted muscle actuator that consists of a polylobed bladder enclosed by fittings and held in place by a wire netting (figure 10c). The bladder is made of a stiff, flexible and fluid-tight sheath, while the netting consists of non-stretchable flexible links arranged in diamond-shaped openings at the nodes. ROMAC actuators have high tensile stiffness, flexibility and fluid tightness. However, same as the previously described netted muscles, they can only withstand low pressures due to their mesh with large holes [7].

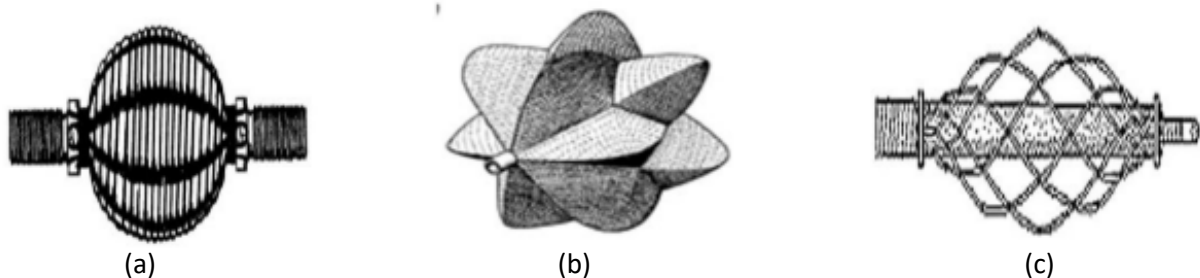


Figure 10: Netted muscle actuators [7]: (a) Kukolj actuator, (b) Yarlott actuator, (c) ROMAC actuator

Embedded muscles actuators have their load-carrying structure embedded within their membrane [7]. There are different types of embedded muscle actuators used for artificial muscles.

- The Morin muscle actuator consists of a rubber tube embedded by threads of high tensile stiffness (figure 11a). This actuator have threads arranged lengthwise or in a double helix around the axis, using fibers such as cotton, rayon, asbestos, or steel [7].
- The Paynter hyperboloid muscle actuator has a spherical elastomeric bladder reinforced by a knitted structure of flexible fibers (figure 11b). It retains the shape of the original bladder and knitting sphere when fully inflated [7].

- The Kleinwachter torsion device is also a type of an embedded muscle actuator which can be used as a torsion device. It has a toroid diaphragm embedded with stiffening filaments and attached at its outer edge to a ring-shaped structure along with its inner edge to a shaft [7] (figure 11c).

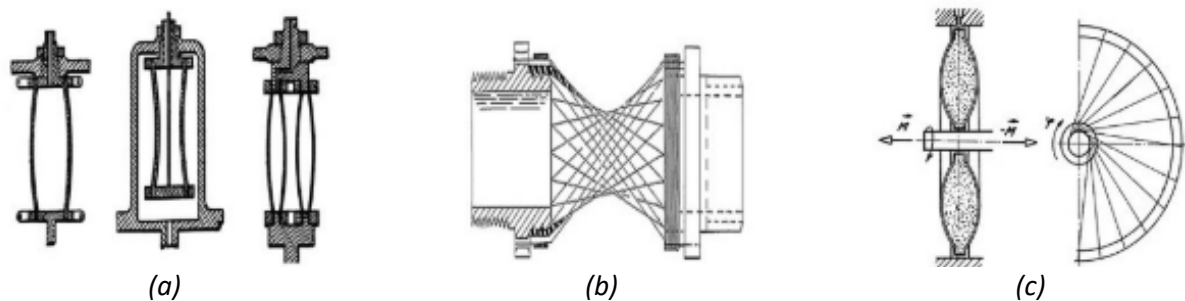


Figure 11: Embedded actuators [7]: (a) Morin actuator, (b) Paynter actuator, (c) Kleinwachter torsion device

Besides these pneumatic actuators there are other pneumatic actuators used for artificial muscles [7] found in the literature.

- The Peano muscle actuator consists of flat layers of thermoplastic, textile reinforced plastic, or textile/silicone composite that are bonded at intervals perpendicular to the direction of contraction (figure 12a). When air pressure is applied, the flat tubes become round [23].
- The series pneumatic muscle actuator is made from a thin rectangular sheet of polyethylene tubes that is sealed on one end so that can inflate [7] (figure 12b).
- The flat pneumatic muscle actuator has Kevlar fibers embedded in a silicon substrate. It comprises an elliptical tube for generating expansion force, a diamond-shaped band for converting it into output contraction force, and a two-stage spline to maintain the elongation of the elliptical tube [7] (figure 12c).

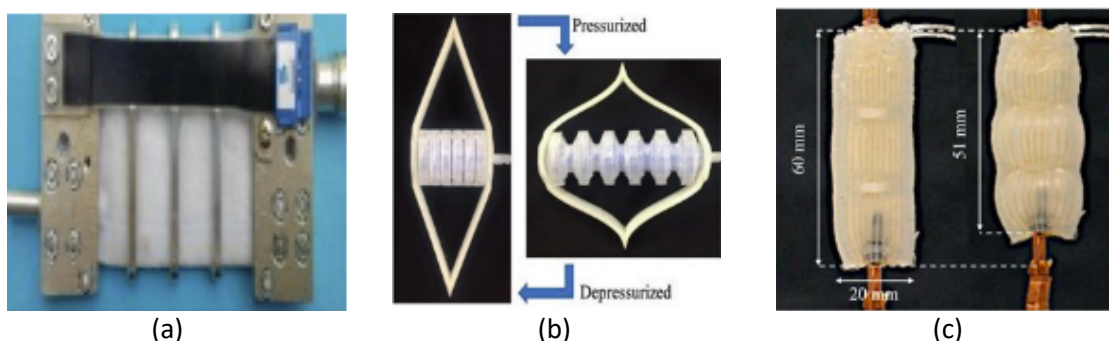


Figure 12: (a) Peano actuator, (b) series pneumatic actuator, (c) flat pneumatic actuator [7]

- The high-displacement pneumatic muscle actuator made of textiles or plastics can sense its pressure and displacement with integrated electronics (figure 13a) and has high displacement capabilities [7].

- The reverse pneumatic artificial muscle actuator, made of silicone rubber and symmetrical double-helix threading, contracts radially under pressure instead of longitudinally (figure 13b) [7]. It is ideal for applications needing high force in limited space [7].

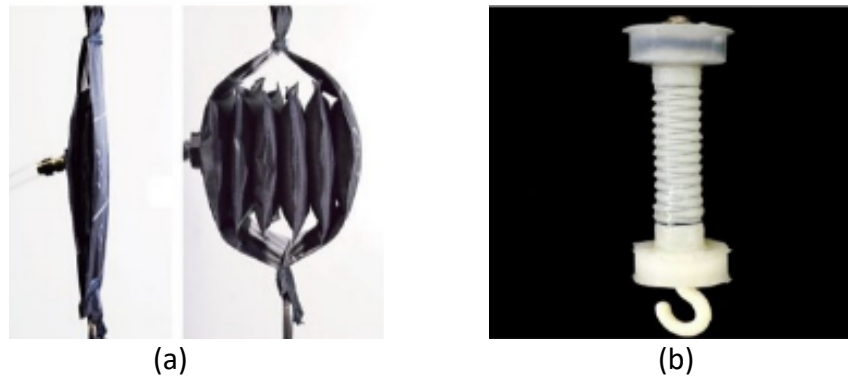


Figure 13: (a) High-displacement pneumatic actuator, (b) reverse pneumatic muscle actuator [7]

In addition to the previously discussed types of pneumatic actuators, further literature was found on two other interesting variations.

- The straight fibre-type pneumatic actuator was described by Zongpeng et al. [16] for the use of knee exoskeletons. This type of actuator is made of woven fibers that are arranged in a parallel fashion to create linear motion [16] (figure 14a). This actuator has a small motion inertia, making it able to move quickly in response to changes in pressure. However this type of actuator has a low control precision [16].
- The PneuNets actuator [23][19], used for hand orthotics [23] and soft robotics [19], consists of a series of channel made of an elastomer that can be inflated like a balloon for actuation [23] (figure 14b). The PneuNets actuator offers several advantages such as being lightweight and having diverse fabrication options [19]. However, this type of actuator also has some disadvantages. For instance, it can be easily punctured and requires tedious fabrication [21]. Additionally, it has a low force output and can be difficult to control [21].

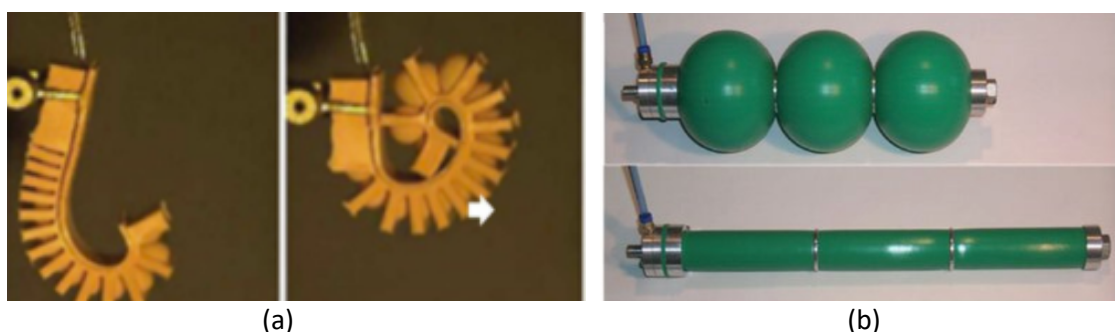


Figure 14: (a) straight fibre-type pneumatic actuator, (b) PneuNets actuator [23]

3.2.1.4 Hydraulic actuators

The functioning principle of hydraulic actuators is quite similar to that of pneumatic actuators, however, instead of using air, hydraulic actuators use pressurized fluid to generate movement. Different types of hydraulic actuators were found in the literature.

Zhaoqi et al. [24] describes two different types of HASEL actuators for the use of artificial muscles.

- Elastomeric HASEL actuators consist of a flexible elastomer layer coated with a conductive electrode. Applying voltage to the electrode causes the elastomer to compress or expand, creating movement [24] (figure 15a). Elastomeric HASEL actuators have the advantages of self-sensing capabilities through capacitance monitoring. However, they require high voltage [24].
- Thermoplastic HASEL actuators have a soft thermoplastic elastomer layer coated with a conductive electrode. They generate movement by compressing or expanding when an electric field is applied to the electrode [24] (figure 15b). Thermoplastic HASEL are also self-sensing through capacitance monitoring and have the advantages of simple and cheap fabrication. However, they also require high voltage and may experience leakages due to the use of dielectric fluid [24].

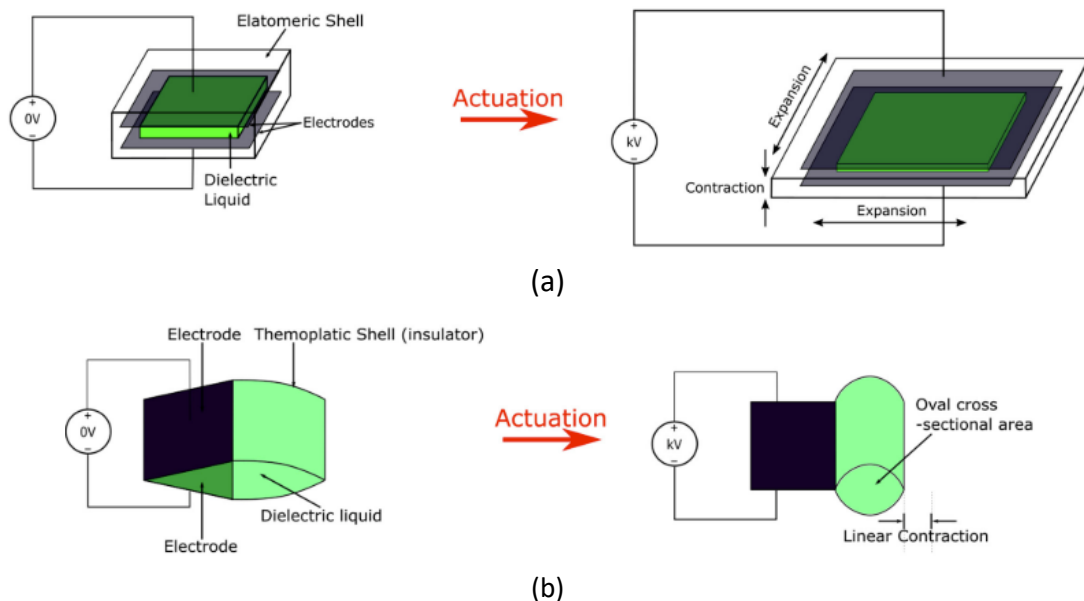


Figure 15: HASEL actuators [24]: (a) elastomeric HASEL actuator, (b) thermoplastic HASEL actuator

De Greef et al. [22] describes a flexible micro actuator for medical instruments and a expansion behaviour based actuator for artificial muscles, particularly in the hand.

- The flexible micro actuator is made of silicone rubber and nylon fibers arranged in a circular pattern. It has three internal chambers, and when one of them is pressurized, the cylinder bends in the opposite direction of that chamber [22] (figure 16a).

- The expansion-based actuator also consists of a chamber, but now connected to two movable parts. Pressurized fluid is introduced through a feeding channel, increasing the volume and height of the chamber, which causes the parts to move relatively to each other [22] (figure 16b). Expansion behaviour-based actuators have the advantages of being highly flexible, capable of handling delicate objects without causing any damage thanks to their own compliance, lightweight, and able to achieve complex motions. However, they require equipment such as pumps, valves, and pipes that can be bulky and may present leakages [22].

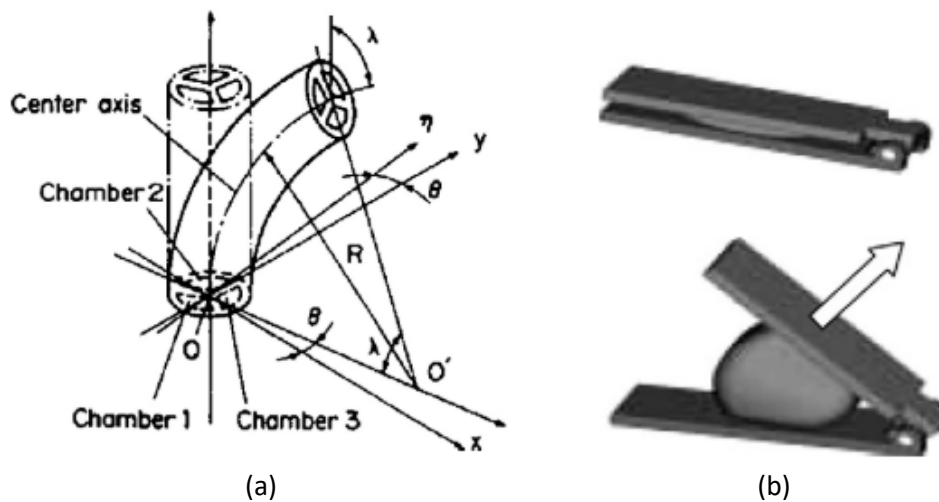


Figure 16: (a) flexible micro actuator, (b) expansion-based actuator [22]

3.2.1.5 Magnetic actuators

Magnetic actuators use a magnetic field to generate movement. Literature was found on different types of magnetic actuators for different applications.

- Magnetorheological elastomer where found to be used for soft robotics [25]. This type of actuator is composed of non-magnetic elastomeric polymer matrix filled with magnetizable particles. The elastomers respond to the external magnetic field with the change of material properties and deformation [25]. Magnetorheological elastomer actuators have the advantage of vibration absorbing, being excited by a field, flexible structure and low production cost [25], but require high magnetic field and permanent magnets.
- A magnetic shape memory alloy actuator, described by Kulagin et al. [26] was used for medical applications such as micropumps and valves. This type of alloy returns to its shape when it is deformed by an external magnetic field [26]. Magnetic shape memory alloys have the advantage of wide actuation frequency, rapid accelerations, and high energy efficiency, but are limited in their temperature range (-40-60 degrees). In addition, they are sensitive to fatigue, have a complex design due to hysteresis and are complex to model the behaviour [26].

- Magnetic hydrogel-based actuator used for artificial muscles, soft robotics and medical devices particularly for the fingers was described by He et al. [27]. These actuators are made by embedding magnetic nanoparticles into a hydrogel matrix, which is a polymer network that can absorb and retain large amounts of water [27]. When the magnetic hydrogel is exposed to a magnetic field, the magnetic particles inside the hydrogel align with the direction of the magnetic field, causing the hydrogel matrix to deform [27]. Magnetic hydrogel based actuators have the advantage of fast response and design diversity [27], but have a complex design and complex fabrication [27].

3.2.1.6 Electroactive actuators

Electroactive actuators are another type of actuator that can be used for skeletal movement. This type of actuator generate movement through electrical energy. Literature within this category was found on piezoelectric actuators [15][28], cellulose paper actuators [29] and electro-ribbon actuators [24].

- Piezoelectric actuators, used for micropumps and micro-robotics [28], convert mechanical or vibration forces into electric charge by using certain materials [15]. These actuators have a fast response, high displacement resolution, high efficiency, and compact structure [28]. However, they require large voltage [15][28] and high temperature thermal processes for incorporation of piezo materials and have large hysteresis nonlinearity [28].
- Cellulose paper actuators were described by Liu et al. [29] for the use of soft robotics and artificial muscles. This type of actuator is made from cellulose-based materials such as paper or thin films. When an electrical charge is applied to the cellulose paper, it causes it to bend, twist or deform in a specific way, creating mechanical motion [29]. The advantages of cellulose paper actuators are their light weight low costs, biodegradability and biocompatibility. However, they have a low output force and slow response [29]
- Electro-ribbon actuators are a relatively new type of actuator that have been developed for origami robots [24]. It uses a principle called dielectrophoretic zipping, which means zipping using Maxwell force with the amplification of a bead of dielectric liquid resulting it to fold or clamp upon activation [24] (figure 17). The advantages of electro-ribbon actuators are that they are easy to fabricate, are light weight and have self-sensing capabilities. However, they require high voltage (0.4kV), have slow actuation and may experience liquid leakage [24].

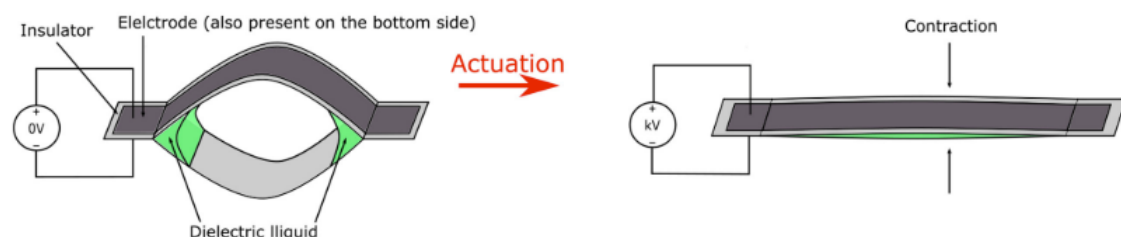


Figure 17: electro-ribbon actuator, before and after actuation [24]

3.2.1.7 Electroactive polymer actuators

Electroactive polymer actuators can be categorized into two subcategories [30]: ionic electroactive polymer actuators, which use ionic motion to generate movement (figure 18) and electronic electroactive polymer actuators, which generate movement through electronic energy (figure 19).

Different ionic electroactive polymer actuators were found in the literature for different applications. Such as ionic polymer metal composition actuators used for soft robotics [25] and artificial muscles [31], ionic polymer gels used for artificial muscles [31][32] and leg orthotics [32], conductive polymer actuators [30] and carbon nanotube actuators [30][33] used for artificial muscles [30].

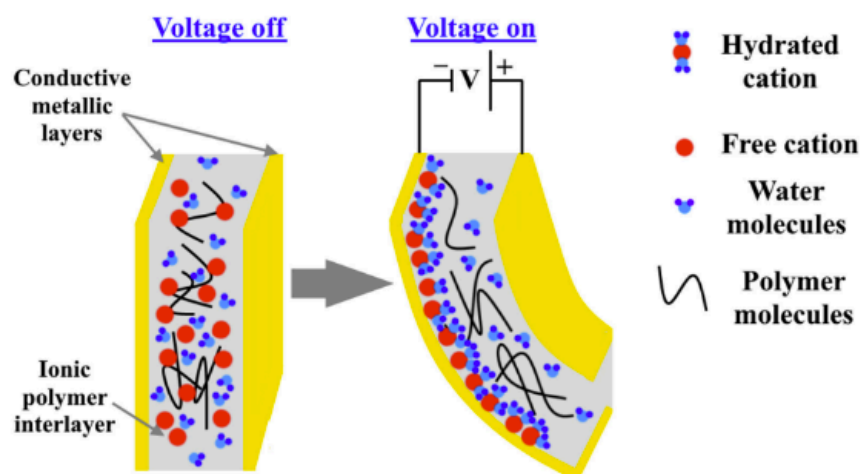


Figure 18: Working principle for ionic electroactive polymer actuators [31]

- Ionic polymer metal composite (IPMC) actuators consist of a polymer membrane with metallic electrodes on both surfaces. Applying voltage to the electrodes causes ion migration in the membrane, resulting in bending of the IPMC actuator [25]. IPMC actuators require low voltage (3V) [25][23][31][34], have bidirectional operation with flexible voltage polarity [23][31][34], variable stiffness [23], self-sensing capabilities [23], fast response [31][34], high ionic conductivity [31], and long-range stroke [34]. However, they have low actuation force [25][23][34], high production costs [25][34], require a humid condition for the electrolyte [25][31], electrolysis occurs above 1.23V [25][31], slow response [23], and low cycle life [31][34].
- Ionic polymeric gel actuators consist of polymer chains and electrolyte solutions. They are activated by changes in the environment from alkaline to acid, or vice versa, which causes the gel to either swell or shrink [31]. They can mimic the strength and energy density of biological muscles [31], require low voltage [31][34], are bistable [31], and lightweight [31]. However, they have weak mechanical properties [31][34], slow response [33], require humid conditions [31][34], electrolysis occurs above a certain voltage [31], slow response [31] and low electromechanical coupling efficiency [31].

- Conductive polymer actuators respond to an applied voltage by either swelling or compressing. This behaviour is due to the oxidation or reduction of the material, which is determined by the polarity of the voltage. When oxidized, the material undergoes crosslinking between generated polarons and dopant anions, resulting in swelling of the actuator [31]. They require low voltage, have high conductivity, high ionic conductivity of the electrolyte, fast response and large deformation. However, they have electrolysis above a certain voltage, low cycle life, high dehydration and low efficiency [31].
- Carbon nanotube actuators have an ionic liquid or electrolyte between two electrodes, one of which is a carbon nanotube. When a voltage is applied, electrochemical reactions occur, and ions move towards the carbon nanotube electrode. This change creates an electrostatic force that causes the nanotube to bend [33]. Carbon nanotube actuators require low voltage [33], are noiseless [33], have high mechanical strength [33], high work per cycle [30][33], and can be used in liquid or air [33]. However, they have poor conductivity of the electrode [33].

Literature regarding dielectric electroactive polymers was found, covering various types of actuators designed for different applications. Dielectric elastomer actuators and liquid crystal elastomer actuators were used for artificial muscles [31][35][24] and soft robotics [34][15], piezo- and ferro- electric polymers and electrostrictive graft elastomers for artificial muscle applications [31][36][30]

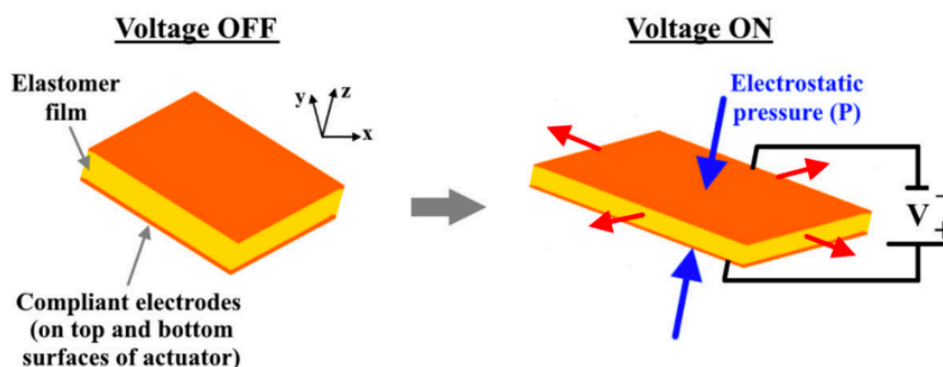


Figure 19: Working principle for dielectric electroactive polymer actuators [31]

- Dielectric elastomers consists of a thin and soft elastomer film placed between two compliant electrodes [31]. When connected to a direct current source, compliant electrodes gather opposite charges that are attracted to each other via Coulomb force, forming an electrostatic pressure. [31]. The formed pressure leads to an deformation of the film in the plane and the is restored when the DC voltage is released [31]. Dielectric elastomers have several advantages, including quiet operation [25], low weight [25], high flexibility [25], large actuation force [25][23], fast actuation response time [25][23][24][34], high value of strain [25][24], self-sensing capability [24], requiring small currents [31], high energy density [31], low costs [31] and ease of fabrication [34]. However, they also have some disadvantages, including high voltage requirement [25][23][31][24][34], unidirectional operation due to the electrostriction effect [25], requiring membrane pre-strain [25][31], difficult fabrication procedure [25], requiring electrolyte [35], and being susceptible to dielectric breakdown [24][34].

- Liquid crystal elastomer actuator consist of an elastomeric backbone and cross-linked side-chains, which are prepared based on crosslinking reaction of reactive-mesogenic monomers [31]. Polymers work by losing and regaining molecular orientation due to phase transitions triggered by external stimuli like light, heat, or electric field [31]. Liquid crystal elastomers can produce high stress and strain [31] and need low electrical voltage (1.5-5 kV) [31][15]. However, they have the disadvantages of slow response and hysteresis [31].
- Piezoelectric polymer actuator converts electrical energy into mechanical motion. When an electric field is applied to a piezoelectric polymer, the material changes shape, producing a displacement or strain [31]. Piezoelectric polymers have the advantages of good mechanical energy density, high elastic modulus, and fast response. However, they also have some disadvantages, including the need for high voltage, complicated production, thin films, and low strain [31].
- Ferroelectric polymer actuator is characterized by an electrical polarization that can be changed in an applied electric field. The external field will apply moments to polarized groups within the polymer [31]. Ferroelectric polymer actuators have the advantages of large actuation force and fast response [31].
- Electro strictive graft elastomer actuator consists of a flexible polymer chain and grafted crystalline groups that rotate and polarize under an electric field. Cross-linking the crystallites creates polarized monomers with partial charges, causing a dipole effect, resulting in electrostrictive strain and deformation [31]. Electrostrictive graft elastomers have the advantages of low costs, strain values up to 5%, and fast response. However, they also have the disadvantage of requiring high voltage [31].

3.2.1.8 Thermal actuators

Thermal actuators generate movement when they come into contact with heat. The actuators work based on the principle of thermal expansion, where they expand upon exposure to heat, generating force and motion. Thermal actuators are commonly used in various applications such as exoskeletons, orthotics and surgical tools. Literature was found on shape memory alloy actuators to generate skeletal movement with knee exoskeletons [16] and ankle-foot orthotics [14]. Other applications consists of surgical tools [28], implantable devices [28] and micro- grippers and pumps [28]. Another type of shape memory actuators, shape memory polymer actuators, are used for endovascular and drug delivery devices [28]. Furthermore, phase changing actuators and twisted and coiled actuators where found to be used for artificial muscles [24][30]. Finally, thermal hydrogel actuators for surgical tools [28], microvalves [28] and drug delivery devices [28]. Bilayer electrothermal actuators were found to be used for applications such as soft robotics [34] and medical devices [34].

- Shape memory alloy and polymer actuators are a class of materials that return to their original shape under thermal cycles due to their reversible changes in crystal structure [15][34]. Shape memory alloy actuators are light and flexible [16], can provide high active stress [23] and have a high elastic modulus [23]. They act as a strain sensor, are noiseless [14] and exhibit large displacement [28].

Furthermore, the actuators can provide a large force [28] have high mechanical robustness [28] and are corrosion-resistant [28]. However, they require exact geometries [16], have slow response and speed [23][28], exhibit hysteresis [23], require high currents [23][28] and have low energy efficiency [14].

- Shape memory polymer actuators have a variable stiffness capability [23][37], high-design diversity [34], ease of fabrication [34], structural flexibility [28], large strains [28], low density [28], tuneable transition temperature [28] and biodegradable properties [28]. However, they have low produced force [23][37], irreversible activation [34], slow response [28] and low recovery stress [28].
- Twisted and coiled polymer actuator is a relatively new type of thermal actuator [24] that is shaped like threads and is a linear actuator that can either contract or extend upon activation through thermal expansion of the twisted fibers [24] (figure 20). Twisted and coiled polymer actuators are lightweight and suitable for small-volume applications. However, they have a long actuation period and low energy efficiency [24].

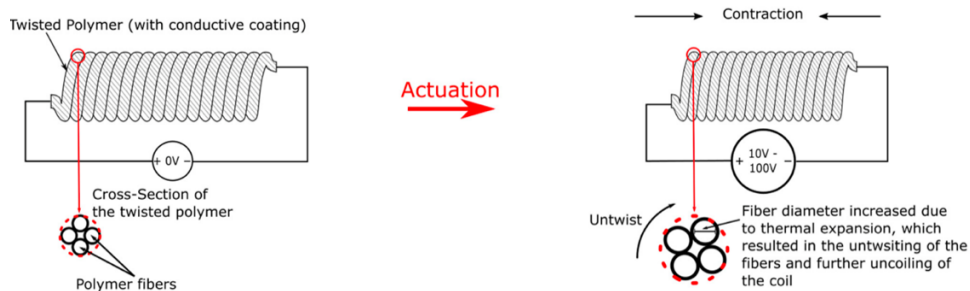


Figure 20: Twisted polymer actuator, before and after actuation [24]

- Phase-changing actuators are a type of thermally activated actuator that uses phase changing materials. When heated, these materials undergo a phase change, resulting in volumetric expansion. They can be driven by any heating method, including embedding heating wires, microwave, near-infrared actuation, and induction heating [24] (figure 21). Phase-changing actuators have very large strain, high specific energy, low voltage actuation (10 – 100 V) and wireless actuation. However, they have a long actuation cycle, limited lifetime, and low energy efficiency [24].

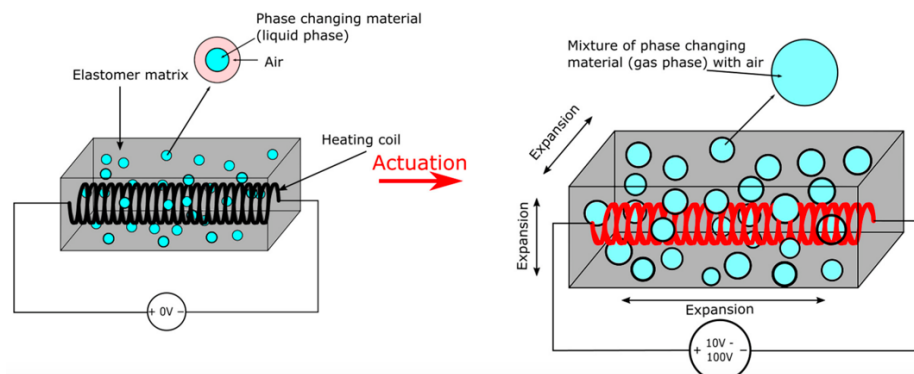


Figure 21: Phase-changing actuator, before and after actuation [24]

- Thermal hydrogel actuators use a hydrogel that changes size when the temperature crosses a certain threshold called the lower critical solution temperature (LCST) [28]. Above the LCST, the hydrogel shrinks by releasing the uptake solution, while below it, the process is reversed. Thermal hydrogel actuators have tuneable degradation features, tuneable mechanical feature and UV-sensitive properties. However, they have a slow response [28].
- Bilayer electrothermal actuators consist of a high coefficient of thermal expansion (CTE) layer, a low CTE layer and a thin conductive film. When an electric current heats the layer, it expands and causes deformation [34] (figure 22). Bilayer electrothermal actuators provide long-range stroke, are lightweight, and can be designed in thin film form. However, they have high driving voltage and low design diversity [34].

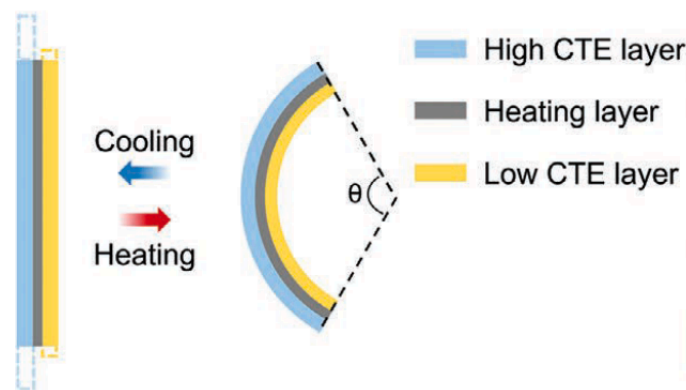


Figure 22: Working principle of a bilayer electrothermal actuator [34]

3.3.2.9 Variable stiffness actuators

Variable stiffness actuators are types of actuators that can change their stiffness. This unique characteristic makes them suitable for a wide range of applications, such as arm and leg exoskeletons [38], robotics and prosthetics. There are many different types and options of variable stiffness actuators, including independent and antagonistic setup.

- An independent setup only moves one motor to vary the output position and contains the possibility to use only one spring [38] (figure 23a). This setup can store and release energy during operation, which allows them to use less power than other actuators [38], the size of the stiffness adjusting motor can be chosen to match exactly the power needed for this purpose, lightweight compared to antagonistic setups [38]. However, the output power of the actuator is defined by the positioning motor's power, which is solely responsible for moving the joint. Similarly, the power of the stiffness adjuster is exclusively utilized for adjusting the stiffness setup. Therefore, any changes to the stiffness setup can only be made by using the power of the stiffness adjuster [38].
- In an antagonistic setup, two motors and two springs are positioned in opposite position to each other (figure 23b). The motors move in opposite directions to adjust the stiffness of the actuator, with co-contraction of the springs resulting in a change of output stiffness [38]. Antagonistic variable stiffness actuators can store and release energy during operation, which allows them to use less power than other actuators. The length between the actuator and the joint can be easily compensated and it can

move the output even if one of the driving motors/electronics is faulty but is still back drivable [38]. However, the maximum output power and torque of only one of the motors and the energy storage of only one spring can be used and for moving the output, both motors and potentially gearboxes have to move, resulting in power losses of all four elements [38].

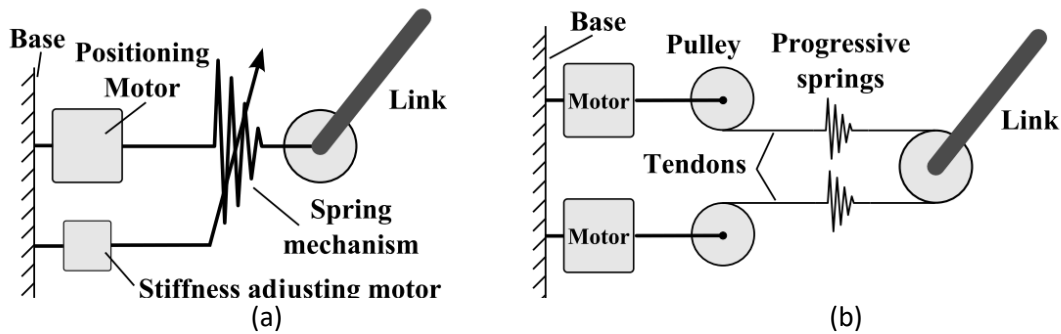


Figure 23: Different variable stiffness principles: (a) independent setup, (b) antagonistic setup [38]

Several other types of variable stiffness actuators were found for applications to enhance skeletal movement. The most common type of variable stiffness actuator, series elastic actuator, was used for prosthetics [17][21], particularly for ankle foot prosthetics [17]. Other actuators, such as a clutch able elastic device based on the hill muscle model or a system where two springs working both in series and in parallel, were used for knee exoskeletons [16].

- The series elastic actuator consists of a spring in series with a stiff actuator, where the actuator stiffness is determined by the spring selection and cannot be changed during operation (figure 24). There are both linear and non-linear variants of this actuator, with the non-linear variant having a spring that is stretched in a non-linear way [39]. The series elastic actuator is able to hold and generate energy when moving thereby increasing efficiency [17] disturbances and shocks are isolated from the gear transmission [18], huge range of speed [21], huge range of torque [21]. However, they have a limited stiffness [18], are bulky [18] and shows low power efficiency [21].

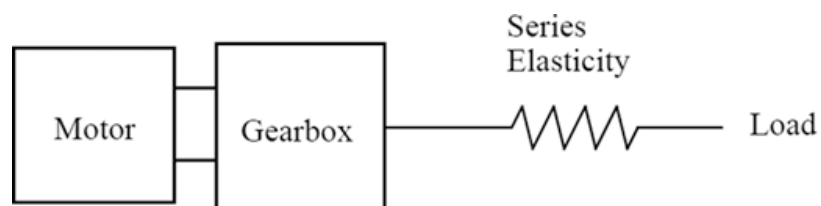


Figure 24: Series elastic actuator [40]

- A clutchable elastic device uses a clutch mechanism and elastic material to move loads (figure 25). It stores potential energy by stretching the elastic material when the clutch is engaged, which is then released when the clutch is disengaged to generate force [16]. This device is easy adaptable to multiple applications but tend to be bulky [16].

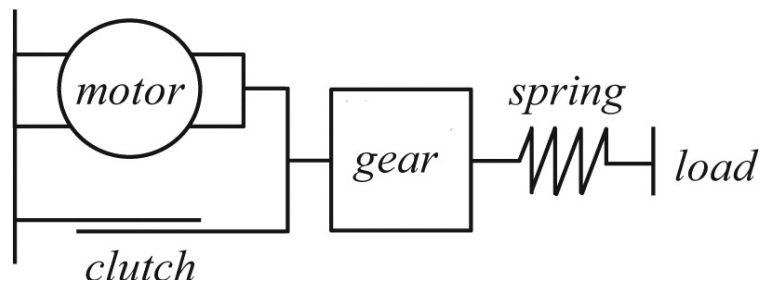


Figure 25: Clutchable elastic device [41]

- Furthermore, Zongpeng et al. [16] describes a setup where two springs working both in series and in parallel. In this system the actuator uses two springs to provide force and displacement [16]. This system behaves similar to biological muscles, but needs multiple complex components and structures [16].

Two types of variable stiffness actuators and three VSA-UT actuators were found to be used for prosthetic applications [42]. Lavate et al. [42] describes two Adjustable Stiffness (AwAS) actuators and three variable stiffness uniform torque (VSA-UT) actuators for the use of prosthetic applications

- AwAS I has two motors: one for controlling the angular position and the other for varying stiffness [42]. The springs' position can be adjusted using a ball screw drive, allowing for real-time adjustment of stiffness while maintaining precise control over the actuator's position [42] (figure 26a).
- AwAS II uses a lever with a moving pivot position to adjust stiffness more efficiently [42] (figure 26b). By controlling the position of the pivot, the stiffness motor doesn't need to counteract the forces of the springs directly. This reduces the amount of energy needed to adjust the stiffness of the actuator. Also, this actuator is lighter and more compact than the AwAS I [42].

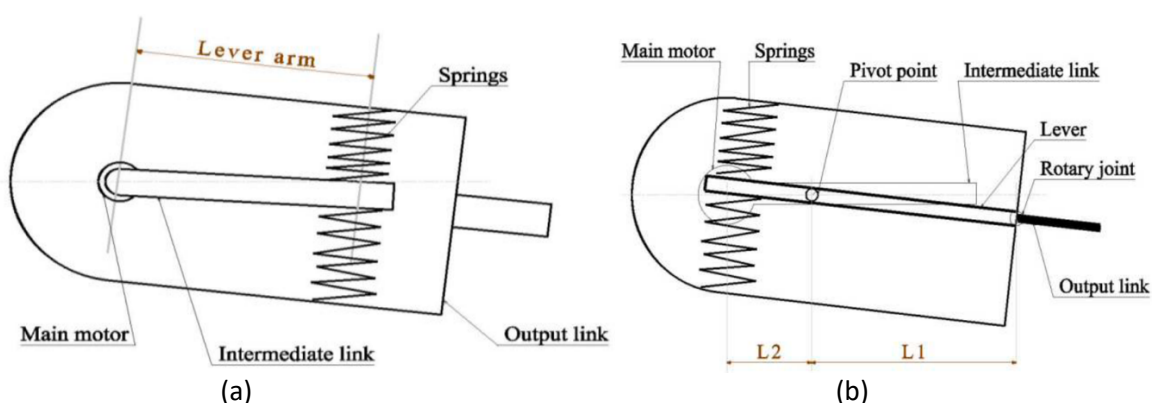


Figure 26: Adjustable stiffness actuators [42]: (a) AwAS I, (b) AwAS II

- VSA-UT I uses a lever arm of variable length to connect the internal spring to the output, with real-time stiffness control achieved by adjusting the point of application of the output force [42] (figure 27a).

- VSA-UT II is a modified version that uses a kinematic structure to move the pivot position along the lever arm using a modified planetary gear mechanism [42] (figure 27b). This allows for real-time adjustment of stiffness while maintaining precise control over position [42].
- mVSA-UT is a compact version of VSA-UT that uses two internal motors in differential configuration to achieve variable stiffness [42].

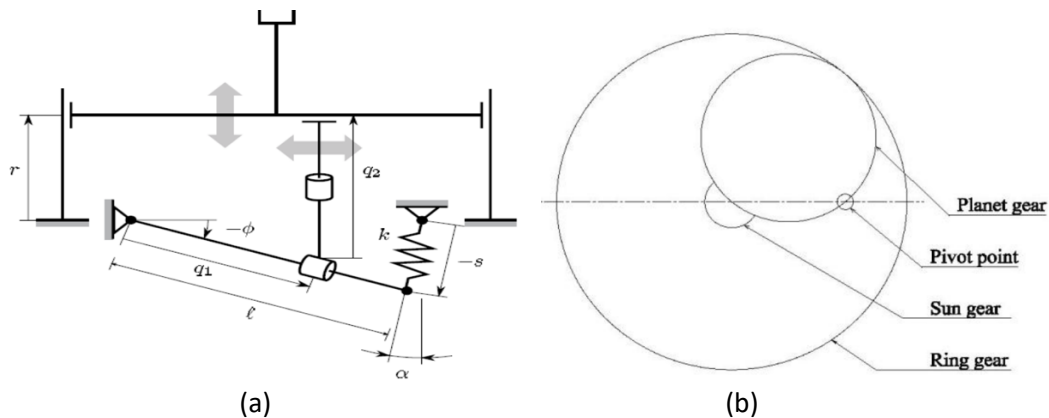


Figure 27: variable stiffness uniform torque actuators [42]: (a) VSA-UT I, (b) VSA-UT II

Finally, a hybrid dual actuator and the CompAct variable stiffness actuator were found to be used for prosthetic applications as well.

- The Hybrid Dual Actuator Unit is composed of a hybrid control module and a drive module with two motors. The hybrid control module uses gear motion to enable real-time control over joint position and stiffness through an adjustable moment arm mechanism [42] (figure 28).
- The CompAct Variable Stiffness Actuator uses a cam-shaped lever arm with a variable pivot position to adjust stiffness. The stiffness variation mechanism consists of a cam-shaped lever with its pivot attached to a rack and pinion, which is driven by a small motor [42]. By changing the position of the pivot, the output stiffness can be varied from zero to infinity [42].

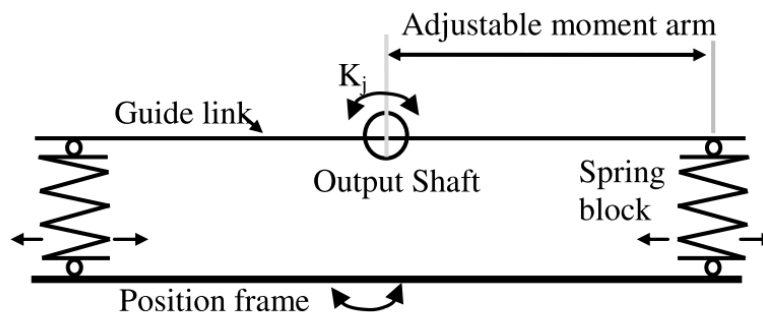


Figure 28: Mechanism of a hybrid dual actuator [42]

3.2.2 Dampers for skeletal movement

Dampers are essential components in many mechanical systems as they provide motion resistance to absorb, dissipate or suppress oscillations, vibrations, and shocks. Research has been conducted on various types of dampers to enhance skeletal movement. The dampers that were found can be categorized into several types based on their mode of operation. Dampers in the following categories will be described: fluid viscous dampers, variable-rheological fluid dampers, electromagnetic dampers and friction dampers. A comprehensive overview can be found in the appendix (Appendix A2, table3).

3.2.2.1 Fluid viscous dampers

Fluid viscous dampers are a type of damper that uses fluids to generate damping force. The dampers are used in a wide range of applications. Meatus and orifice dampers were found to be used in medical devices [43]. But besides this application they are mainly utilized in automotive applications [43] and are not directly relevant to this literature study.

- Oil dampers, on the other hand, are used in ankle-foot and knee orthotics [44][45][46]. These dampers provides resistance to the motion of the ankle or knee joint during walking [46]. The resistance is created by forcing oil through small holes, which slows down the movement of the joint and helps to control its speed and range of motion (OpenAI 2021, [2]).

3.2.2.2 Magnetorheological dampers

Variable-rheological fluid dampers are a class of damping devices that have numerous applications in different fields such as medical devices [43], prosthetics [43][47] (particularly for the knee [47][48]), rehabilitative systems [43], and wearable robotics [43].

There are two main types of variable-rheological fluid dampers: electrorheological [43] and magnetorheological fluid dampers [49][43][48][47].

- Electrorheological fluid dampers use electrically polarizable microscopic particles in a suspended carrier medium [43]. When an external electric field is applied, they align along the field lines and act as a barrier to the flow of the carrier [43]. They have a fast response time and simple mechanics, but they have a tendency to chemically and mechanically react with diverse materials, making precise damper component selection necessary [43].
- Magnetorheological fluid dampers consist of microscopic particles suspended in a carrier medium that can be polarized magnetically [43]. When an external magnetic field is applied, the particles align along the field lines and act as a barrier to the flow of the carrier [43]. Magnetorheological fluid dampers have fast response time, simple mechanics, simple configuration, step-less damping force adjustment, large viscosity, large control range, low costs, and low power feeding. However, they are prone to particles sticking together due to residual magnetization, making redispersion difficult and forming a hard layer [43].

Within magnetorheological and electrorheological dampers, there are several working modes, including flow mode, shear mode, and squeeze mode.

- In the flow mode, the fluid is forced to flow through a narrow orifice, where the external field is applied [49] (figure 29a). The flow mode provides large damping force but requires a complex design [49].
- In the shear mode, plates in relative motion are used to generate shear strain in the fluid [49] (figure 29b). The shear mode has a simple design but has a lower damping force. In the squeeze mode, a volume contains the variable-rheology fluid that is squeezed away [49].
- In the squeeze mode, the fluid is squeezed by applying force on a moveable plate [49] (figure 29c). It provides a large damping force but is only suitable for low and slight vibrations [49].

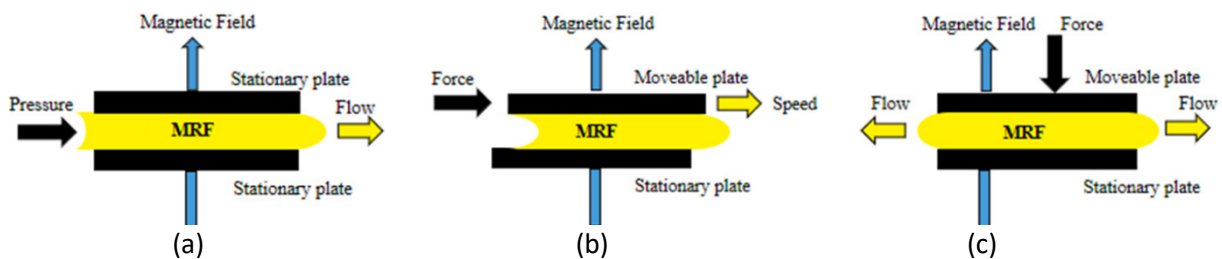


Figure 29: Rheological damper working modes [49]: (a) flow mode, (b) shear mode, (c) squeeze mode

There are also different shapes of magnetorheological fluid dampers, including annular-shaped, radial-shaped, and annular-radial shaped [49].

- In annular shaped damper, the fluid passes through the damping gap in a cylindrical manner and flows axially along the valve [49] (figure 30a). An annular-shaped magnetorheological fluid damper enable a fast response time, narrow dimensions and high damping force but are limited by axial valve dimensions [49].
- For radial shaped dampers, the fluid flows radially along the fluid path before the magnetic flux is directed into the fluid path [49] (figure 30b). Radial-shaped magnetorheological fluid dampers have large damping force and are suitable for broader and shorter bypass fluids but have a complex design [49].
- The annular-radial shaped damper is a combination of the two [49] (figure 30c). They have large damping force and good working performance but are difficult to compact [49].

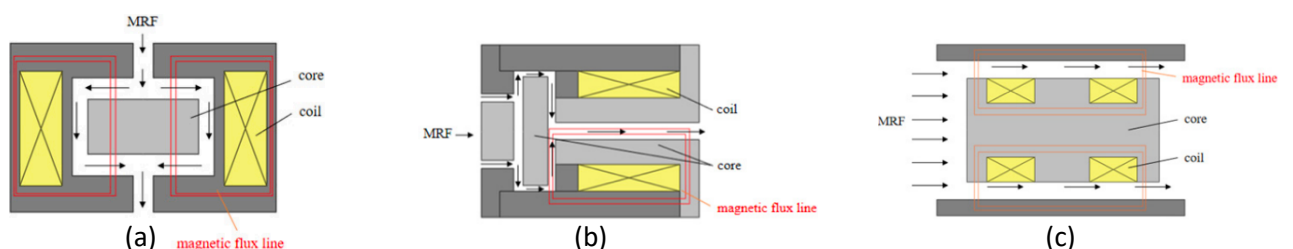


Figure 30: Magnetorheological fluid damper shapes [49]: (a) annular shaped, (b) radial shaped, (c) annular-radial shaped

Additionally, dampers can be classified as either linear or rotary based on their operating principle.

- Linear magnetorheological dampers consist of a piston that moves back and forth inside a cylinder filled with MR fluid [47]. Linear magnetorheological fluid dampers have the capability to change their damping stiffness by varying the magnetic field strength inside the damper [50]. However, they require large installation space, are less resistant to damage, use relatively large amounts of expensive fluid, and have high costs [50].
- Rotary MR fluid dampers are designed to operate based on angular velocity and incorporate one or more MR fluid working modes as the working principle [50]. They have several advantages, including compactness, low weight, and lower costs. However, they exhibit hysteresis behaviour, and the MR brake has low endurance [50].

There are three subtypes of linear MR dampers: mono tube, twin tube, and double-ended dampers [47][50].

- The mono tube MR damper consists of only one tube or reservoir, and the movement of the piston rod causes a volume change in the reservoir which is compensated for by an accumulator mechanism [47] (figure 31a).
- The twin tube MR damper has two fluid reservoirs with an inner housing filled with MR fluid, an outer housing and two valves [47] (figure 31b).
- The double-ended MR damper has two piston rods of the same diameter that enter the reservoir from both ends and does not require an accumulator mechanism [47] (figure 31c).

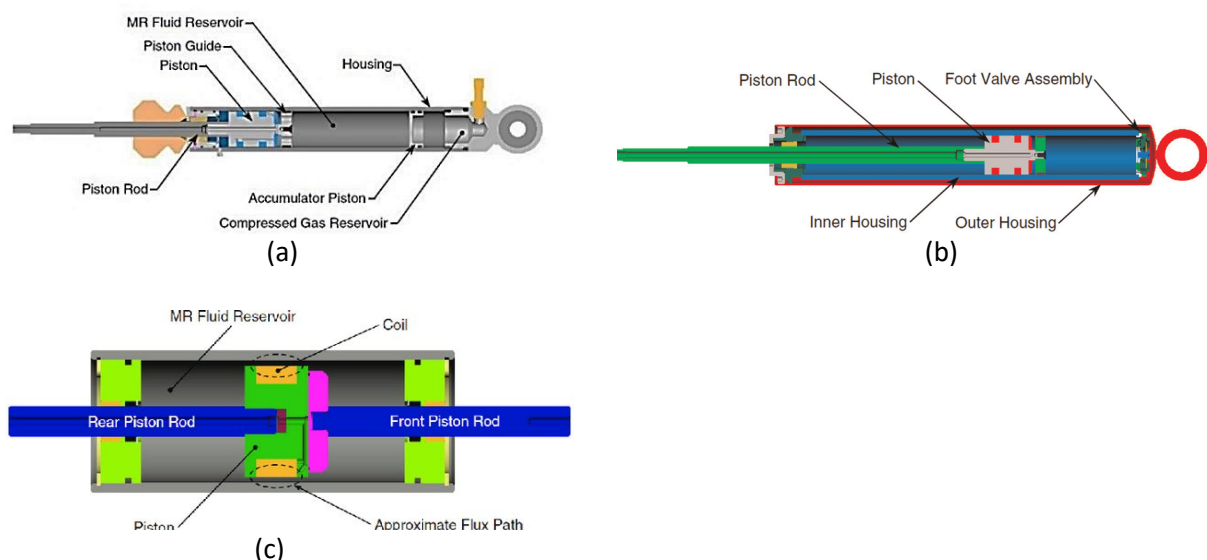


Figure 31: Linear magnetorheological dampers [51]: (a) mono tube-, (b) twin tube-, (c) double-ended damper

Rotary MR fluid dampers can be further classified into continuous angle and limited angle dampers, each with their own subtypes.

- The limited angle rotary MR fluid damper provides variable damping force over a limited range of rotation but cannot rotate continuously [50]. It has a larger damping torque than the continuous angle damper [47][50] but has a complex manufacturing process [50].
- The continuous angle damper on the other hand, has the capability to rotate with an infinite rotation angle [47] but had a lower damping force [47].

There are three subtypes within continuous angle dampers: drum type, disc type, and hybrid brake type. These type are capable of reducing the angular speed of a rotating shaft immersed in the fluid [50] but it also has lower endurance and are not compact [50].

- The continuous angle damper with drum type brake generates the damping force using a rotating drum, with the shear mode occurring in the radial gap of the rotor [50] (figure 32a).
- The continuous angle damper with disc type brake uses a rotating disc in order to generate the damping force, with the shear mode occurring in the axial gap of the rotor [50] (figure 32b).

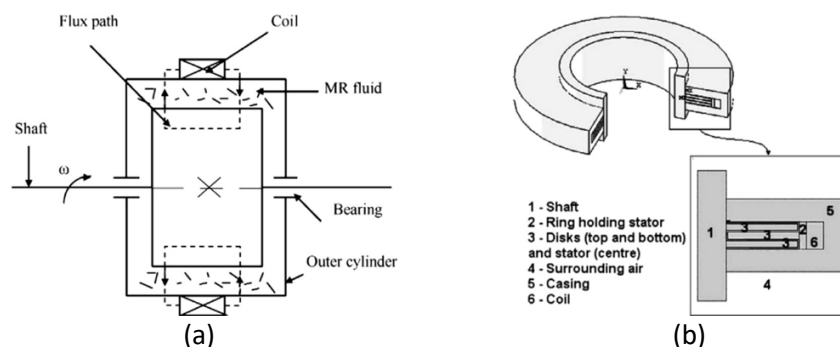


Figure 32: Continuous angle dampers [50]: (a) drum type brake damper, (b) disc type brake damper

- The continuous angle with hybrid brake is a combination of the two, with the housing made from magnetic material to guide the flux through the axial gap [50].

The hybrid brake can have various configurations, including single coil, double coil, and T-shaped.

- The single coil configuration has one electromagnetic coil wrapped around the cylinder containing the fluid [50] (figure 33a).
- The double coil configuration has two electromagnetic coils wrapped around the cylinder in opposite directions [50] (figure 33b).
- The T-shaped configuration is shaped like a T and has rotor and stator coil configurations [47] (figure 33c).

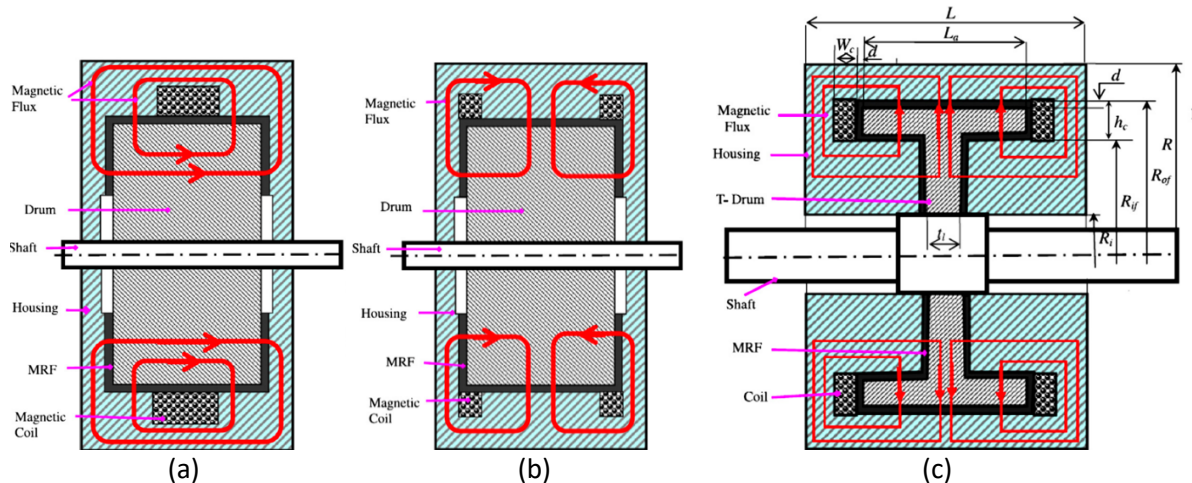


Figure 33: Hybrid type brake dampers [50]: (a) single coil-, (b) double coil-, T-shaped configuration

3.2.2.3 Electromagnetic dampers

Electromagnetic dampers use electromagnetic fields to create a resistance force in a moving object. Two types of electromagnetic dampers that have been found in the literature were eddy current dampers and motor-like electromagnetic dampers. Both dampers were used in prosthetics and other medical devices [43].

- Eddy current are passive electromagnetic devices composed of a conductive material moving through a magnetic field. They exploit the Foucault currents induced inside a plate moving in a magnetic field [43] (figure 34a). Eddy current dampers have several advantages, including the ability to avoid friction and their durability. They also have fast and precise dynamics. However, they have a low energy dissipation density [43].
- Motor-like electromagnetic dampers are based on the same principles as eddy current dampers, but their design is similar to that of electric motors [43]. They consist of a conductive body that forms a rotor and a stator to generate a magnetic field (figure 34b). This magnetic field can be either constant with permanent magnets or variable with other coils [43]. Motor-like electromagnetic dampers also have the advantage of avoiding friction and being durable, with fast and precise dynamics. However, they also have a low energy dissipation density [43].

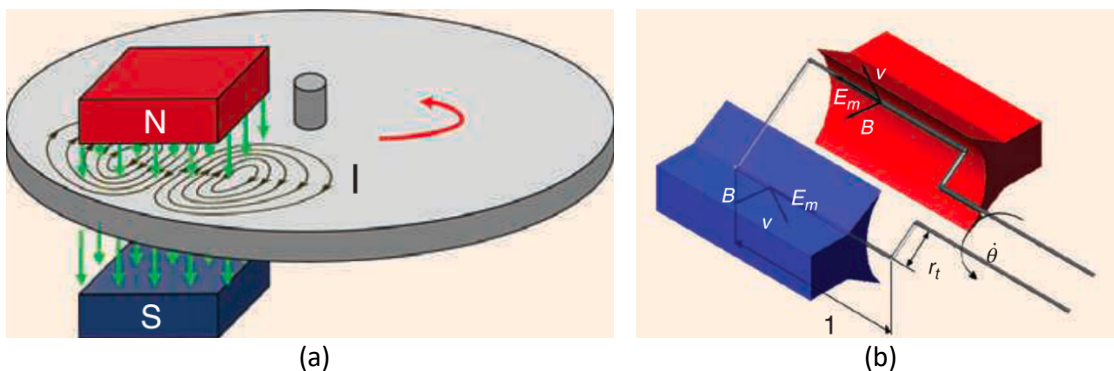


Figure 34: Electromagnetic dampers [43]: (a) eddy current-, (b) motor-like electromagnetic damper

3.2.2.4 Friction dampers

Friction dampers are a type of mechanical damping system that rely on the principle of friction to dissipate energy and reduce vibrations. There are two types of friction dampers for skeletal movement found in the literature: viscoelastic dampers and braking effect dampers. Both of them were used in rehabilitative systems, wearable robotics and haptic systems [43].

- Viscoelastic dampers use a viscoelastic material to absorb and dissipate mechanical energy. They use the same physical element to implement elasticity and damping, making them simple and easy to implement [43]. When a force is applied to the damper, the viscoelastic material deforms and absorbs the energy, then slowly returns to its original shape (figure 35a). However, the impossibility to decouple the elastic and damping effects can be a disadvantage of this type of damper [43].
- Braking effect dampers use dry friction between two stacked surfaces to generate damping [43] (figure 35b). They can emulate any type of damping effect with proper control and generate high forces but require careful pad location regulation and can cause braking on the link [43].

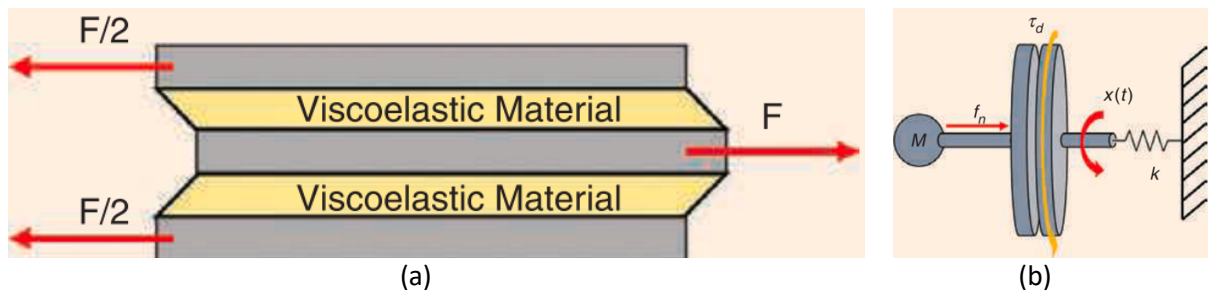


Figure 35: Friction dampers [43]: (a) viscoelastic damper, (b) braking effect damper

3.2.3 Springs for skeletal movement

Springs are an essential mechanical component that store mechanical energy when subjected to external forces and release it when those forces are removed. There were several categories of springs for skeletal movement found in the literature. Springs in the following categories will be described: Non-linear springs, compression springs and torsion springs. Furthermore, cam-based springs, lockable parallel springs, gas springs and rubber springs will be discussed. A comprehensive overview can be found in the Appendix (A3, table 4).

3.2.3.1 Non-linear springs

Springs are used in many mechanical systems to store and release energy. They are classified as either linear or nonlinear depending on the relationship between the applied force and the resulting deformation. Linear springs have a constant force-displacement relationship, where the force applied is directly proportional to the deformation of the spring. Nonlinear springs, on the other hand, have a nonlinear force-displacement relationship, where the force applied is not directly proportional to the deformation of the spring [52]. There were several types of nonlinear springs found in the literature, each with different applications. Variable dimension helical springs for midsole foot orthotics [53], Kresling pattern springs for artificial muscles [54] and shape memory alloy springs for artificial muscles [55] and ankle-foot orthotics [56].

- Variable dimension helical springs are helical springs with a non-uniform pitch coil diameter or wire diameter along the length of the spring [53]. These spring have a high strength to weight ratio, low costs and controllable suspension [53].
- Kresling pattern springs, on the other hand, are made by folding paper into a cylindrical bellow-type structure consisting of similar triangles arranged in cyclic symmetry and connected together [54] (figure 36). They stretch or compress when an external axial load or torque is applied, depending on the direction of the applied load [54].

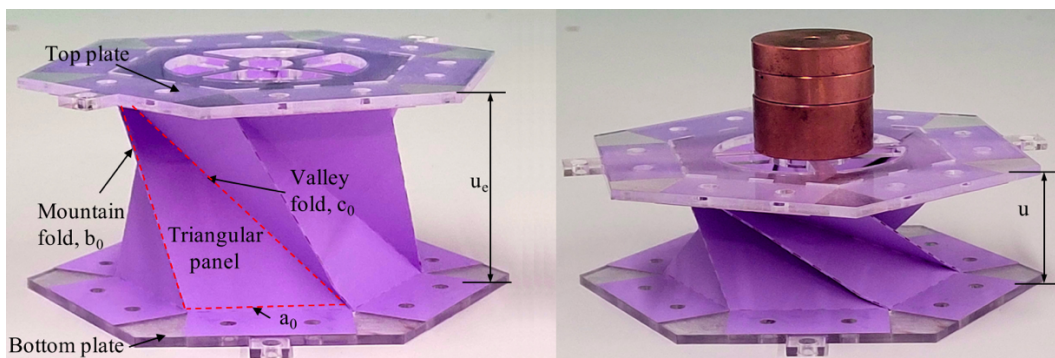


Figure 36: Kresling pattern spring, unloaded and loaded [54]

- Shape memory alloy springs are made out of an alloy, often Nitinol, that deforms under thermal conditions [55][57]. They can be formed into bundles [55] and offer various advantages such as the ability to be made into various shapes [58], lightweight and, flexible [55], high force and strain similar to that of human skeletal muscles [55]. They can also be However, the relaxation of SMA spring is highly affected by the cooling speed [59].

3.2.3.2 Compression springs

Compression springs are a very common type of springs and are widely used in various applications. They are designed to resist compressive forces and provide resistance when an external force is applied to the spring in a compressed state. Compression springs come in a variety of shapes and types. Compression springs that were found in the literature include coil springs for exoskeletons and leg prosthetics [60], CoiLeaf springs for ankle exoskeletons and ankle-foot prosthetics [61]. Wrap spring clutch/brake springs were found to be used in knee exoskeletons and constant force springs in arm exoskeletons [62].

- Coil springs are a commonly used type of spring made of steel wire that has been wound into a helical shape (figure 37a). Each turn of the coil provides a certain amount of force when the spring is compressed or stretched [60].
- Leaf springs are made from multiple thin metal plates, or "leaves," stacked on top of each other and held together by a center bolt acting as a pivot point. (OpenAI 2021 [3] input: leaf springs). Leaf springs compress and absorb the impact and are used in applications such as ankle exoskeletons and ankle-foot prosthetics [61]. They are flexible [63], have a simple structure [63], high load carrying capacity [63], small size [63] and are easy to adjust the stiffness [64].
- CoiLeaf springs are a combination of coil springs and leaf springs [61] (figure 37b).

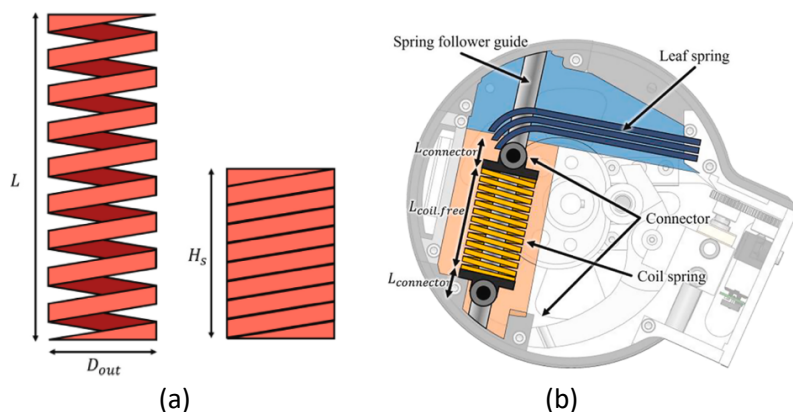


Figure 37: Compression springs: (a) coil spring [60], (b) CoiLeaf spring mechanism [61]

- Wrap spring clutch/brake utilizes steel coverings between inner and outer rotors that clamp and transmit torque as a result of the outer rotor's quick movement due to an interference fit, and are released by the outer rotor's slow speed for independent rotation [65] (figure 38a). This type provides high accuracy, repeatability, high torque to size ratio, low power consumption, and durability [74].
- Constant force springs provide constant force over a large displacement range. They are made of a tightly wound thin band of spring steel in a spool [62] (figure 38b). Although the force follows a curve at smaller displacements due to the initial shape and mechanics of the spring, the force remains nearly constant after the initial unwinding [62]. An advantage of constant force springs is their ability to provide a constant force over a wide range of motion. However, these springs may experience resonance as a result of stick-and-slip friction [62].

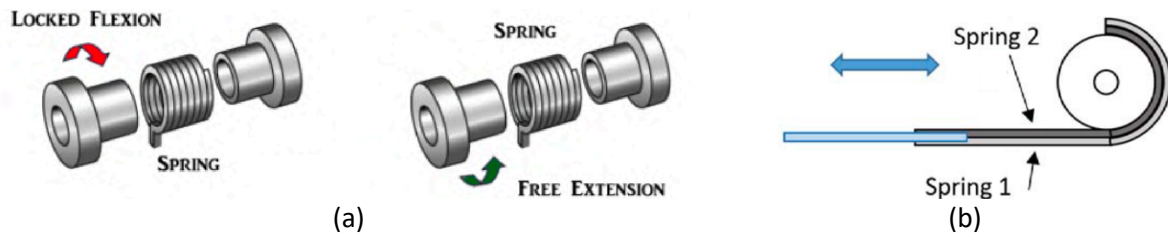


Figure 38: Compression springs: (a) wrap spring clutch/brake mechanism [65], (b) constant force spring [62]

3.2.3.3 Torsion springs

- Torsion springs are coiled springs that generate a moment proportional to the angular displacement and can be found in various applications including knee exoskeletons [67][66].
- Another variation that was used for artificial muscles is the carbon nanotube torsional spring, which is made of carbon nanotube material [68]. This material enables a high stiffness and extendibility. However, they have a low energy density compared to mechanical springs [68].

3.2.3.4 Other types

- Cam based springs were used in ankle prosthetics [69]. This is a type of mechanical spring that uses a specially designed cam shape to provide a non-linear force-displacement [69] (figure 39a).
- Lockable parallel springs were used in ankle and knee prosthetics [70]. This spring can be locked to maintain a constant force or tension. It's anchored to a carriage that moves on a rail. An ellipsoid part contacts the rail, creating a lock in one direction due to friction cone [70] (figure 39b). They are power efficient and have the ability to generate a passive stiffness when the device runs out of power [70].

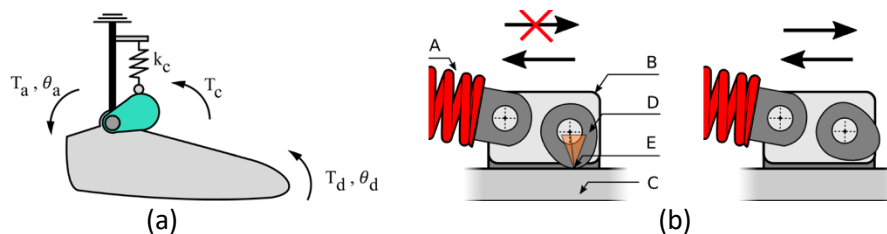


Figure 39: (a) Cam based spring mechanism [69], (b) working principle of a lockable parallel spring [70]

- Gas spring stores energy by compressing the gas inside the cylinder. The bigger the pressure, the air chamber inside gas spring will be reduced and accumulates the gas pressure and stores larger energy [71]. This type of spring was used in knee exoskeletons [72] and leg prosthetics [71]. They offer advantages such as acting as a brake or lock and providing a smoother response than a mechanical spring [72][71]
- Lastly, rubber springs, mechanical springs made of a rubber material, were used in exoskeletons and orthotics for the elbow, hand and fingers [73]. Rubber springs offer advantages such as a less limited elongation range than steel springs and being lightweight. However, they also have disadvantages such as the Mullins effect and hysteresis, which can affect their performance [73].

3.3 Implantability

This chapter focuses on the implantability criteria for actuators, dampers, and springs used in mechatronics for facilitating skeletal movement. The information presented in this chapter was initially sourced from ChatGPT (OpenAI, 2021 [4][5][6]) and was altered based on the knowledge gathered from articles about actuators, dampers and springs. This provides a comprehensive overview of the criteria that must be met for successful implantation.

3.3.1 Implantability criteria for actuators

Implantable actuators for skeletal movement must meet specific criteria in order to be suitable for use. Based on ChatGPT (OpenAI, 2021 [4]), these criteria include biocompatibility, size and shape, flexibility, force output, range of motion, durability and response time. Control and feedback was initially considered a criteria but was excluded due to the scope of this literature review. Based on knowledge gathered from articles about actuators, criteria of voltage range and weight were included.

A detailed description of each criteria was provided:

- **Biocompatibility:** The actuator must be made from biocompatible materials that are safe for implantation and do not cause an adverse immune response or rejection by the body. There are various materials that can be used for implantable actuators, such as titanium alloys, cobalt-chromium alloys, and certain polymers.
- **Size and shape:** The actuator must be small enough to be implanted in the desired location within the skeletal system, and its shape must be compatible with the surrounding bone and muscle tissue to minimize any damage or irritation to the tissue.
- **Weight:** Weight is another important consideration for implantable actuators for skeletal movement. In general, implantable devices should be lightweight to minimize the overall load on the body and reduce the risk of complications such as tissue damage, implant migration, or discomfort.
- **Flexibility:** Another important consideration for implantable actuators for skeletal movement is flexibility. The flexibility of the device can affect how well it can conform to the shape of the body and how well it can adapt to different movements.
- **Force output:** The actuator must be able to provide a specific force output that is appropriate for the intended application. The force output can vary depending on the specific location and function of the implant.
- **Range of motion:** The actuator must be able to provide a range of motion that is appropriate for the intended application.
- **Durability:** The actuator must be designed to have a long fatigue life and be able to withstand the repeated mechanical stresses associated with skeletal movement. The fatigue life will depend on the specific material and design of the actuator.
- **Voltage range:** The actuator must operate within a specific voltage range that is compatible with the surrounding tissue and any external power source.
- **Response time:** In general, implantable actuators for skeletal movement should be designed to have a fast response time in order to enable rapid and precise movements. The response time of the device can be influenced by a variety of factors, including the control system design, the communication interface between the device and external controllers, and the mechanical properties of the actuator.

3.3.2 Implantability criteria for dampers

Similar to implantable actuators, implantable dampers also have specific criteria that must be met to ensure their safe and effective use within the skeletal system. Based on ChatGPT (OpenAI, 2021 [5]), these criteria include biocompatibility, size and shape, flexibility, durability and response time. Based on knowledge gathered from articles about dampers, criteria of damping force, damping flexibility and weight were included.

An overview with description of each criteria was given:

- **Biocompatibility:** The damper must be made from biocompatible materials that are safe for implantation and do not cause an adverse immune response or rejection by the body. There are various materials that can be used for implantable dampers, such as titanium alloys, cobalt-chromium alloys, and certain polymers.
- **Size and shape:** The damper must be small enough to be implanted in the desired location within the skeletal system, and its shape must be compatible with the surrounding bone and muscle tissue to minimize any damage or irritation to the tissue.
- **Weight:** Weight is another important consideration for implantable dampers for skeletal movement. In general, implantable devices should be lightweight to minimize the overall load on the body and reduce the risk of complications such as tissue damage, implant migration, or discomfort.
- **Flexibility:** Another important consideration for implantable dampers for skeletal movement is flexibility. The flexibility of the device can affect how well it can conform to the shape of the body and how well it can adapt to different movements.
- **Damping force:** the damper should be designed to provide the appropriate amount of damping force for the specific skeletal movement it is intended to dampen.
- **Damping flexibility:** the damper should have the ability to adjust the damping force according to the changing needs of the skeletal movement, such as during different phases of gait.
- **Durability:** The damper must be designed to have a long fatigue life and be able to withstand the repeated mechanical stresses associated with skeletal movement. The fatigue life will depend on the specific material and design of the damper.
- **Response time:** In general, implantable dampers for skeletal movement should be designed to have a fast response time in order to enable rapid and precise movements. The response time of the device can be influenced by a variety of factors, including the control system design, the communication interface between the device and external controllers, and the mechanical properties of the damper.

3.3.3 Implantability criteria for springs

When using springs for implantation, the following criteria was considered based on ChatGPT (OpenAI, 2021 [6]): biocompatibility, size and shape, flexibility, spring stiffness, range of motion, durability and response time. Based on knowledge gathered from articles about springs, criteria of the spring strength, and weight were also included.

A detailed description of each criteria was provided:

- **Biocompatibility:** The spring must be made from biocompatible materials that are safe for implantation and do not cause an adverse immune response or rejection by the body. There are various materials that can be used for implantable springs, such as titanium alloys, cobalt-chromium alloys, and certain polymers.
- **Size and shape:** The spring must be small enough to be implanted in the desired location within the skeletal system, and its shape must be compatible with the surrounding bone and muscle tissue to minimize any damage or irritation to the tissue. The size and shape of the spring will depend on the specific location and function of the implant.
- **Weight:** The implantable spring should be lightweight to minimize the load on the skeletal structure and avoid any additional stress or strain.
- **Flexibility:** The implantable spring should have some degree of flexibility to allow for natural movement of the skeletal structure. This is important to ensure that the movement feels natural and does not cause discomfort or pain.
- **Spring strength:** The spring should have sufficient strength to provide support to the skeletal structure and resist any deformation or breakage.
- **Spring stiffness:** The spring stiffness should be adequate to provide the necessary support for the skeletal movement. The stiffness can vary depending on the application, but generally, it should be high enough to support the movement without causing discomfort or damage to surround tissues.
- **Range of motion:** The spring must be able to provide a range of motion that is appropriate for the intended application.
- **Durability:** The spring must be designed to have a long fatigue life and be able to withstand the repeated mechanical stresses associated with skeletal movement. The fatigue life will depend on the specific material and design of the spring.
- **Response time:** The spring should respond quickly to changes in the skeletal movement. This is important to ensure that the movement feels natural and does not cause discomfort or pain.

3.3.4 Assessment of implantability criteria

An assessment of the advantages and disadvantages of actuators, dampers and springs was conducted using the implantability criteria. The aim of the assessment was to evaluate the suitability of the different actuators for implantation in the human body. Each advantage and disadvantage was analysed and assessed based on implantability criteria in order to determine whether it was feasible to implant the actuator, damper or spring. A table containing the comparison of each advantage and disadvantage with the implantability criteria will provide an overview of the suitability of each technique for implantation or further research (Appendix B1,B2,B3, table 4,5a,5b,6).

3.4 Suitability of mechatronic techniques for implantation

By evaluating each actuator, damper and spring, it was possible to determine which techniques were the most suitable for implantation, which ones needed more research and which ones weren't suitable for implantation. Table 1 shows the results of the assessment:

	Actuators suitable for skeletal movement	Dampers suitable for skeletal movement	Springs suitable for skeletal movement
Likely implantable	Yoshimura pattern origami actuator Miura-ori pattern origami actuator Kresling pattern origami actuator McKibben pneumatic actuator Carbon nanotube actuator	Magnetorheological fluid damper: annular shaped Rotary magnetorheological fluid damper: limited angle	Leaf spring Shape memory alloy spring
Likely not implantable	Servo motor DC brushless motor Rotary pneumatic actuator Pneumatically driven microcage actuator Pneumatic balloon actuator Flexible rubber micro actuator PneuNets actuator Elastomeric HASEL actuator Thermoplastic HASEL actuator Expansion behaviour based hydraulic actuator Magnetic shape memory alloy actuator Magnetic hydrogel based actuator Piezoelectric actuator Cellulose paper actuator Electro-ribbon actuator Ionic polymer metal composition actuator Dielectric elastomer actuator Piezoelectric polymer actuator Electrostrictive graft elastomer actuator Shape memory alloy actuator Phase changing actuator Bilayer electrothermal actuator Series elastic actuator Clutchable elastic device Two springs acting in series and parallel	Magnetorheological or electrorheological fluid damper: flow mode Magnetorheological fluid damper: radial shaped Magnetorheological fluid damper: annular-radial shaped Linear magnetorheological fluid damper Rotary magnetorheological fluid damper: continuous angle with drum type brake Rotary magnetorheological fluid damper: continuous angle with disc type brake Rotary magnetorheological fluid damper: continuous angle with hybrid brake Rotary magnetorheological fluid damper: continuous angle with hybrid brake (single coil) Rotary magnetorheological fluid damper: continuous angle with hybrid brake (double coil) Rotary magnetorheological fluid damper: continuous angle with hybrid brake (T-shaped)	Constant force spring Rubber spring
Further research	Convoluted skin vacuum actuator Pleated skin vacuum actuator Linear pneumatic actuator HASEL actuator Pleated pneumatic actuator Antagonistic pleated pneumatic actuator Sleeved bladder actuator Yarlott netted muscle actuator Kukolj netted muscle actuator ROMAC actuator Morin muscle actuator Paynter hyperboloid actuator Kleinwachter torsion device Peano muscle actuator Series pneumatic muscle actuator Flat pneumatic muscle actuator Reverse pneumatic artificial muscle actuator Straight fiber type pneumatic actuators High-displacement pneumatic muscle actuator Flexible micro actuator Magnetorheological elastomer actuator Ionic polymer gel actuator Conductive polymer actuator Liquid crystal elastomer actuator Ferroelectric polymer actuator Shape memory polymer actuator Twisted and coiled polymer actuator Thermal actuator Nonlinear series elastic actuator Independent variable stiffness actuator Antagonistic variable stiffness actuator AwAS I AwAS II VSA-UT VSA-UT II mVSA-UT Hybrid dual actuator unit CompAct variable stiffness actuator	Oil damper Electrorheological fluid damper Magnetorheological or electrorheological fluid damper: shear mode Magnetorheological or electrorheological fluid damper: squeeze mode Linear magnetorheological fluid damper: mono tube Linear magnetorheological fluid damper: twin tube Linear magnetorheological fluid damper: double ended Linear magnetorheological fluid damper: double ended Rotary magnetorheological fluid damper Rotary magnetorheological fluid damper: continuous angle Eddy current damper Motor-like electromagnetic damper Viscoelastic damper Braking effect damper	Non-linear spring Variable dimension helical spring Kresling pattern spring Coil spring CoilLeaf spring Wrap spring clutch/brake Torsion spring Carbon nanotube torsial spring Cam based spring Lockable parallel spring Gas spring

Table 1: Classification matrix implantability. Likely implantable, likely not implantable, further research (vertical axis). Actuators-, dampers- and springs for skeletal movement (horizontal axis).

Discussion

The aim of this study was to evaluate the suitability of actuators, dampers, and springs for implantation to facilitate skeletal movement. The implantability criteria were used to assess the advantages and disadvantages of each technique. The results show that while each technique has its advantages and disadvantages, some techniques are more suitable for implantation than others.

For actuators, McKibben pneumatic actuators, were found to be suitable technique for implantation due to their biocompatibility, weight, flexibility, force output and durability. Carbon nanotube actuators are possible implantable due to their low voltage requirement, durability and biocompatibility. Furthermore, Yoshimura-, Miura-ori- and Kresling pattern origami actuators were found to be the most suitable technique for implantation due to their biocompatibility, size and shape and range of motion. For some actuators, however, it was clear that they were not implantable, mainly due to their high voltage requirement, size and weight and biocompatibility. For the remaining actuators, the available information was insufficient to determine the implantability. Further research is required to evaluate their potential for implantation.

The dampers that were found to be suitable for implantation include magnetorheological fluid dampers due to their biocompatibility, size and shape, damping adjustment, and response time. Rotary magnetorheological fluid dampers with limited angle were also likely implantable due to their acceptable size and shape, weight, and damping force. However, a few dampers were not likely to be implantable mainly because of their durability and size and shape. For some dampers, there was insufficient information to evaluate whether they are implantable or not, so further research is needed to determine their potential for implantation.

For springs, leaf springs and shape memory alloy springs were found to be suitable for implantation. Leaf springs have the advantage of their size and shape, flexibility, range of motion and spring stiffness. Shape memory alloy springs are likely implantable because of their low weight, flexibility, spring strength and stiffness, range of motion and durability. However, constant force springs and rubber springs were unlikely to be suitable for implantation due to their durability, which may limit their lifespan in the body. For the remaining springs, there was not enough information available to determine their implantability. Further research is needed to evaluate their potential for implantation.

In conclusion, this study provides an evaluation of the implantability of actuators, dampers, and springs for skeletal movement. While each technique has its advantages and limitations, the results of this study can help the development of new implantable devices for skeletal movement, which can contribute to the development for artificial muscles.

5

Limitations

While the findings and discussion presented in this report provide valuable insights into the potential for implantable actuators, dampers, and springs to facilitate skeletal movement, there are several limitations that need to be acknowledged.

Firstly, only one search database, Google Scholar, was used to gather information for this study. It is possible that relevant studies and information may have been missed. Using additional databases and search engines could have provided a more comprehensive overview of the subject and potentially yielded different results.

Secondly, there was a lot of variation in the information available for each technique, making it difficult to make direct comparisons between them. Furthermore, the implantability assessment was based on the available information, and not all criteria were met for each technique. Therefore, the list of potentially implantable techniques may not be entirely accurate. Additionally, for some techniques, there was limited information available, necessitating further research to determine their implantability.

Another limitation of this study is that the criteria used in this study were based on the output of ChatGPT (OpenAI, 2021), it may not have been comprehensive enough. As a result, a new study should be conducted to provide a more thorough overview of the criteria for implantable devices for skeletal movement.

In addition, only actuators, springs, and dampers were evaluated, while other techniques used in mechatronics, such as sensors and microcontrollers, were not included. Therefore, the results of this study provide only a limited perspective on the potential for implantable devices for skeletal movement.

Finally, the study did not include an evaluation of the control, electrical components, and embedded systems necessary for the operation of the evaluated actuators, dampers, and springs. These components are essential for the safe and effective functioning of implantable devices and can significantly affect their implantability. Future research could address this limitation by exploring these components in more depth.

6

Conclusion

In conclusion, this study aimed to evaluate the suitability of different techniques for implantation to facilitate skeletal movement, including actuators, dampers, and springs. The implantability criteria were used to assess the advantages and disadvantages of each technique, and the results were analysed to determine which technique was likely suitable for implantation, which ones were not likely for implantation and which one needed further research.

The assessment of the implantability criteria showed that all five actuators (McKibben pneumatic actuators, carbon nanotube actuators, Yoshimura-, Miura-ori- and Kresling pattern origami actuators) two dampers (magnetorheological fluid dampers, rotary magnetorheological fluid dampers: limited angle) and two springs (leaf springs, shape memory alloy springs) were most likely to be implantable.

However, it is important to note that there were several limitations to this study, including the use of one search database and chatGPT, the exclusion of other techniques commonly used in mechatronics and the variation in advantages and disadvantages which made a comparison between the techniques difficult. Nonetheless, the findings of this study provide valuable insights into the potential for implantable devices to facilitate skeletal movement and techniques to be used for artificial muscles.

7.1 Articles

- [1] M. Craddock, E. Augustine, S. Konerman, and M. Shin, "Biorobotics: An Overview of Recent Innovations in Artificial Muscles," *Actuators*, vol. 11, no. 6, 2022, doi: 10.3390/act11060168.
- [2] H. M. Herr and R. D. Kornbluh, "New horizons for orthotic and prosthetic technology: artificial muscle for ambulation," *Smart Struct. Mater. 2004 Electroact. Polym. Actuators Devices*, vol. 5385, no. July 2004, p. 1, 2004, doi: 10.1117/12.544510.
- [3] A. G. Dunning and J. L. Herder, "A review of assistive devices for arm balancing," *IEEE Int. Conf. Rehabil. Robot.*, 2013, doi: 10.1109/ICORR.2013.6650485.
- [4] J. H. Lee, S. Okamoto, and S. Matsubara, "Development of Multi-Fingered Prosthetic Hand Using Shape Memory Alloy Type Artificial Muscle," *Comput. Technol. Appl.*, vol. 3, pp. 477–484, 2012.
- [5] T. T. Tollefson and C. W. Senders, "Restoration of eyelid closure in facial paralysis using artificial muscle: Preliminary cadaveric analysis," *Laryngoscope*, vol. 117, no. 11, pp. 1907–1911, 2007, doi: 10.1097/MLG.0b013e31812e0190.
- [6] L. G. Ledgerwood, S. Tinling, C. Senders, A. Wong-Foy, H. Pahlad, and T. T. Tollefson, "Artificial muscle for reanimation of the paralyzed face: Durability and biocompatibility in a gerbil model," *Arch. Facial Plast. Surg.*, vol. 14, no. 6, pp. 413–418, 2012, doi: 10.1001/archfacial.2012.696.
- [7] B. Kalita, A. Leonessa, and S. K. Dwivedy, "A Review on the Development of Pneumatic Artificial Muscle Actuators: Force Model and Application," *Actuators*, vol. 11, no. 10, pp. 1–28, 2022, doi: 10.3390/act11100288.
- [8] R. Tiwari, M. A. Meller, K. B. Wajcs, C. Moses, I. Reveles, and E. Garcia, "Hydraulic artificial muscles," *J. Intell. Mater. Syst. Struct.*, vol. 23, no. 3, pp. 301–312, 2012, doi: 10.1177/1045389X12438627.
- [9] C. Naresh, P. S. C. Bose, and C. S. P. Rao, "Shape memory alloys: A state of art review," *IOP Conf. Ser. Mater. Sci. Eng.*, vol. 149, no. 1, 2016, doi: 10.1088/1757-899X/149/1/012054.
- [10] Y. Bar-cohen and J. P. L. Caltech, "Artificial Muscles using Electroactive Polymers (EAP): Capabilities , Challenges and Potential," pp. 1–14, 2005.
- [11] F. Carpi and D. De Rossi, "Electroactive polymer artificial muscles: An overview," *WIT Trans. Ecol. Environ.*, vol. 138, pp. 353–364, 2010, doi: 10.2495/DN100311.
- [12] M. J. Page *et al.*, "PRISMA 2020 explanation and elaboration: Updated guidance and exemplars for reporting systematic reviews," *BMJ*, vol. 372, 2021, doi: 10.1136/bmj.n160.
- [13] L. Roever, "PICO: model for clinical questions," *Evid. Based. Med.*, vol. 3, no. 2, pp. 1–2, 2018, doi: 10.4172/2471-9919.1000115.
- [14] K. Subramaniam, R. Shenoy, V. Velu, A. A. Zainuddin, L. G. Kurappa, and V. Amirtham, "A Review of Actuators in Ankle-Foot Rehabilitation Therapy," vol. 2, no. December, pp. 71–74, 2022.

- [15] N. El-Atab *et al.*, “Soft Actuators for Soft Robotic Applications: A Review,” *Adv. Intell. Syst.*, vol. 2, no. 10, p. 2000128, 2020, doi: 10.1002/aisy.202000128.
- [16] Z. Wu, M. Yang, Y. Xia, and L. Wang, “Mechanical Structural Design and Actuation Technologies of Powered Knee Exoskeletons: A Review,” *Applied Sciences (Switzerland)*, vol. 13, no. 2. 2023, doi: 10.3390/app13021064.
- [17] A. R. Ismawan, R. Ismail, T. Prahasto, M. Ariyanto, and B. Setiyana, “A Review of Existing Transtibial Bionic Prosthesis: Mechanical Design, Actuators and Power Transmission,” *J. Biomed. Sci. Bioeng.*, vol. 1, no. 2, pp. 65–72, 2022, doi: 10.14710/jbiomes.2021.v1i2.65-72.
- [18] C. Yang *et al.*, “Current developments of robotic hip exoskeleton toward sensing, decision, and actuation: A review,” *Wearable Technol.*, vol. 3, 2022, doi: 10.1017/wtc.2022.11.
- [19] C. Thalman and P. Artemiadis, “A review of soft wearable robots that provide active assistance: Trends, common actuation methods, fabrication, and applications,” *Wearable Technologies*, vol. 1. 2020, doi: 10.1017/wtc.2020.4.
- [20] S. Joe, F. Bernabei, and L. Beccai, “A Review on Vacuum-Powered Fluidic Actuators in Soft Robotics,” in *Rehabilitation of the Human Bone-Muscle System*, IntechOpen, 2022
- [21] N. Shankar, T. Kamma, B. Mahesh Krishna, C. Harish Kumar, and B. Shalem, “Smart Actuators: A Review Smart Actuators: A Review Notations-Inertia of Motor-Motor Damping Coefficient-Inertia of Load-Load Damping Coefficient-Spring Constant-Angular displacement variable for Motor-Angular displacement variable f ,” 2021, Accessed: Mar. 29, 2023. [Online]. Available: <https://www.researchgate.net/publication/358565034>.
- [22] A. De Greef, P. Lambert, and A. Delchambre, “Towards flexible medical instruments: Review of flexible fluidic actuators,” *Precision Engineering*, vol. 33, no. 4. pp. 311–321, 2009, doi: 10.1016/j.precisioneng.2008.10.004.
- [23] A. Pagoli, F. Chapelle, J. A. Corrales-Ramon, Y. Mezouar, and Y. Lapusta, “Review of soft fluidic actuators: Classification and materials modeling analysis,” *Smart Materials and Structures*, vol. 31, no. 1. 2022, doi: 10.1088/1361-665X/ac383a.
- [24] Z. Ma and D. Sameoto, “A Review of Electrically Driven Soft Actuators for Soft Robotics,” *Micromachines*, vol. 13, no. 11, 2022, doi: 10.3390/mi13111881.
- [25] J. Bernat, P. Gajewski, J. Kołota, and A. Marcinkowska, “Review of Soft Actuators Controlled with Electrical Stimuli: IPMC, DEAP, and MRE,” *Applied Sciences (Switzerland)*, vol. 13, no. 3. 2023, doi: 10.3390/app13031651.
- [26] I. Kulagin, M. Li, V. Laitinen, and H. Handroos, “Review of MSM Actuators: Applications, Challenges, and Potential,” *IEEE Access*, vol. 10, no. July. IEEE, pp. 83841–83850, 2022, doi: 10.1109/ACCESS.2022.3197278.
- [27] Y. He, “Magnetic hydrogel-based flexible actuators: A comprehensive review on design, properties, and applications | Enhanced Reader,” 2023. .
- [28] M. Nazibul Hasan, “MEMS actuators for biomedical applications: A review,” 2020. <chrome-extension://dagcmkpagilhakfdhnbomgmjdpkdklff/enhanced-reader.html?pdf=http%3A%2F%2Fwww.hms.harvard.edu%2Fbss%2Fneuro%2Fbornlab%2Fnb204%2Fstatistics%2Fbootstrap.pdf> (accessed Mar. 29, 2023).
- [29] Y. Liu, S. Shang, S. Mo, P. Wang, B. Yin, and J. Wei, “Soft actuators built from cellulose paper: A review on actuation, material, fabrication, and applications,” *J. Sci. Adv. Mater. Devices*, vol. 6, no. 3, pp. 321–337, Sep. 2021, doi: 10.1016/J.JSAMD.2021.06.004.

- [30] Y. Bar-cohen, “Electroactive polymer (EAP) actuators — background review,” pp. 1–14, 2019.
- [31] A. V Maksimkin, T. Dayyoub, D. V Telyshev, and A. Y. Gerasimenko, “Electroactive Polymer-Based Composites for Artificial Muscle-like Actuators: A Review,” *Nanomaterials*, vol. 12, no. 13. 2022, doi: 10.3390/nano12132272.
- [32] Z. Liu, Y. D. Liu, Q. Shi, and Y. Liang, “Electroactive dielectric polymer gels as new-generation soft actuators: a review,” *Journal of Materials Science*, vol. 56, no. 27. pp. 14943–14963, 2021, doi: 10.1007/s10853-021-06260-y.
- [33] U. Kosidlo *et al.*, “Nanocarbon based ionic actuators-a review,” *Smart Mater. Struct.*, vol. 22, no. 10, 2013, doi: 10.1088/0964-1726/22/10/104022.
- [34] J. Ahn *et al.*, “A Review of Recent Advances in Electrically Driven Polymer-Based Flexible Actuators: Smart Materials, Structures, and Their Applications,” *Advanced Materials Technologies*, vol. 7, no. 11. pp. 2200041–2200042, 2022, doi: 10.1002/admt.202200041.
- [35] Y. Wang *et al.*, “Dielectric elastomer actuators for artificial muscles: A comprehensive review of soft robot explorations,” *Resour. Chem. Mater.*, vol. 1, no. 3–4, pp. 308–324, Sep. 2022, doi: 10.1016/j.recmm.2022.09.001.
- [36] A. O’Halloran, F. O’Malley, and P. McHugh, “A review on dielectric elastomer actuators, technology, applications, and challenges,” *J. Appl. Phys.*, vol. 104, no. 7, 2008, doi: 10.1063/1.2981642.
- [37] X. Tang, H. Li, Y. Yang, J. Luo, H. Wang, and P. Jiang, “A Review of Soft Actuator Motion : Actuation , Design ,” vol. 11, no. 11, pp. 1–25, 2022.
- [38] S. Wolf *et al.*, “Variable Stiffness Actuators: Review on Design and Components,” *IEEE/ASME Transactions on Mechatronics*, vol. 21, no. 5. pp. 2418–2430, 2016, doi: 10.1109/TMECH.2015.2501019.
- [39] B. Vanderborcht *et al.*, “Variable impedance actuators: A review,” *Rob. Auton. Syst.*, vol. 61, no. 12, pp. 1601–1614, 2013, doi: 10.1016/j.robot.2013.06.009.
- [40] Y.-L. Cheng *et al.*, *Series Elastic Actuator: Design, Analysis and Comparison*, vol. 11, no. tourism. 2016.
- [41] E. J. Rouse, L. M. Mooney, and H. M. Herr, “Clutchable series-elastic actuator: Implications for prosthetic knee design,” *Int. J. Rob. Res.*, vol. 33, no. 13, pp. 1611–1625, 2014, doi: 10.1177/0278364914545673.
- [42] Mr. S. A. Lavate and Dr. R. G. Todkar, “Variable Stiffness Actuators : A General Review,” *Int. J. Eng. Res.*, vol. V4, no. 07, pp. 201–205, 2015, doi: 10.17577/ijertv4is070214.
- [43] S. Monteleone, F. Negrello, M. G. Catalano, M. Garabini, and G. Grioli, “Damping in Compliant Actuation: A Review,” *IEEE Robot. Autom. Mag.*, vol. 29, no. 3, pp. 47–66, 2022, doi: 10.1109/MRA.2021.3138388.
- [44] C. Zhou, Z. Yang, K. Li, and X. Ye, “Research and Development of Ankle–Foot Orthoses: A Review,” *Sensors*, vol. 22, no. 17, pp. 1–15, 2022, doi: 10.3390/s22176596.
- [45] H. Abe, K. Kadowaki, N. Tsujimoto, and T. OKANUKA, “A Narrative Review of Alternate Gait Training Using Knee-ankle-foot Orthosis in Stroke Patients with Severe Hemiparesis,” *Phys. Ther. Res.*, vol. 24, no. 3, pp. 195–203, 2021, doi: 10.1298/ptr.r0015.
- [46] T. Y. S Yamamoto, A Hagiwara, T Mizobe, O Yokoyama, “Development of an ankle – foot orthosis with an oil damper Enhanced Reader.pdf.” 2005.

- [47] M. Rahman, Z. C. Ong, S. Julai, M. M. Ferdaus, and R. Ahamed, "A review of advances in magnetorheological dampers: their design optimization and applications," *J. Zhejiang Univ. Sci. A*, vol. 18, no. 12, pp. 991–1010, 2017, doi: 10.1631/jzus.A1600721.
- [48] H. Lv, S. Zhang, Q. Sun, R. Chen, and W. J. Zhang, "The Dynamic Models, Control Strategies and Applications for Magnetorheological Damping Systems: A Systematic Review," *J. Vib. Eng. Technol.*, vol. 9, no. 1, pp. 131–147, 2021, doi: 10.1007/s42417-020-00215-4.
- [49] Y. Zhang, J. Guo, J. Yang, and X. Li, "Recent Structural Developments and Applications of Magnetorheological Dampers (MRD): A Review," 2023.
- [50] F. Imaduddin, S. A. Mazlan, and H. Zamzuri, "A design and modelling review of rotary magnetorheological damper," *Mater. Des.*, vol. 51, pp. 575–591, 2013, doi: 10.1016/j.matdes.2013.04.042.
- [51] C. J. Poynor, "Innovative Designs for Magneto-Rheological Dampers," pp. 1–12, 2001.
- [52] Kobelev V., "Smart springs," pp. 1–12, 2013.
- [53] M. Ali, A. Nazir, and J. Y. Jeng, "Mechanical performance of additive manufactured shoe midsole designed using variable-dimension helical springs," *Int. J. Adv. Manuf. Technol.*, vol. 111, no. 11–12, pp. 3273–3292, 2020, doi: 10.1007/s00170-020-06227-4
- [54] S. Khazaaleh, R. Masana, and M. F. Daqaq, "Functional, Durable, and Scalable Origami-Inspired Springs," 2021, [Online]. Available: <http://arxiv.org/abs/2105.06769>.
- [55] S. J. Park, U. Kim, and C. H. Park, "A Novel Fabric Muscle Based on Shape Memory Alloy Springs," *Soft Robot.*, vol. 7, no. 3, pp. 321–331, 2020, doi: 10.1089/soro.2018.0107.
- [56] H. M. Afifah, I., & Sopiany, "Toward Creating Normal Ankle Joint Behavior for Drop Foot Patients Using an Ankle Foot Orthosis (AFO) with Superplastic NiTi Springs," vol. 87, no. 1,2, pp. 149–200, 2017.
- [57] E. A. Allen, "Design and modeling of a pneumasoft robotics catheter device using resistance-based modeling of nitinol springs" no. July, 2022.
- [58] T. Devashena and K. Dhanalakshmi, "Simultaneous Measurements in Shape Memory Alloy Springs to Enable Structural Health Monitoring by Self-Sensing Actuation," *Arab. J. Sci. Eng.*, vol. 46, no. 6, pp. 6015–6025, 2021, doi: 10.1007/s13369-020-05259-y.
- [59] K. Choi, S. J. Park, M. Won, and C. H. Park, "Soft fabric muscle based on thin diameter SMA springs," *Smart Mater. Struct.*, vol. 31, no. 5, 2022, doi: 10.1088/1361-665X/ac6550.
- [60] J. O. van der Weijde, *Self-sensing of coil springs and twisted and coiled polymer muscles*. 2022.
- [61] J. Moon, J. Ryu, J. Kim, and G. Lee, "CoilLeaf spring: A hybrid system of coil and leaf springs for maximizing space utilization and energy storage," *Mech. Mach. Theory*, vol. 178, no. September, p. 105094, 2022, doi: 10.1016/j.mechmachtheory.2022.105094.
- [62] P. W. Hill, E. T. Wolbrecht, and J. C. Perry, "Gravity Compensation of an Exoskeleton Joint Using Constant- Force Springs," *2019 IEEE 16th Int. Conf. Rehabil. Robot.*, pp. 311–316, 2019.
- [63] Y. Lu, Y. Yang, Y. Xue, J. Jiang, Q. Zhang, and H. Yue, "A Variable Stiffness Actuator Based on Leaf Springs: Design, Model and Analysis," *Actuators*, vol. 11, no. 10, 2022, doi: 10.3390/act11100282.
- [64] X. Wu, Z. Zhao, J. Wang, D. Xu, and W. Chen, "A novel design of variable stiffness linkage with distributed leaf springs," *Proc. 2016 IEEE 11th Conf. Ind. Electron. Appl. ICIEA 2016*, pp. 789–794, 2016, doi: 10.1109/ICIEA.2016.7603689.

- [65] V. A. S. Mani, N. Goldfarb, and G. S. Fischer, "Design, development and characterization of a wrap spring clutch/brake mechanism as a knee joint for an assistive exoskeleton," *Proc. ASME Des. Eng. Tech. Conf.*, vol. 9, 2020, doi: 10.1115/DETC2020-22444.
- [66] R. Chaichaowarat, D. F. P. Granados, J. Kinugawa, and K. Kosuge, "Passive knee exoskeleton using torsion spring for cycling assistance," *IEEE Int. Conf. Intell. Robot. Syst.*, vol. 2017-Septe, pp. 3069–3074, 2017, doi: 10.1109/IROS.2017.8206146.
- [67] K. B. Bumbard, H. Herrington, C. H. Goh, and A. Ibrahim, "Incorporation of Torsion Springs in a Knee Exoskeleton for Stance Phase Correction of Crouch Gait," *Appl. Sci.*, vol. 12, no. 14, 2022, doi: 10.3390/app12147034.
- [68] S. Liu, C. Martin, D. Lashmore, M. Schauer, and C. Livermore, "Carbon nanotube torsional springs for regenerative braking systems," *J. Micromechanics Microengineering*, vol. 25, no. 10, 2015, doi: 10.1088/0960-1317/25/10/104005.
- [69] J. Realmuto, G. Klute, and S. Devasia, "Nonlinear passive cam-based springs for powered ankle prostheses," *J. Med. Devices, Trans. ASME*, vol. 9, no. 1, 2015, doi: 10.1115/1.4028653.
- [70] F. Heremans and R. Ronsse, "Design of an energy efficient transfemoral prosthesis using lockable parallel springs and electrical energy transfer," *IEEE Int. Conf. Rehabil. Robot.*, pp. 1305–1312, 2017, doi: 10.1109/ICORR.2017.8009429.
- [71] C. N. Rosyidi, U. S. Maret, P. Fitriawati, U. S. Maret, R. D. Astuti, and U. S. Maret, "Optimization Model for Gas Spring of Endoskeletal Prosthetic Leg with Optimization Model for Gas Spring of Endoskeletal Prosthetic Leg with Maximum Energy Storage Criteria," no. May 2014, pp. 799–804, 2012.
- [72] P. Geng, "Design Analysis of Passive Impedance Control of Medical Exoskeleton Using Cable Drive and Gas Spring By Masters of Science , Plan II University of California at Berkeley," 2016.
- [73] J. C. Perry and A. Rathod, "Energy density and hysteresis comparison in natural rubber tube springs for wearable exoskeleton applications," *IEEE Int. Conf. Rehabil. Robot.*, vol. 2019-June, pp. 21–27, 2019, doi: 10.1109/ICORR.2019.8779400.

7.2 Other

- [74] Design World (2017, October 30). *What is a wrap spring clutch or brake?* [Video]. YouTube. <https://www.youtube.com/watch?v=92Ti7LBjfYQ>

7.3 ChatGPT

[1] Input:
DC brushless motor

Output:

A DC brushless motor, also known as a BLDC (Brushless DC) motor, is a type of electric motor that uses electronic commutation instead of brushes to control the movement of the rotor. It operates on direct current (DC) power and has a stator and a rotor. The stator consists of a series of permanent magnets arranged around the circumference of the motor, while the rotor is made up of a series of electromagnets.

[2] Input:
Oil dampers

Output:

Oil dampers create resistance by forcing oil through small holes, which slows down the movement of the joint and helps to control its speed and range of motion. This makes them effective at absorbing and dissipating kinetic energy in various applications, such as in automobiles, industrial machinery, and aerospace.

[3] Input:
Leaf springs

Output:

Leaf springs are a type of suspension system commonly used in vehicles such as trucks, vans, and trailers. They are made up of several thin, flexible strips of metal, called leaves, which are stacked on top of each other and secured to the vehicle's frame and axle.

[4] Input:
Implantability criteria for implantable actuators for skeletal movement.

[5] Input:
Implantability criteria for implantable dampers for skeletal movement.

[6] Input:
Implantability criteria for implantable springs for skeletal movement.

	Hydraulic actuators	Advantages	Disadvantages	Applications	Location(s)
Ma, Zhaoyi (2022)	Elastomeric HASEL actuator	Self healing (M222) Self sensing through capacitance monitoring (M222)	Requires high voltage (M222)	Artificial muscles (M222)	
Ma, Zhaoyi (2022)	Thermoplastic HASEL actuator	Self healing (M222) Self sensing through capacitance monitoring (M222)	Requires high voltage (M222) Dielectric fluid may leak (M222)	Artificial muscles (M222)	
De Greef, Aline (2009)	Flexible micro actuator			Medical instruments (DA09)	
De Greef, Aline (2009)	Expansion behaviour based hydraulic actuator	Highly flexible (DA09) They can handle delicate objects without causing any damage (DA09) Lightweight (DA09) Can achieve complex motions (DA09)	Needs equipment that can be bulky (DA09) Can present leakages (DA09)	Artificial muscles (DA09)	Hand (DA09)
	Magnetic actuators	Advantages	Disadvantages	Applications	Location(s)
Bernat, Jakub (2023)	Magnetorheological elastomer actuator	Vibration absorbing (BJ23) Excited by field (BJ23) Flexible structure (BJ23) Low production cost (BJ23)	Requires high magnetic field (BJ23) Most commonly required permanent magnets (BJ23)	Soft robotics (BJ23)	
Kulagin, Ivan (2022)	Magnetic shape memory alloy actuator	Wide actuation frequency (KI22) Rapid accelerations (KI22) High energy efficiency (KI22)	Limited temperature range (-40-60 degrees) (KI22) Sensitive to fatigue (KI22) Complex design due to hysteresis and complex to model the behavior (KI22)	Micropumps (KI22) Valves (KI22)	
He, Yuen (2022)	Magnetic hydrogel based actuator	Fast response (HY22) Design diversity (HY22)	Complex design (HY22) Complex fabrication (HY22)	Artificial muscles (HY22) Soft robotics (HY22) Medical devices (HY22)	Fingers (HY22)
	Electroactive actuators	Advantages	Disadvantages	Applications	Location(s)
El-Atab, Nazeek (2020) Nazibul Hasan, Mohammed (2020)	Piezoelectric actuator	Fast response (NM20) High displacement resolution (NM20) High efficiency (NM20) Compact structure (NM20)	Require large voltage (EN20)(NM20) Require high temperature (NM20) Large hysteresis nonlinearity (NM20)	Micropumps (NM20) Micro-robotics (NM20)	
Liu, Yan (2021)	Cellulose paper actuator	Light weight (LY21) Low costs (LY21) Biodegradable (LY21) Biocompatible (LY21)	Low output force (LY21) Slow response (LY21)	Soft robotics (LY21) Artificial muscles (LY21)	
Ma, Zhaoyi (2022)	Electro-ribbon actuator	Easy fabrication (M222) Lightweight (M222) Self-sensing (M222)	Requires high voltage (0.4kV)(M222) Slow actuation (M222) Liquid leakage (M222)	Origami (M221)	
	Ionic electroactive polymer actuators	Advantages	Disadvantages	Applications	Location(s)
Bernat, Jakub (2023) Pagoli, Amir (2022) Maksimkin, Aleksey V (2022) Ahn, Junseong (2022)	Ionic polymer metal composition actuator	Requires low voltage (3V) (BJ23)(AP22)(MA22)(AJ22) Flexible (can bend over 360 degrees) (BJ23)(AP22)(MA22) Variable stiffness (AP22) Self sensing (AP22) Fast response (MA22)(AJ22) High ionic conductivity (MA22) Long-range stroke (AJ22)	Low actuation force in bending (BJ23)(AP22)(AJ22) High production costs (BJ23)(AJ22) Electrolyte requires humid condition (BJ23)(MA22) Electrolysis occurs over 1.23V (BJ23)(MA22) Slow response (AP22) Low cycle life (MA22)(AJ22)	Soft robotics (BJ23) Artificial muscles (MA22)	
Maksimkin, Aleksey V (2022) Ahn, Junseong (2022) Liu, Zhiwei (2021)	Ionic polymeric gel actuator	Can mimic strength and energy density of biological muscles (MA22) Require low voltage (MA22)(AJ22) Bistable (MA22) Lightweight (AJ22)	Weak mechanical properties (MA22)(AJ22) Slow response (MA22) Require humid conditions (MA22)(AJ22) Electrolysis occurs above a certain voltage (MA22) Low response (MA22) Low electromechanical coupling efficiency (MA22)	Artificial muscles (MA22)(LZ21) Orthotics (LZ21)	Leg (LZ21)
Maksimkin, Aleksey V (2022) Bar-cohen, Yoseph (2019)	Conductive polymer actuator	Require low voltage (MA22) High conductivity (MA22) High ionic conductivity of the electrolyte (MA22) Fast response (MA22) Large deformation (MA22)	Electrolysis above a certain voltage (MA22) Low cycle life (MA22) High dehydration (MA22) Low efficiency (BY19)	Artificial muscles (MA22)(BY29)	
Bar-cohen, Yoseph (2019) Kosidlo, U. (2013)	Carbon nanotube actuator	Require low voltage (KU13) Noiseless (KU13) High mechanical strength (KU13) High work per cycle (BY19)(KU13) Can be used in liquid or air (KU13),	Poor conductivity of the electrode (KU13)	Artificial muscles (BY19)	
	Electronic electroactive polymer actuators	Advantages	Disadvantages	Applications	Location(s)
Bernat, Jakub (2023) Pagoli, Amir (2022) Maksimkin, Aleksey V (2022) Wang, Yuhao (2022) Ma, Zhaoyi (2022) Ahn, Junseong (2022)	Dielectric elastomer actuator	Quiet operation (BJ23) Low weight (BJ23) Large actuation force (BJ23)(PA22) Fast actuation response time (BJ23)(PA23)(MA22)(AJ22) Very flexible (BJ23) High value of strain (BJ23)(MA22) Self sensing capability (ZM22) Requiring small currents (MA22) High energy density (MA22) Low costs (MA22) Ease of fabrication (AJ22)	High voltage requirement (BJ23)(AP22)(MA22)(ZM22)(AJ22) Unidirectional operation due to electrostriction effect (BJ23) Requiring membrane pre-strain (BJ23)(MA22) Difficult fabrication procedure (AP22) Requiring electrolyte (WY22) Susceptible to dielectric breakdown (ZM22)(AJ22)	Artificial muscles (MA22)(WY22)(M222) Soft robotics (AJ22)	
Maksimkin, Aleksey V (2022) El-Atab, Nazeek (2020)	Liquid crystal elastomer actuator	Produce high stress and strain (MA22) Need low electrical voltage (1.5-5 kV) (MA22)(EN20)	Slow response (MA22) Hysteresis (MA22)	Artificial muscles (MA22) Soft robotics (EN20)	
Maksimkin, Aleksey V (2022) O'Halloran, Ailish (2008)	Piezoelectric polymer actuator	Good mechanical energy density (MA22) High elastic modulus (MA22) Fast response (MA22)	Need high voltage (MA22) Complicated production (MA22) Thin films (MA22) Low strain (MA22)	Artificial muscles (MA22)(OA08)	
Bar-cohen, Yoseph (2019)	Ferroelectric polymer actuator	Large actuation force (BY19) Fast response (BY19)		Artificial muscles (BY19)	
Maksimkin, Aleksey V (2022)	Electrostrictive graft elastomer actuator	Low costs (MA22) Strain values up to 5% (MA22) Fast response (MA22)	Need high voltage (MA22)	Artificial muscles (MA22)	

Table 2b: Characteristics actuators: f.i.t.r. author, year, actuator type, advantage(s) and disadvantage(s), application(s) and location(s)

	Thermal actuators	Advantages	Disadvantages	Applications	Location(s)
Wu, Zongpeng (2023) Pagoli, Amir (2022) Subramaniam, Krishnan (2022) Tang, Xianzhi (2022) El-Atab, Nazek (2020) Nazibul Hasan, Mohammed (2020)	Shape memory alloy actuator	Soft (W223), light and flexible (W223)(SK22) High active stress (AP22)(XT22) High elastic modulus (AP22) Conductivity without the need for an external heater (AP22) Act as a strain sensor at the same time (AP22) Noiseless (SK22) Large displacement (NM20) Large force (NM20) High mechanical robustness (NM20) Corrosion-resistan (NM20)	Geometries must be exact (W223) Slow reponse and speed (AP22)(NM20) Hysteresis (AP22) Require high currents (AP22)(NM20) Low energy efficiency (SK22)	Exoskeletons (W223) Orthotics (SK22) Surgical tools (NM20) Implantable devices (NM20) Microgrippers (NM20) Micropumps (NM20)	Knee (W223) Ankle-foot (SK22)
Pagoli, Amir (2022) Tang, Xianzhi (2022) Ahn, Junseong (2022)	Shape memory polymers actuator	Variable stiffness capability (PA22)(TX22) High-design diversity (AJ22) Ease of fabrication (AJ22) Structural flexibility (NM20) Large strains (NM20) Low density (NM20) Tunable transition temperature (NM20) Biodegradable properties (NM20)	Low produced force (PA22)(TX22) Irreversible actuation (AJ22) Slow response (NM20) Low recovery stress (NM20)	Endovascular devices (NM20) Drug delivery devices (NM20)	
Ma, Zhaoyi (2022) Bar-cohen, Yoseph (2019)	Twisted and coiled polymer actuator	Linear contraction (MZ22) Small-volume applications (MZ22) Lightweight applications (MZ22)	Long actuation period (MZ22) Low energy efficiency (MZ22)	Robotics (MZ22) Prosthetics (MZ22) Artificial muscles ((BY29)	Arms (MZ22)
Ma, Zhaoyi (2022)	Phase changing actuator	Very large strain (MZ22) High specific energy (MZ22) Low voltage actuation (MZ22) Wireless actuation (MZ22)	Long actuation cycle (MZ22) Limited lifetime (MZ22) Low energy efficiency (MZ22)	Artificial muscles (MZ22)	
Nazibul Hasan, Mohammed (2020)	Thermal hydrogel actuator	Tunable degradation features (NM20) Tunable mechanical features (NM20) UV-sensitive (NM20)	Slow response (NM20)	Surgical tools (NM20) Miscorvalves (NM20) Drug delivery devices (NM20)	
Ahn, Junseong (2022)	Bilayer electrothermal actuator	Long- range stroke (AJ22) Lightweight (AJ22) Can be designed in thin film form (AJ22)	High driving voltage (AJ22) Low design diversity (AJ22)	Soft robotics (AJ22) Medical devices (AJ22)	
	Variable stiffness actuators	Advantages	Disadvantages	Applications	Location(s)
Wolf, Sebastian (2016)	Independent variable stiffness actuator	Use less power than other actuators (WS16) Size of the stiffness adjusting motor can be chosen to match the power needed (WS16) Lightweight compared to antagonistic setups (WS16) Stiffness variation (WS16)	Only the power of the positioning motor can be used to move the joint and thus this defines the output power of the actuator and also for changing the stiffness setup only the power of the stiffness adjuster can be used (WS16)	Robotics (WS16)	Arms (WS16) Legs (WS16)
Wolf, Sebastian (2016)	Antagonistic variable stiffness actuator	Use less power than other actuators. (WS16) Length between the actuator and the joint can be easily compensated (WS16) It can move the output, but is still backdrivable (WS16) Stiffness variation (WS16)	The maximum output power and torque of only one of the motors and also the energy storage of only one spring can be used (WS16) For moving the output both motors and potentially gearboxes have to move and as a result the power losses of all four elements show up (WS16)	Robotics (WS16)	Arms (WS16) Legs (WS16)
Ismawan, Ade Reza (2022) Yang, Canjun (2022) Shankar, NVS (2021) Vanderborght, B (2013)	Series elastic actuator	Able to hold and generate energy when moving thereby increasing efficiency (IA22) Disturbances and shocks are isolated from the gear transmission (YC22) Huge range of speed (SN21) Huge range of torque (SN21)	Limited stiffness (YC22) Bulky (YC22) Low power efficiency (SN21)	Prosthetics (IA22)(SN21)	Ankle-foot (IA22)
Wu, Zongpeng (2023)	Clutchable elastic device	Adaptable to multiple applications (W223)	Bulky system (W223)	Exoskeletons (W223)	Knee (W223)
Wu, Zongpeng (2023)	Two springs working both in series and in parallel	Behaves similar to biological muscles (W223)	Multiple components and complex structure (W223)	Exoskeletons (W223)	Knee (W223)
S. A. Lavate (2015)	AwAS I	Capable of minimizing energy consumption through exploiting the natural dynamics in real time for both fixed and variable frequency motions (SL15)		Robotics (SL15) Prosthetics (SL15)	
S. A. Lavate (2015)	AwAS II	Lighter and more compact setup than the previous version (SL15)		Robotics (SL15) Prosthetics (SL15)	
S. A. Lavate (2015)	VSA-UT			Robotics (SL15) Prosthetics (SL15)	
S. A. Lavate (2015)	VSA-UT II			Robotics (SL15) Prosthetics (SL15)	
S. A. Lavate (2015)	mVSA-UT			Robotics (SL15) Prosthetics (SL15)	
S. A. Lavate (2015)	Hybrid dual actuator unit			Robotics (SL15) Prosthetics (SL15)	
S. A. Lavate (2015)	CompAct variable stiffness actuator			Robotics (SL15) Prosthetics (SL15)	

Table 2c: Characteristics actuators: f.l.t.r. author, year, actuator type, advantage(s) and disadvantage(s), application(s) and location(s)

A2 Characteristics dampers

Author, Year	Damper type(s)	Remarks	Relevance	Applications	Location(s)
Monteleone, Simone (2022)	Fluid dynamic dampers	Advantages	Disadvantages	Applications	Location(s)
	Meatus damper	Wide spectrum of energy dissipation density led by the vast range of viscosity levels held by these fluids, making them suitable for compact, high-damping solutions. (MS22)	Slow damping response (MS22) Require precise seals to avoid leaks (MS22)	Medical devices (MS22)	
Monteleone, Simone (2022)	Orifice damper	Wide spectrum of energy dissipation density led by the vast range of viscosity levels held by these fluids, making them suitable for compact, high-damping solutions. (MS22)	Slow damping response (MS22) Require precise seals to avoid leaks (MS22)	Medical devices (MS22)	
Zhou Congcong (2022) Abe, Hiroaki (2021) S Yamamoto (2015)	Oil damper			Orthotics (ZC22)	Ankle-foot (ZC22)(AH21)(SY15) Knee (AH21)
Monteleone, Simone (2022)	Variable-rheological fluid dampers	Advantages	Disadvantages	Applications	Location(s)
	Electrorheological fluid damper	Fast response (MS22) Simple mechanics (MS22)	ER fluids, have a tendency to chemically and mechanically react with diverse materials (MS22) Necessitating precise damper component selection (MS22)	Medical devices (MS22) Prosthetics (MS22) Rehabilitative systems (MS22) Wearable robotics (MS22)	
Zhang, Yanjuan (2023) Monteleone, Simone (2022) Lv, Hongzhan (2021) Rahman, Mahmud (2017)	Magnetorheological fluid damper	Fast response (MS22)(RM17)(ZY23) Simple mechanics (MS22) Simple configuration (ZY23) Compact design (ZY23)(RM17) Step-less damping force adjustment (ZY23) Large viscosity (RM17) Large control range (RM17) Low costs (RM17) Low power feeding (RM17)	Particles are liable to stick together due to residual magnetization, making redispersion difficult and forming a hard layer (MS22)	Medical devices (MS22) Prosthetics (MS22)(RM17) Rehabilitative systems (MS22) Wearable robotics (MS22)	Knee (LH21)(RM17)
Zhang, Yanjuan (2023) Monteleone, Simone (2022)	Magnetorheological or electrorheological fluid damper: flow mode	Large damping force (ZY23)	Complex design (ZY23)		
Zhang, Yanjuan (2023) Monteleone, Simone (2022)	Magnetorheological or electrorheological fluid damper: shear mode	Simple design (ZY23)	Lower damping force (ZY23)		
Zhang, Yanjuan (2023) Monteleone, Simone (2022)	Magnetorheological or electrorheological fluid damper: squeeze mode	Large damping force (ZY23)	Only for low and slight vibrations (ZY23)		
Zhang, Yanjuan (2023)	Magnetorheological fluid damper: Annular shaped	Fast response (ZY23) Narrow dimensions (ZY23) High damping force (ZY23)	Adjustment range limited by axial valve dimensions (ZY23)		
Zhang, Yanjuan (2023)	Magnetorheological fluid damper: Radial shaped	Large damping force (ZY23) Suitable for broader and shorter bypass fluids (ZY23)	Complex design (ZY23)		
Zhang, Yanjuan (2023)	Magnetorheological fluid damper: Annular-radial shaped	Large damping force (ZY23) Good working performance (ZY23)	Complex design (ZY23) Difficult to compact (ZY23)		
Rahman, Mahmud (2017) Imaduddin, Fitriani (2013)	Linear magnetorheological fluid damper	Capability to change its damping stiffness by varying the magnetic field strength inside the damper(IF13)	Large installation space requirement (IF13) Less resistant to damage (IF13) Uses relatively large amounts of expensive fluid (IF13) High costs (IF13)		
Khedkar, Yashpal M. (2019) Rahman, Mahmud (2017)	Linear magnetorheological fluid damper: mono tube				
Khedkar, Yashpal M. (2019) Rahman, Mahmud (2017)	Linear magnetorheological fluid damper: twin tube				
Khedkar, Yashpal M. (2019) Rahman, Mahmud (2017)	Linear magnetorheological fluid damper: double ended				
Rahman, Mahmud (2017) Imaduddin, Fitriani (2013)	Rotary magnetorheological fluid damper	Compact and low weight (IF13) Uses smaller quantity of fluid (IF13) Lower costs (IF13)	Hysteresis behaviour (IF13)		
Rahman, Mahmud (2017) Imaduddin, Fitriani (2013)	Rotary magnetorheological fluid damper: continuous angle	Ability to switch with endless rotational angle (RM17)	Lower damping torque (RM17)(IF13)		
Rahman, Mahmud (2017) Imaduddin, Fitriani (2013)	Rotary magnetorheological fluid damper: continuous angle with drum type brake	Capable of reducing the angular speed of a rotating shaft immersed in the fluid (IF13)	Compactness of the MR brake (IF13) Low endurance (IF13)		
Rahman, Mahmud (2017) Imaduddin, Fitriani (2013)	Rotary magnetorheological fluid damper: continuous angle with disc type brake	Capable of reducing the angular speed of a rotating shaft immersed in the fluid (IF13)	Compactness of the MR brake (IF13) Low endurance (IF13)		
Rahman, Mahmud (2017) Imaduddin, Fitriani (2013)	Rotary magnetorheological fluid damper: continuous angle with hybrid brake	Capable of reducing the angular speed of a rotating shaft immersed in the fluid (IF13)	Compactness of the MR brake (IF13) Low endurance (IF13)		
Rahman, Mahmud (2017) Imaduddin, Fitriani (2013)	Rotary magnetorheological fluid damper: continuous angle with hybrid brake (single coil)	Capable of reducing the angular speed of a rotating shaft immersed in the fluid (IF13)	Compactness of the MR brake (IF13) Low endurance (IF13)		
Rahman, Mahmud (2017) Imaduddin, Fitriani (2013)	Rotary magnetorheological fluid damper: continuous angle with hybrid brake (double coil)	Capable of reducing the angular speed of a rotating shaft immersed in the fluid (IF13)	Compactness of the MR brake (IF13) Low endurance (IF13)		
Rahman, Mahmud (2017) Imaduddin, Fitriani (2013)	Rotary magnetorheological fluid damper: continuous angle with hybrid brake (T-shaped)	Capable of reducing the angular speed of a rotating shaft immersed in the fluid (IF13)	Compactness of the MR brake (IF13) Low endurance (IF13)		
Rahman, Mahmud (2017) Imaduddin, Fitriani (2013)	Rotary magnetorheological fluid damper: limited angle	Larger damping torque (RM17)(IF13) Lower weight and have a space saving compared to linear damper (IF13)	Not the ability to switch with endless rotational angle (RM17) Complex manufacturing (IF13)		
Monteleone, Simone (2022)	Electromagnetism dampers	Advantages	Disadvantages	Applications	Location(s)
	Eddy current damper	Avoid friction (MS22) Durable (MS22) Fast and precise dynamics (MS22)	Low energy dissipation density (MS22)	Prosthetics (MS22) Medical devices (MS22)	
Monteleone, Simone (2022)	Motor-like electromagnetic damper	Avoid friction (MS22) Durable (MS22) Fast and precise dynamics (MS22)	Low energy dissipation density (MS22)	Prosthetics (MS22) Medical devices (MS22)	
Monteleone, Simone (2022)	Friction dampers	Advantages	Disadvantages	Applications	Location(s)
	Viscoelastic damper	Employ the same physical element to implement elasticity and dampening (MS22)	The impossibility to decouple the elastic and damping effects (MS22)	Rehabilitative systems (MS22) Wearable robotics (MS22) Haptic systems (MS22)	
Monteleone, Simone (2022)	Braking effect damper	Able to emulate any type of generalized damping effect if proper control is applied (MS22) High damping forces (MS22)	The pad location must be regulated to avoid compromising the control quality (MS22) Passive dry friction dampers would result in constant braking on the link (MS22)	Rehabilitative systems (MS22) Wearable robotics (MS22) Haptic systems (MS22)	

Table 3: Characteristics dampers: f.i.t.r. author, year, damper type, advantage(s) and disadvantage(s), application(s) and location(s)

A3 Characteristics springs

Author, Year	Spring type(s)	Remarks	Relevance	Location(s)
	Non-linear springs	Advantages	Disadvantages	Applications
Ali, Mubasher (2020)	Variable dimension helical springs	High strength to weight ratio (AM20) Low costs (AM20) Controllable suspension (AM20)		Orthotics (AM20) Midsole foot (AM20)
Khazaaleh, Shadi (2021)	Kresing pattern springs			Artificial muscles (KS21)
Choi, Kyungjun (2022) Allen, Emily A (2022) Devashena, T. (2021) Park, Seong Jun (2020) Afifah, I. (2017)	Shape memory alloy springs	Can be made into various shapes (DT21) Memorizes its original shape (PS20) Lightweight (PS20) Flexible (PS20) High force (PS20) Strain similar to that of human skeletal muscles (PS20) Can be formed in bundles (PS20)	Relaxation of SMA spring is highly affected by the cooling speed (CK22)	Artificial muscles (PS20) Orthotics (AI17) Ankle-foot (AI17)
	Compression springs	Advantages	Disadvantages	Applications
van der Weijde, J.O. (2022)	Coil springs			Exoskeletons (VJ22) Prosthetics (VJ22) Leg (VJ22)
Liu, Yifan (2022) Moon, Junyoung (2022) Wu, Xingming (2016)	Leaf springs	Flexible (LY22) Simple structure (LY22) High load carrying capacity (LY22) Small size (LY22) Easy to adjust stiffness (WX16)		Exoskeletons (MY22) Prosthetics (MY22) Ankle (MY22) Ankle foot (MY22)
Moon, Junyoung (2022)	Coil/Leaf springs			Exoskeletons (MY22) Prosthetics (MY22) Ankle (MY22) Ankle foot (MY22)
Mani, Vishnu Aishwaryan Subra (2020) Design World (2017), Youtube Elliott, Grant (2014)	Wrap spring clutch/brake	High accuracy (DW) Repeatability (DW) High torque to size ratio (DW) Low power consumption (DW) Durable (DW)		Exoskeletons (MV20)(EG14) Knee (MV20)(EG14)
Hill, Parker W. (2019)	Constant force springs	Ability to provide a constant force over a wide range of motion (HP19)	Resonance as a result of stick-and-slip friction (HP2019)	Exoskeletons (HP19) Arm (HP19)
	Torsion springs	Advantages	Disadvantages	Applications
Bumbard, Katy Baker (2022) Chaichaowarat, Ronnapree (2017)	Torsion springs			Exoskeletons (BK22)(CR17) Knee (BK22)(CR17)
Liu, Sanwei (2015)	Carbon nanotube torsial springs	High stiffness (LS15) High extensibility (LS15)	Low energy density compared to mechanical springs (LS15)	Artificial muscles (LS15)
	Cam based springs	Advantages	Disadvantages	Applications
Realmuto, Jonathan (2015)	Cam based springs			Prosthetics (RU15) Ankle (RU15)
	Lockable parallel springs			
Heremans, François (2017)	Lockable parallel springs	Ability to generate a passive stiffness when the device runs out of power (HF17) Power efficient (HF17)		Prosthetics (HF17) Ankle (HF17) Knee (HF17)
	Rubber springs			
Geng, Peter (2016) Rosyidi, Cucuk Nur (2012)	Gas springs	Acts as a brake or lock during initial stance phase (GP16) Smoother response than a mechanical spring (RC12)		Exoskeletons (GP16) Prosthetics (RC12) Knee (GP16) Leg (RC12)
Perry, Joel C. (2019)	Rubber springs	Less limited elongation range than steel springs (PJ19) Lightweight (PJ19)	Mullins effect (PJ19) Hysteresis (PJ19)	Exoskeletons (PJ19) Orthotics (PJ19) Elbow (PJ19) Hand (PJ19) Fingers (PJ19)

Table 4: Characteristics springs: f.i.t.r. author, year, spring type, advantage(s) and disadvantage(s), application(s) and location(s)

B1 Implantability assessment actuators

	Servo motor	DC brushless motor	Convolute vacuum actuator	Pleated vacuum actuator	Yoshimura pattern origami actuator	Miura-ori pattern origami actuator	Kresling pattern origami actuator	Linear pneumatic actuator	Rotary pneumatic actuator	HASEL actuator	Pneumatically driven microcage actuator	Pneumatic balloon actuator	Flexible rubber micro actuator	Pleated pneumatic actuator	Antagonistic pleated pneumatic actuator	McKibben pneumatic actuators	Sleeved bladder actuator	Yarlott netted muscle actuator	Kukolj netted muscle actuator	ROMAC actuator	Morin muscle actuator	Paynter hyperboloid actuator	Kleinwachter torsion device	Peano muscle actuator	Series pneumatic muscle actuator	Flat pneumatic muscle actuator	High-displacement pneumatic muscle actuator	Reverse pneumatic artificial muscle actuator	Straight fiber type pneumatic actuators	PneuNets actuator	Elastomeric HASEL actuator	Thermoplastic HASEL actuator	Flexible micro actuator			
Biocompatibility	x	x	x	x	+	+	+	x	-	x	-	-	-	x	+	+	x	-	-	-	x	x	x	x	x	x	x	x	x	x	x	x	x	x	x	
Size and shape	-	-	x	x	+	+	+	x	±	x	±	±	±	+	x	x	x	x	x	+	x	x	x	x	x	x	x	x	x	x	x	x	x	x	x	
Weight	x	-	x	x	x	x	x	x	+	x	+	+	x	x	x	+	x	x	x	x	x	x	x	x	x	x	x	x	x	x	x	x	x	x	x	
Flexibility	-	x	x	x	x	x	x	x	x	x	x	x	x	x	x	+	x	x	x	+	x	x	x	x	x	x	x	x	x	x	x	x	x	x	x	
Force output	+	+	x	x	x	x	x	x	x	x	x	x	x	x	+	x	x	x	x	x	x	x	x	x	x	x	x	x	x	x	x	x	x	x	x	
Range of motion	-	-	x	x	+	+	+	x	x	+	x	x	x	x	x	±	x	x	x	x	x	x	x	x	x	x	x	x	x	x	x	x	x	x	x	
Durability	x	x	x	x	x	x	x	x	x	x	x	x	x	x	x	+	x	x	x	x	x	x	x	x	x	x	x	x	x	x	x	x	x	x	x	x
Voltage range	x	x	x	x	x	x	x	x	x	x	x	x	x	x	x	x	x	x	x	x	x	x	x	x	x	x	x	x	x	x	x	x	x	x	x	x
Response time	x	x	x	x	x	x	x	x	x	x	x	x	x	+	-	x	x	x	x	x	x	x	x	x	x	x	x	x	x	x	x	x	x	x	x	x

Table 5a: Implantability assessment actuators. Implantability criteria (vertical axis), type of actuator (horizontal axis). Meeting the criteria (+), not meeting the criteria (-), can possibly meet the criteria (±), unclear (x).

	Expansion behaviour based hydraulic actuators	Magnetorheological elastomer actuator	Magnetic shape memory alloy actuator	Magnetic hydrogel based actuator	Piezoelectric actuator	Cellulose paper actuator	Electro-ribbon actuator	Ionic polymer metal composition actuator	Ionic polymeric gel actuator	Conductive polymer actuator	Carbon nanotube actuator	Dielectric elastomer actuator	Liquid crystal elastomer actuator	Piezoelectric polymer actuator	Ferroelectric polymer actuator	Electrostrictive graft elastomer actuator	Shape memory alloy actuator	Shape memory polymers actuator	Twisted and coiled polymer actuator	Phase changing actuator	Thermal hydrogel actuator	Bi-layer electrothermal actuator	Independent variable stiffness actuator	Antagonistic variable stiffness actuator	Series elastic actuator	Clutchable elastic device	Two springs working both in series and in parallel	AWAS I	AWAS II	VSA-UT	VSA-UT II	mVSA-UT	Hybrid dual actuator unit	CompAct variable stiffness actuator			
Biocompatibility	-	-	-	x	-	+	-	x	+	x	+	-	-	x	x	x	x	x	x	x	x	x	x	x	x	x	+	x	x	x	x	x	x	x	x	x	
Size and shape	-	x	-	-	+	x	x	x	x	x	x	x	x	x	x	x	-	+	x	x	x	+	+	x	-	-	-	x	+	x	x	x	x	x	x	x	
Weight	x	x	x	x	x	+	+	x	+	x	x	+	x	x	x	x	+	x	+	x	x	+	+	x	x	x	x	x	x	+	x	x	x	x	x	x	x
Flexibility	+	+	x	x	x	x	x	x	x	x	x	+	x	x	x	x	+	x	x	x	x	x	x	x	x	x	x	x	x	x	x	x	x	x	x	x	x
Force output	x	x	x	x	x	x	x	-	x	x	x	x	x	x	+	x	+	x	x	x	x	x	x	x	+	x	x	x	x	x	x	x	x	x	x	x	x
Range of motion	+	x	x	x	x	x	x	+	x	x	x	x	x	x	x	x	+	x	x	x	x	x	x	+	x	x	x	x	x	x	x	x	x	x	x	x	x
Durability	x	x	-	x	x	x	x	-	x	-	±	x	x	x	x	x	x	x	x	-	x	x	x	x	x	x	x	x	x	x	x	x	x	x	x	x	x
Voltage range	x	x	x	x	-	-	-	+	+	+	+	-	+	-	x	-	-	x	x	+	x	-	x	x	x	x	x	x	x	x	x	x	x	x	x	x	x
Response time	x	x	+	+	+	-	-	±	-	+	x	+	-	+	+	+	-	-	-	-	-	-	x	x	x	x	x	x	x	x	x	x	x	x	x	x	x

Table 5b: Implantability assessment actuators. Implantability criteria (vertical axis), type of actuator (horizontal axis). Meeting the criteria (+), not meeting the criteria (-), can possibly meet the criteria (±), unclear (x).

B2 Implantability assessment dampers

	Oil damper	Electrorheological fluid damper	Magnetorheological fluid damper	Magnetorheological or electrorheological fluid damper: flow mode	Magnetorheological or electrorheological fluid damper: shear mode	Magnetorheological or electrorheological fluid damper: squeeze mode	Magnetorheological fluid damper: Annular shaped	Magnetorheological fluid damper: Radial shaped	Magnetorheological fluid damper: Annular-radial shaped	Linear magnetorheological fluid damper	Linear magnetorheological fluid damper: mono tube	Linear magnetorheological fluid damper: twin tube	Linear magnetorheological fluid damper: double ended	Rotary magnetorheological fluid damper	Rotary magnetorheological fluid damper: continuous angle	Rotary magnetorheological fluid damper: continuous angle with drum type brake	Rotary magnetorheological fluid damper: continuous angle with disc type brake	Rotary magnetorheological fluid damper: continuous angle with hybrid brake	Rotary magnetorheological fluid damper: continuous angle with hybrid brake (single coil)	Rotary magnetorheological fluid damper: continuous angle with hybrid brake (double coil)	Rotary magnetorheological fluid damper: continuous angle with hybrid brake (T-shaped)	Rotary magnetorheological fluid damper: limited angle	Eddy current damper	Motor-like electromagnetic damper	Viscoelastic damper	Braking effect damper	
Biocompatibility	X	±	±	X	X	X	X	X	X	X	X	X	X	X	X	X	X	X	X	X	X	X	X	X	X	X	X
Size and shape	X	X	+	-	+	X	+	-	-	-	X	X	X	+	X	-	-	-	-	-	-	+	X	X	X	X	X
Weight	X	X	X	X	X	X	X	X	X	X	X	X	X	+	X	X	X	X	X	X	X	+	X	X	X	X	X
Flexibility	X	X	X	X	X	X	X	X	X	X	X	X	X	X	X	X	X	X	X	X	X	X	X	X	X	X	X
Damping force	X	X	X	+	-	+	+	+	+	X	X	X	X	X	-	X	X	X	X	X	X	+	X	X	X	X	+
Damping Adjustment	X	X	+	X	X	-	-	X	X	+	X	X	X	X	X	+	+	+	+	+	+	X	X	X	X	X	+
Durability	X	X	X	X	X	X	X	X	X	-	X	X	X	X	X	-	-	-	-	-	-	X	+	+	X	X	X
Response time	X	+	+	X	X	X	+	X	X	X	X	X	X	X	X	X	X	X	X	X	X	X	+	+	X	X	X

Table 6: Implantability assessment dampers. Implantability criteria (vertical axis), type of damper (horizontal axis). Meeting the criteria (+), not meeting the criteria (-), can possibly meet the criteria (±), unclear (x).

B3 Implantability assessment springs

	Non-linear spring	Variable dimension helical spring	Kresing pattern spring	Shape memory alloy spring	Coil spring	Leaf spring	CoilLeaf spring	Wrap spring clutch/brake	Constant force spring	Torsion spring	Carbon nanotube torsial spring	Cam based spring
Biocompatibility	x	x	x	x	x	x	x	x	x	x	x	x
Size and shape	x	x	x	x	x	±	x	x	x	x	x	x
Weight	x	x	x	±	x	x	x	x	x	x	x	x
Flexibility	x	x	x	±	x	±	x	x	x	x	x	x
Spring strength	x	±	x	±	x	x	x	±	x	x	x	x
Spring stiffness	x	±	x	±	x	±	x	x	-	x	±	x
Range of motion	x	x	x	±	x	x	x	x	±	x	±	x
Durability	x	x	x	±	x	x	x	±	-	x	x	x
Response time	x	x	x	-	x	x	x	x	x	x	x	x

Table 7: Implantability assessment springs. Implantability criteria (vertical axis), type of spring (horizontal axis). Meeting the criteria (+), not meeting the criteria (-), can possibly meet the criteria (±), unclear (x).